Assessing shale gas reservoir potential using multi-scaled SEM pore network characterizations and quantifications: The Ciñera-Matallana pull-apart basin, NW Spain

Ethan J. Richardson [a, b], Michael Montenari [a,*]

[a] Geography, Geology and the Environment, Keele University, Newcastle under Lyme, United Kingdom

[b] 35 Thoresby Road, York, United Kingdom

*Corresponding author: m.montenari@keele.ac.uk (M. Montenari)

Keywords: Shale gas; Unconventional hydrocarbon reservoirs; Quantitative pore network characterization; SEM; Ciñera-Matallana coalfield; Spain

Abstract

In recent years, unconventional hydrocarbon reservoirs (UHRs), specifically shale gas plays, have become a vast source of economically viable hydrocarbons, in response to better drilling and stimulation techniques. To further improve recovery, more detailed pore network modeling needs to be conducted by means of detailed pore network characterizations, based upon predefined pore size and pore type classification schemes. Through the quantification of the nano/microporous properties of the pore network, a better understanding on how hydrocarbon storage and migration phenomena operate within UHRs and how well they might respond to stimulation can be developed. Kasimovian-Gzhelian (Late Carboniferous) lacustrine sediments from the Upper Pastora Formation of the Ciñera-Matallana coalfield, NW Spain, were investigated to identify the potential for shale gas, by conducting a detailed pore network analysis using SEM-based porosity data, alongside traditional methods of formation evaluation. Here we show that the Upper Pastora Formation demonstrates shale gas potential and that the nanoporous network is a complex multifaceted and multi-scaled system composed of various pore types and sizes, each with specific dynamic properties and varying contributions toward total porosity. The present contribution provides a full pore net-work characterization and quantification, based on pore type and size, followed by a quantification of the porosity percentage held within each pore type and size. This work will provide an insight into the need for pore network characterizations along-side pore property quantifications with regard to computational fluid flow models and as such the need to carry out this work in conjunction with more traditional methods of shale gas exploration.

1. INTRODUCTION

Unconventional hydrocarbon reservoirs (UHRs) are reservoirs characterized by low permeability but with great hydrocarbon potential, most notable of which are shale gas plays, tights gas sands and
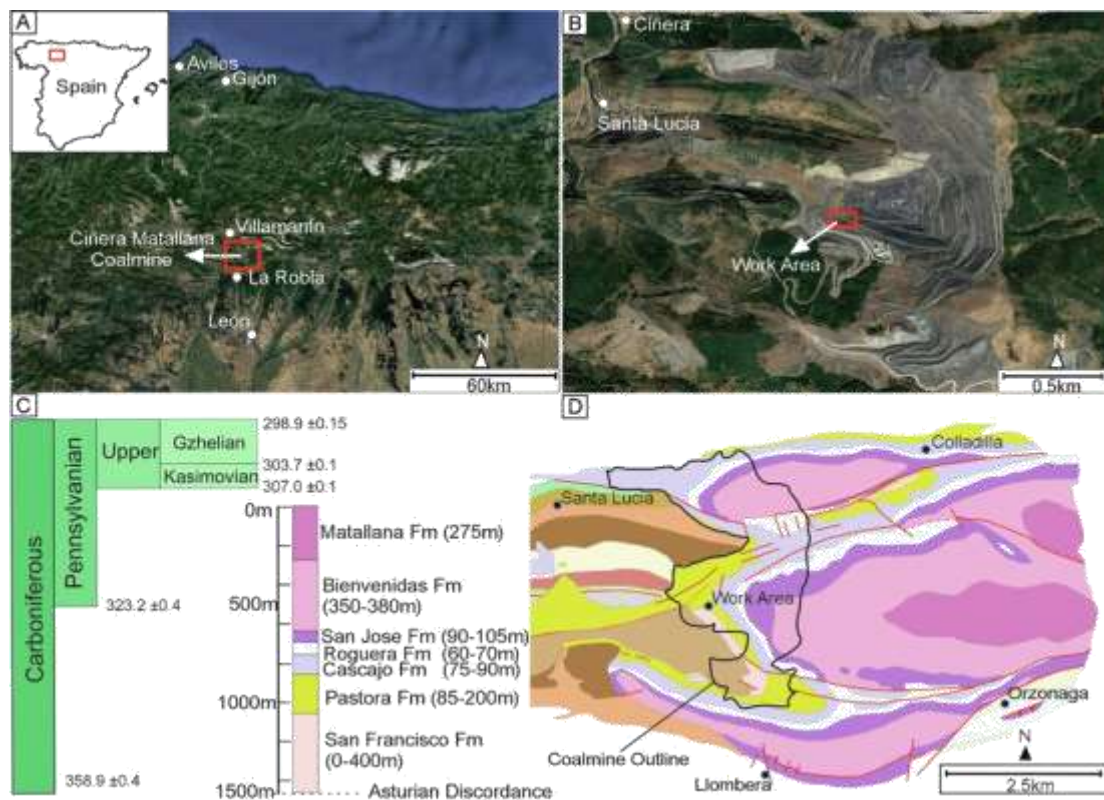
Fig. 1. Location map of the Ciñera-Matallana Coalmine. (A) Aerial view of Cantabria NW Spain. (B) Aerial view of the Ciñera-Matallana coalmine. (C) Late Carboniferous timescale (D) Geological map of the area surrounding the Ciñera-Matallana coalmine, with the coalmine's out-line highlighted in black ((A) and (B) adapted from Google Maps, (C) adapted from Cohen et al, 2013 (updated), (D) adapted from IGME, 1989).
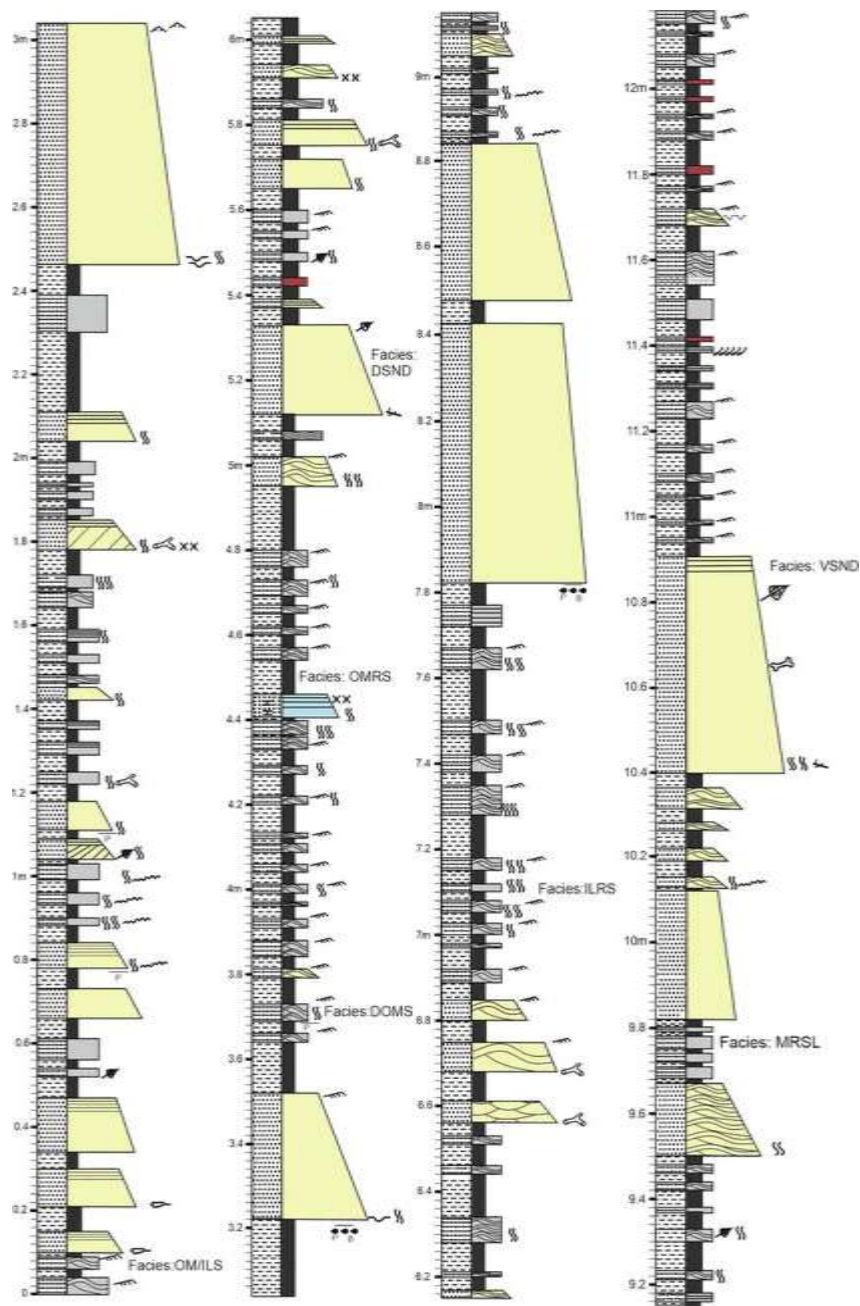
Facies:OM/ILS

Facies: DSND

Facies: OMRS

Facies:DOMS

Facies:ILRS

Facies: VSND

Facies: MRSL

Fig. 2. High-resolution 12-m sedimentary log of the Upper Pastora Formation with sampled microfacies locations.

coalbed methane (Chengzao, 2017). One of the most productive UHRs which has currently been reshaping the global energy industry, are shale gas plays, characterized by high organic matter (OM) content and low–ultra low permeability (0.0001 mD). These reservoirs hold a much greater volume of hydrocarbons than their conventional counterparts (Zendehboudi and Bahadori, 2016). Acting as both source and seal, large quantities of gas are held in very small nano/μm scale pores within dissolved, adsorbed and free gas states, throughout a multi-scaled system, spread over several orders of magnitude. With shales representing the most abundant type of sedimentary rock on Earth (Boyer et al., 2013) and unproven, but technically recoverable shale gas reserves estimated at 7576.6 trillion cubic feet (Tcf), from 46 of the world's most shale rich countries, this UHR is a highly valuable resource (EIA, 2013). However, traditional methods of recovery cannot be used due to poor flow proper-ties within the pore network, requiring hydraulic fracturing to increase recovery (Guo et al., 2018).

Extending over 19,000 km^2, the Cantabrian Massif has been subject to a limited number of hydrocarbon exploration campaigns, with only two hydrocarbon wells spanning the entire area (González et al., 2017). Despite the Central Carboniferous Basin being identified as offering source rock potential and the presence of mine gas, predominately consisting of methane and traces of ethane, having long been recognized, no published shale gas/oil reports for the Cantabrian Massif exist (European Commission, 2016). The Ciñera-Matallana Basin, located in the South-ern Cantabrian Zone, was identified by Lemos de Sousa and Pinheiro (1996) as the most important coalfield with real natural gas prospects in the Cantabrian Massif. Further work by Cienfuegos and Loredo (2010) within the Asturian Central Coal Basin located further to the north, estimated that coal bed methane (CBM) resources contain a minimum of 25,100 Mm^3 of gas. This is clear evidence of the great potential in the Cantabrian Massif for CBM, but currently, no methane has been economically extracted in the region (Álvarez et al., 2018). As

with most studies into UHRs within the Cantabrian Massif, CBM has been the dominant focus, while shale gas potential has remained untested and is at a very preliminary stage of understanding and exploration (Mackenzie, 2018).

Fig. 3. Key for sedimentary structures.

Fig. 4. Outcrop of the Upper Pastora Formation. (A–C) Interbedded sequence of argillaceous sediment of the Upper Pastora Formation with 5-m staff for scale. The formation is clearly marked with large intermittent sandstone beds which interrupt the more finely bedded siltstone/shale sequence. (D) Sandstone bed with weak hummocky cross-stratification. (E) Very finely interbedded shales/siltstones between two large dolomitized sand-stone beds. (F) Siltstone displaying quasi-planar laminations at the top of the bed with a carbonate base. (G) Basal bioturbation (thalassinoides) in a larger sandstone bed. (H) Calamite fossil. (I) Clustered group of fossilized plant material.
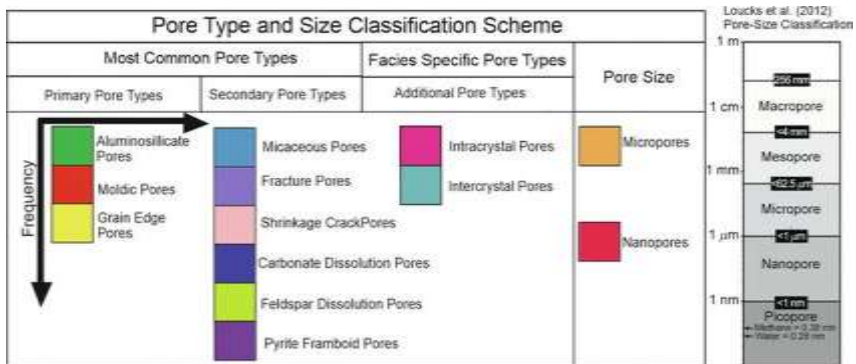
Fig. 5. Pore type and size classification key listing the most frequent pore types found throughout all microfacies.
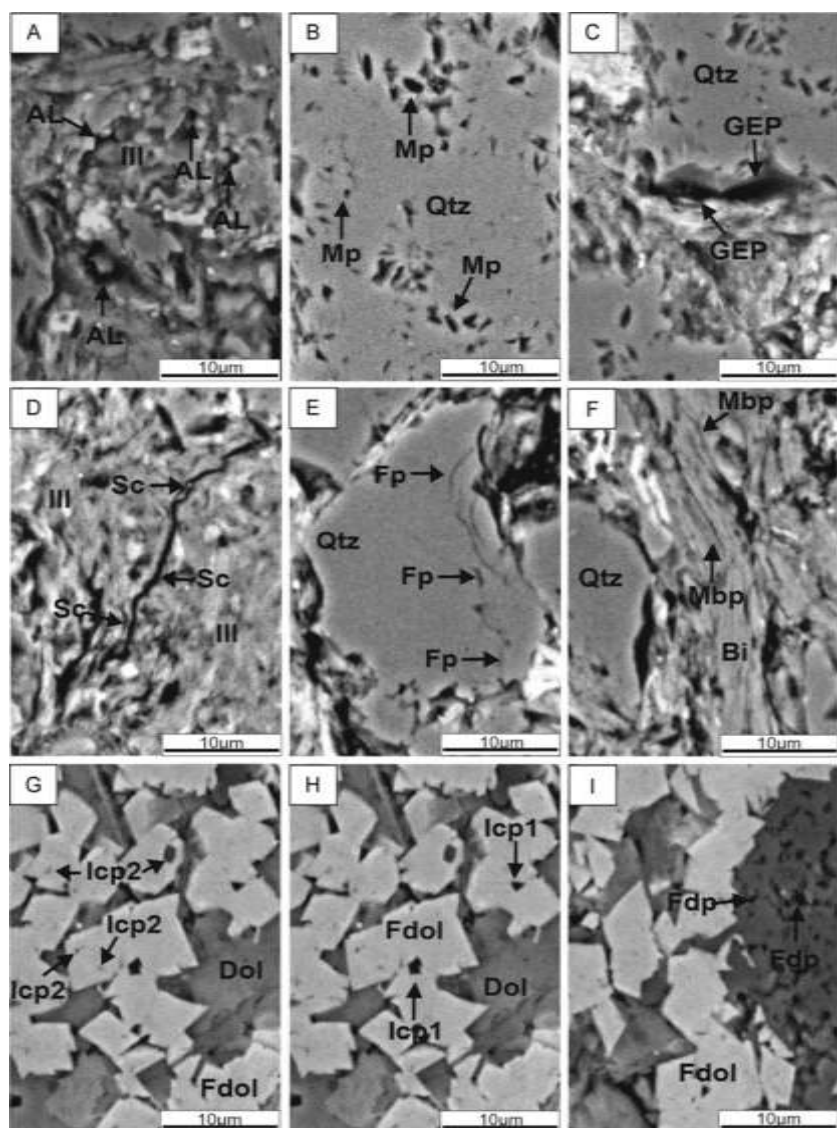
Fig. 6. Scanning electron microscope (Backscatter electron, BSE) images depicting the spectrum of pore types used for the characterization of microfacies pore networks. (A) Aluminosilicate pores (AL) found between grains. (B) Moldic pores (MP) isolated within mineral phases, showing elongate pore morphologies. (C) Grain edge pore (GEP) located adjacent to a rigid grain. (D) Shrinkage crack pore (SCP) located within the illite matrix. (E) Facture pores (FP) concentrated around a small area within a quartz grain. (F) Micaceous pores (MBP) found closely grouped within a biotite grain. (G) Intracrys-tal pores (ICP1) found isolated within ferroan dolomite crystals. (H) Intercrystal pores (ICP2) found between closely packed ferroan dolomite crystals. (I) Feldspar dissolution pores (FDP) found within a highly weathered feldspar grain displaying a high pore den-sity. There are also carbonate dissolution pores which are referred to as (CDP).

1st Sample0063

1st Sample0063   201

Porosity:15.43%

Microporosity:13.76%
Microporosity:1.67%

200μm

13
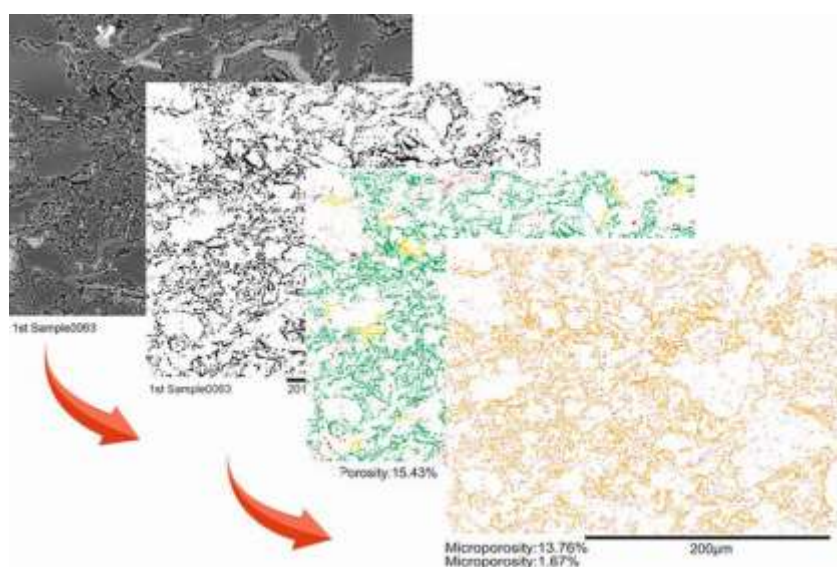
Fig. 7. The process of image binarization and subsequent pore type and pore size characterization from a back scattered electron image (example: OMRS microfacies, for explanations see text).

A preliminary study by Álvarez et al. (2018), aimed at assessing UHR source rock potential of 12 Silurian and Carboniferous lithostratigraphic units across the Cantabrian Zone, found that according to TOC results, the Naranco, San Emiliano, Fito Ereñes, and Barcaliente Formations offer a moderately good potential for hydrocarbon generation. However, thermal maturity data based on vitrinite reflectance indicated that all Silurian/Carboniferous dated strata were too immature for the development of thermogenic gas as they clearly plotted within the oil generation window.

While the search for shale gas potentials within the Cantabrian Massif is still in an initial exploration phase, around the world the potential of shale gas has already been realized as a cleaner alternative to coal which can be used as a "bridging fuel" during the transition to a CO_2 neutral future. Furthermore, shale gas has proved to be a cost efficient source of energy which reduces expenditure on imports and increases energy security while bolstering domestic economic prosperity through the generation of regional job opportunities (Bazilian et al., 2014). However, our understanding of the physicochemical properties and characteristics of micro- and nanometric pores, which largely control hydrocarbon migration and storage in shale gas reservoirs, still remains largely insufficient in both predicting and maximizing well productivity. It appears that the rapidly increasing demand and the subsequent production of shale gas was not accompanied by an adequate investment into the detailed research of the very fundamentals of shale gas generation and exploitation. The knowledge of how these fundamental properties within the pore network operate in response to recovery, is still in an early if not rudimentary stage, especially with regard to the physical properties that control the flow regimes (King et al., 2015).
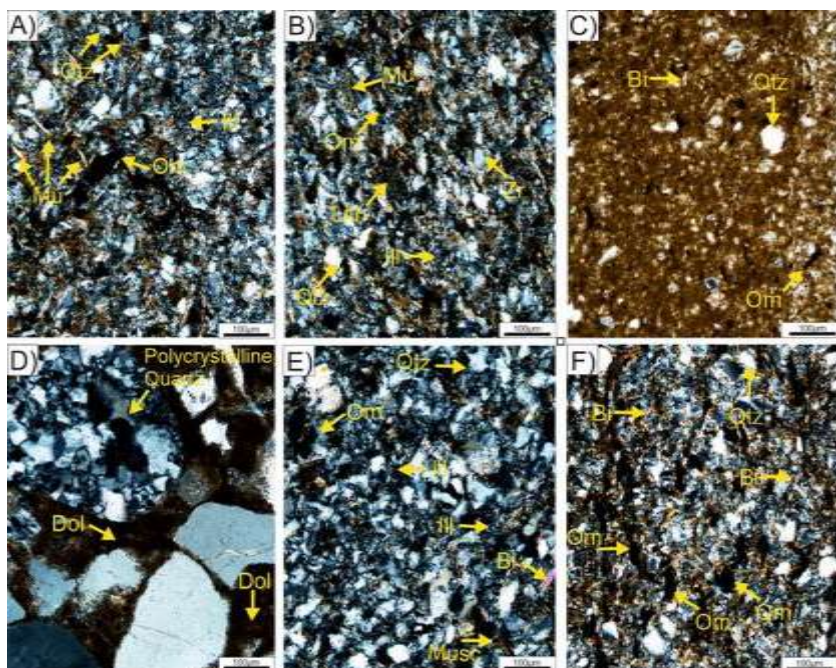
Fig. 8. Annotated thin section (100 μm-scale) of the seven most abundant microfacies found along the 12-m logged section. (A) OM/ILS. (B) DOMS. (C) OMRS. (D) DSND. (E) ILRS. (F) MRSL (all images with crossed polarisers). Bi = Biotite, Dol = Dolomite, Ill = Illite, Mu and Musc = Muscovite, OM = Organic matter, Qtz = Quartz, Zr = Zircon.

One of the major issues facing the industry is the sustainability of the so-called shale gas revolution with the significant decline in production after the initial 12-month flow-back period. Production data from
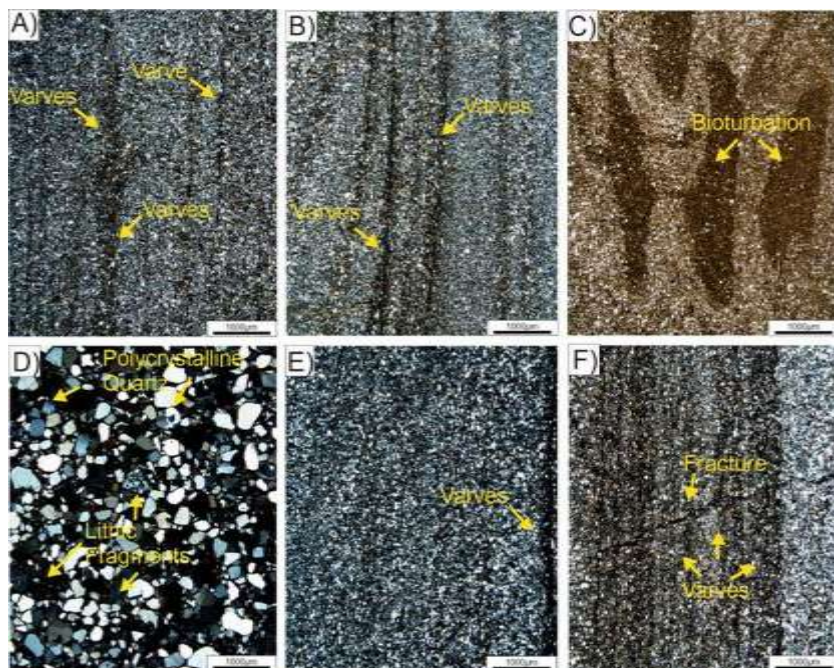
Fig. 9. Annotated thin section (1000 µm-scale) of the seven most abundant microfacies found along the 12-m logged section. (A) OM/ILS. (B) DOMS. (C) OMRS. (D) DSND. (E) ILRS. (F) MRSL (all images with crossed polarisers).
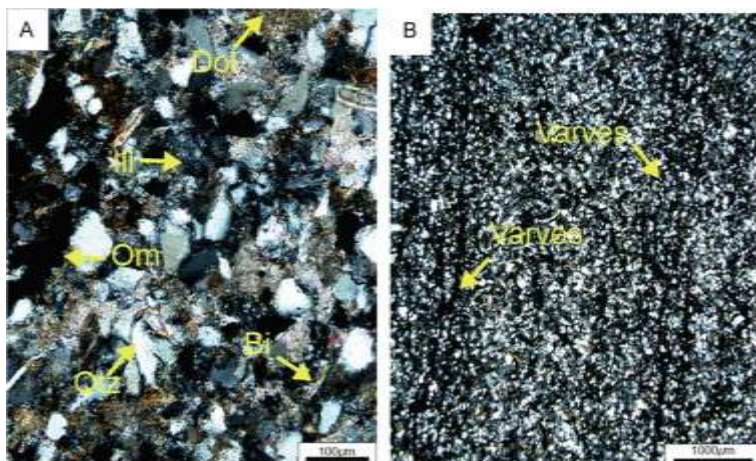
Fig. 10. Annotated thin section of VSND facies. (A) 100 µm-scale and (B) 1000 µm-scale. Bi = Biotite, Dol = Dolomite, Ill = Illite, Om = Organic matter, Qtz = Quartz (all images with crossed polarisers).
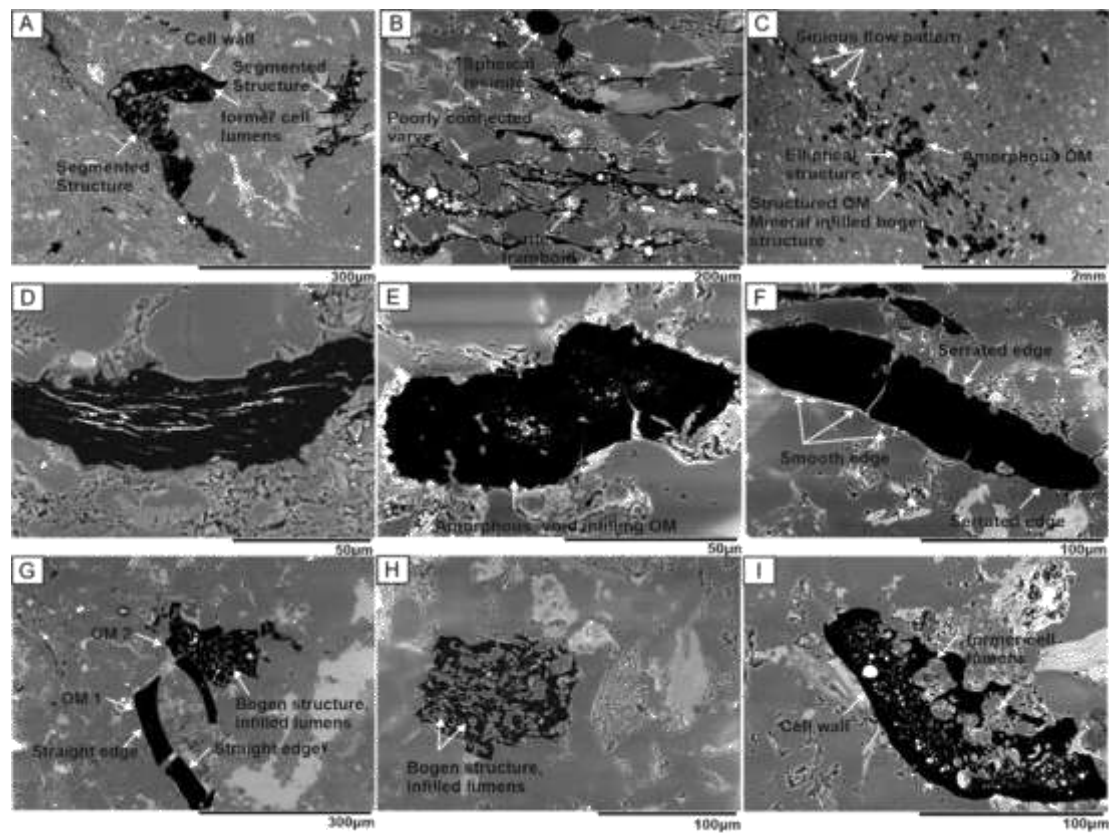
Fig. 11. Scanning electron microscope (BSE) images depicting organic matter morphologies with interpretation of maceral type. (A) Segmented structures representing remnant woody cell wall structures (vitrinite). (B) Poorly connected varve showing sinuous flow patterns presumed to be of algal/phytoplanktonic origin. (C) Phytoclastic varve showing various OM structures but poor connectivity with discrete sinuous flow paths. (D) Inertodetrinite, structured morphology with a mineral infilled bogen structure. (E) Unidentifiable OM, amorphous with low relief (void-filling). (F) Cutinite, serrated pattern more dominate on one side. (G) Two types of OM, Om1 with straight edge morphology (Telovitrinite), Om2 bogen structure and infilled cell lumens (fusinite). (H) Fusinite, well pronounced bogen structure. (I) Unidentifiable organic maceral, cell wall and in-filled lumens are well pronounced.
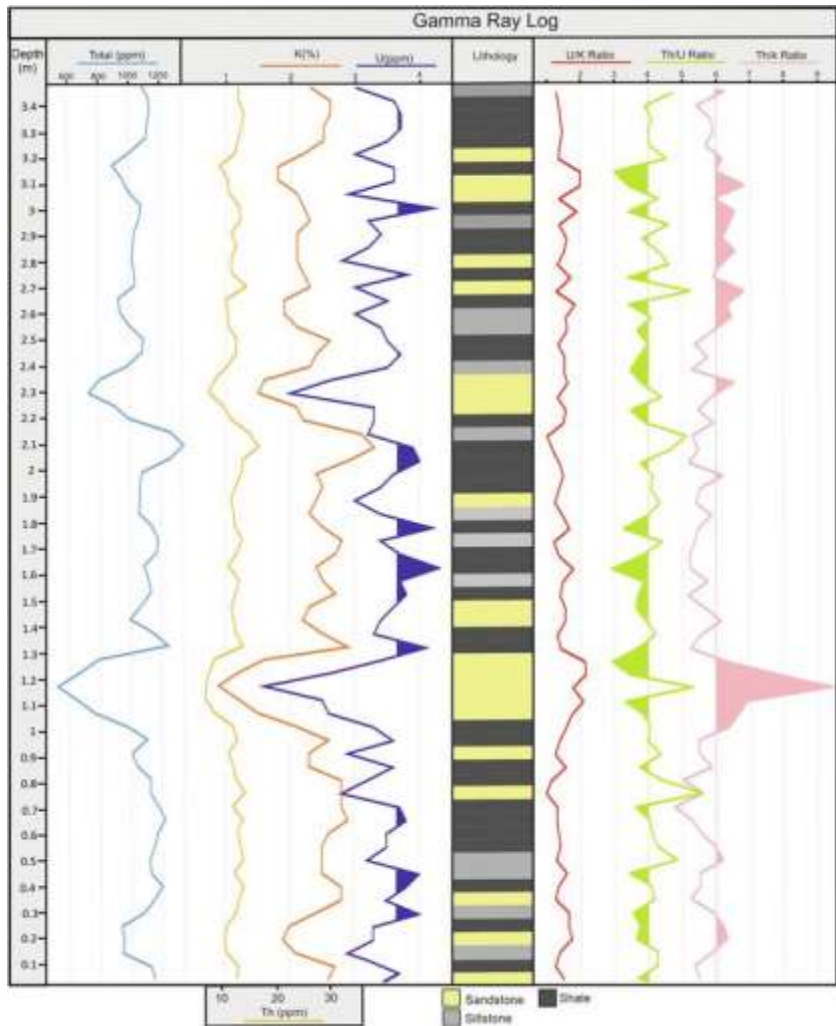
Fig. 12. 3.4 meter high-resolution gamma ray log depicting variations in the total signal, thorium (Th), potassium (K), and uranium (U) concentrations along the sedimentary log as well as Th/U, Th/K and U/K ratios.

the Late Devonian to Early Carboniferous Bakken Shale and the early Late Cretaceous (Cenomanian to Turonian) Eagleford Shale gas plays in the U.S. have shown a 60% decrease in production after the first 12 months, while gas wells in 5 of the most productive shale gas plays across the U.S. have reported that after 3 years, wells only achieve between 5% and 20% of their initial production rate (Hu et al., 2015). Further production data from wells located in the Early Carboniferous Barnett Shale (Texas) also show that over a 10-year period high performing wells produce 33% of their gas within the first 12 months and low performing wells 22% (Middleton et al., 2017). Such production data has given rise to the assumption that there are two fundamentally different physical mechanisms controlling shale gas production, with regard to initially high, followed by later sustained but significantly lower production rates seen in tail-end production. This significantly reduced production rate is generally attributed to desorption processes. The majority of shale gas production, however, occurs in this latter stage but over a prolonged period, which highlights the need for research to maximize the recoverability during tail-end production. It is estimated that by enhanced desorption alone, wells could yield up to 20–30% more gas over a 5–10-year period (Middleton et al., 2015). This phenomenon, which is becoming more and more apparent in mature wells across U.S. shale gas plays, has led to the conclusion that future decline rates of shale gas have been underestimated and as a result well longevity and estimated ultimate recovery (EUR)
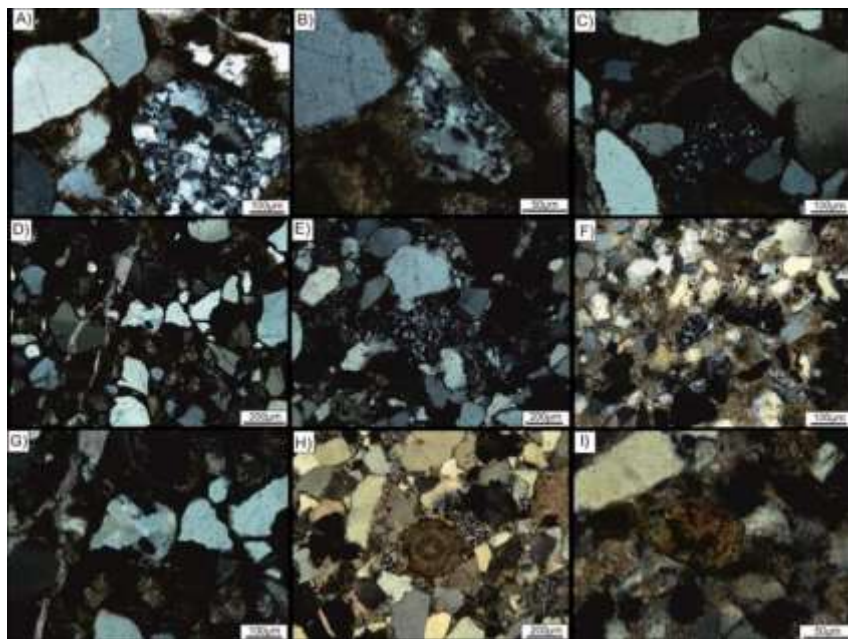
Fig. 13. (A–G) Polycrystalline quartz grains found in coarse grained sandstones showing varying degrees of polycrystallinity and variable microfabrics (all images with crossed po-larisers). (H) Bone fragment. (I) Palynomorph.

severely overestimated (McGlade et al., 2013). To overcome this, new wells are constantly being drilled to make up for the rapid decline of mature wells in order to maintain shale gas production (Wang, 2018). However, another way in which these problems could be addressed is through developing a deeper understanding of the multi-scaled distribution of different pore types throughout the pore network, using an integrated analytical approach aimed at providing a full, visual, quantitative analysis of the pore network and associated properties.

Pore Size Frequency vs Area (50μm)

Facies:OM/ILS

Facies:DOMS

Facies:ORMS

Facies:DSND

Facies:ILRS

Facies:MRSL

Facies:VSND

23
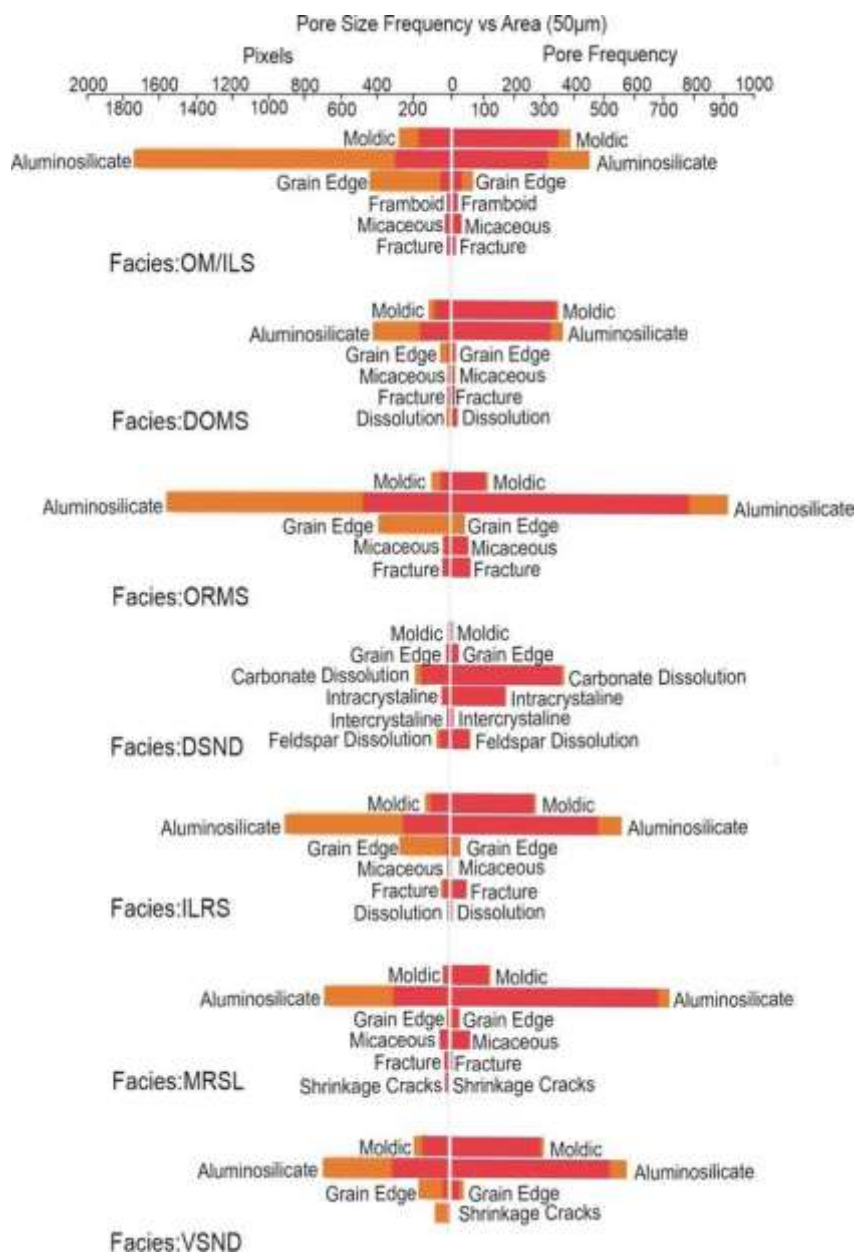
Fig. 14. Pore size frequency and area changes in relation to pore types within different microfacies, highlighting the disproportionate relationship between nanopore frequency and area occupied within the pore network (50 μm - scale).

Pore Size Frequency vs Area (200μm)

Facies:OM/ILS

Facies:DOMS

Facies:ORMS

Facies:DSND

Facies:ILRS

Facies:MRSL

Facies:VSND
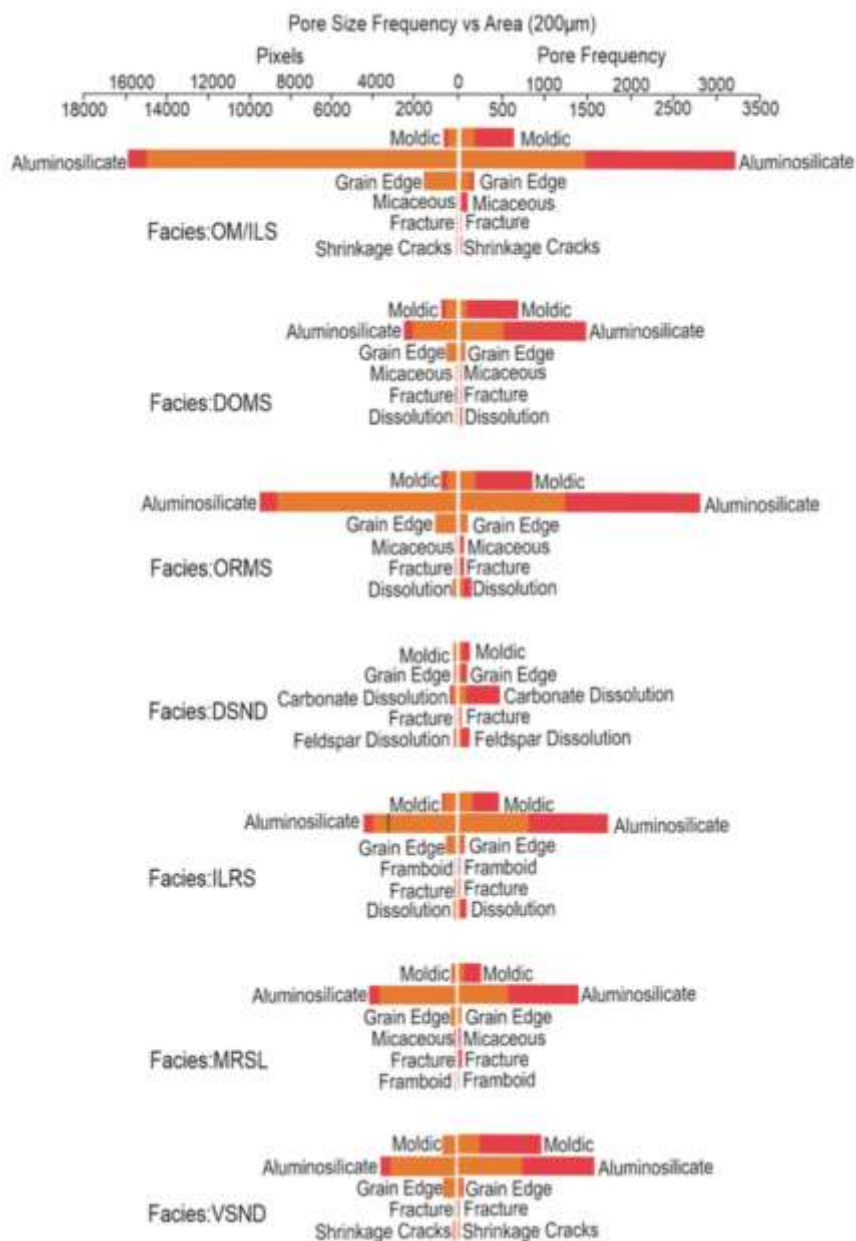
Fig. 15. Pore size frequency and area changes in relation to pore types within different microfacies, highlighting the disproportionate relationship between nanopore frequency and area occupied within the pore network. (200 µm - scale).

Pore Type Porosity vs Frequency

Facies	Scale (µm)	Porosity (%)
VSND	50µm	8.53%
	200µm	6.98%
MRLS	50µm	6.94%
	200µm	6.34%
ILRS	50µm	10.56%
	200µm	7.7%
DSND	50µm	2.7%
	200µm	0.91%
OMRS	50µm	17.08%
	200µm	15.43%
DOMS	50µm	4.86%
	200µm	5.25%
OM/ILS	50µm	19.35%
	200µm	24.47%
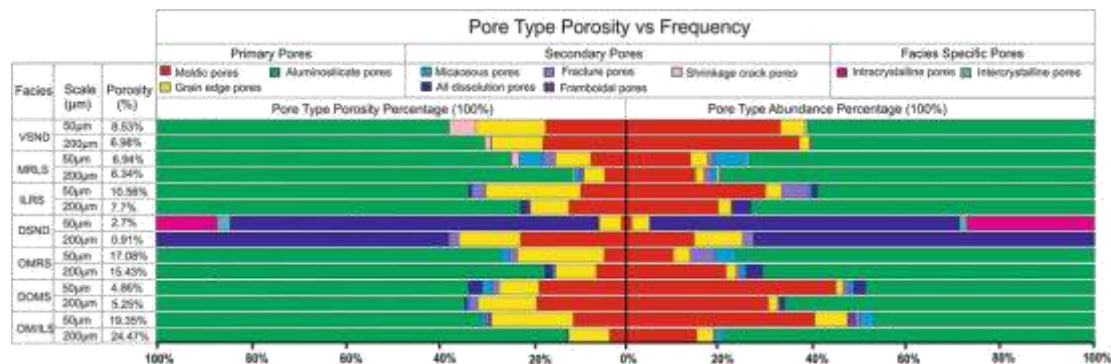
Fig. 16. Pore type abundance in relation to porosity across all facies types within the nanopore system (50 μm) and micropore system (200 μm). The chart highlights the disparity between the abundance of specific pore types throughout the pore network and their disproportionate contribution toward porosity, best exemplified by GEP and MP pores.
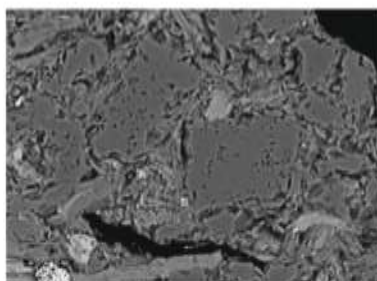
Facies:OM/ILS
Scale:50μm
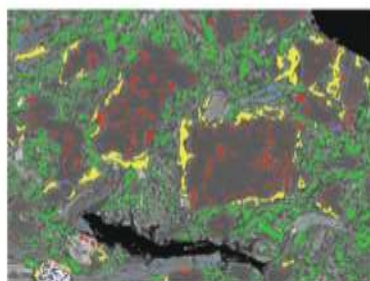
Total Porosity:19.35%
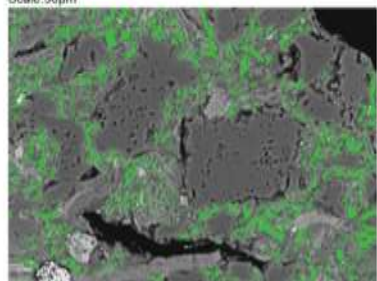
Pore Type:Aluminosilicate Pores (AL)
Total Porosity:13.36%
Porosity (100%):69.04%
Pore Frequency (100%):46.96%
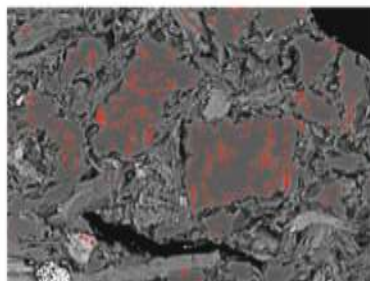
Pore Type:Moldic Pores (MP)
Total Porosity:2.17%
Porosity (100%):11.19%
Pore Frequency (100%):40.27%
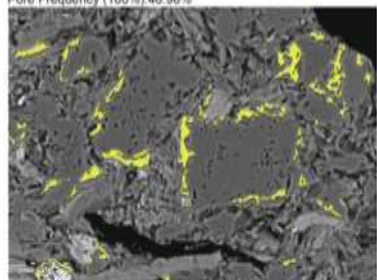
Pore Type:Grain Edge Pores (GEP)
Total Porosity:3.39%
Porosity (100%):17.53%
Pore Frequency (100%):7%
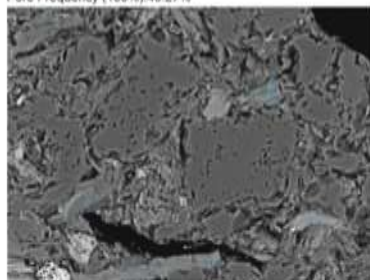
Pore Type:Micaceous Pores (MBP)
Total Porosity:0.2%
Porosity (100%):1.04%
Pore Frequency (100%):2.99%
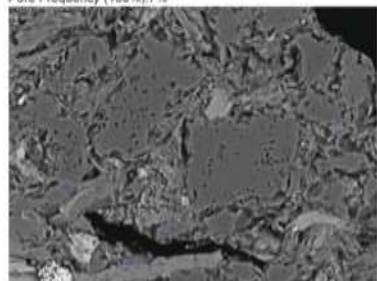
Pore Type:Fracture Pores (FP)
Total Porosity:0.12%
Porosity (100%):0.61%
Pore Frequency (100%):1.13%
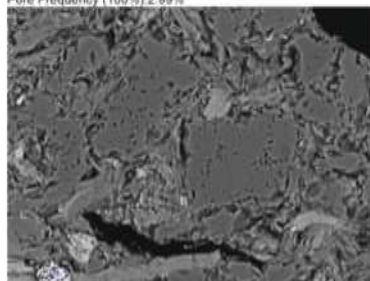
Pore Type:Framboid Pores (FHP)
Total Porosity:0.11%
Porosity (100%):0.59%
Pore Frequency (100%):1.65%

29

Upon completion, associated changes in specific pore type abundances, permeability and flow-back data will provide a deeper understanding of pore type controls on gas storage and migration mechanisms. Further research into hydrocarbon migration and storage in fine clastic materials such as shales is vital for evaluating the long term behavior of shale gas reservoirs, the economic viability of recovery operations and the reduction of exploration risks (Ross and Bustin, 2009). However, up to the present date there remains only a moderate understanding of the full characteristics of pore systems in shales, with only limited work conducted on the systematic quantification of pore networks, and with detailed imaging being rare (Curtis et al., 2012; Ma et al., 2018).

In order to better understand important productivity controlling factors, the pore network must be systematically measured and quantitatively described (Anovitz and Cole, 2015). In this paper, we approach this problem by (1) identifying and quantifying the petrographic loci of the porosity; (2) establishing a pore network characterization, followed by (3) identifying which pore types have a similar mode of occurrence and as such, display similar properties, which in turn are considered to be different from other pore types found throughout the net-work. This is an area which has previously been understudied, with most published research focusing on understanding the factors controlling pore type genesis and rarely conducting an in-depth analysis into pore type contributions toward total porosity (Chen et al., 2019). As the majority of hydrocarbons within shale gas plays are thought to be stored within nanopores, which have a very low permeability (Scotchman, 2016), this characterization will quantify both the nanoporous and microporous systems as separate entities. As decreasing pore radii result in multiple flow regimes operating within one and the same pore network, Darcy's law can

Fig. 17. Facies OMILS pore type characterization (50 μm Scale).

Facies:OM/LS
Scale: 50µm
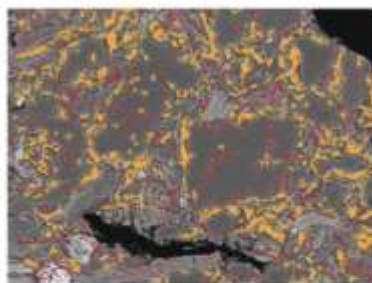
Microporosity:14.83%
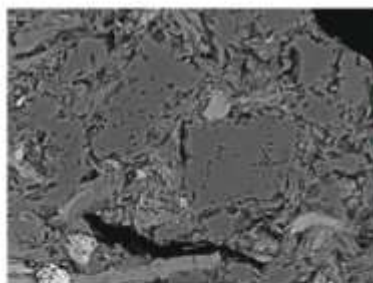Nanoporosity:4.52%
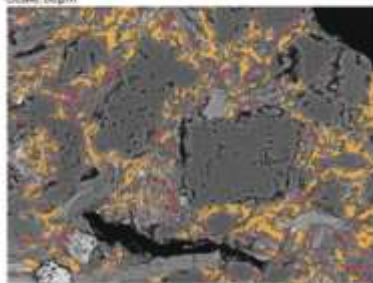
Pore Type:Aluminosilicate Pores (AL)
Total Porosity:13.36%
Microporosity:11.04%   Micropore Frequency (100%):30.82%
Nanoporosity:2.32%   Nanopore Frequency (100%):69.08
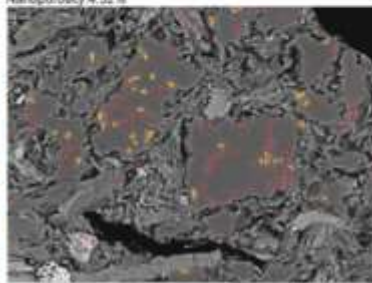
Pore Type:Moldic Pores (MP)
Total Porosity:2.17%
Microporosity:0.83%   Micropore Frequency (100%):10.23%
Nanoporosity:1.34%   Nanopore Frequency (100%):89.77%
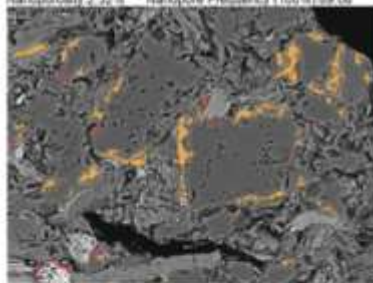
Pore Type:Grain Edge Pores (GEP)
Total Porosity:3.39%
Microporosity:2.96%   Micropore Frequency (100%):57.35%
Nanoporosity:0.43%   Nanopore Frequency (100%):42.65%
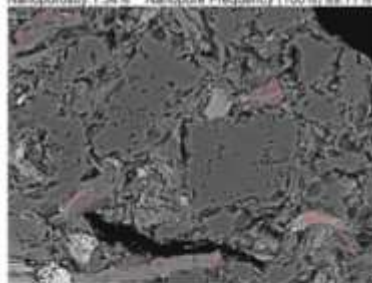
Pore Type:Micaceous Pores (MBP)
Total Porosity:0.2%
Microporosity:N/A   Micropore Frequency (100%):N/A
Nanoporosity:0.2%   Nanopore Frequency (100%):100%
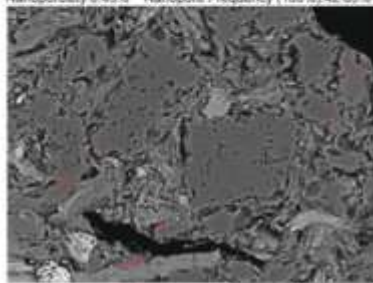
Pore Type:Fracture Pores (FP)
Total Porosity:0.12%
Microporosity:N/A   Micropore Frequency (100%): N/A
Nanoporosity:0.12%   Nanopore Frequency (100%):100%
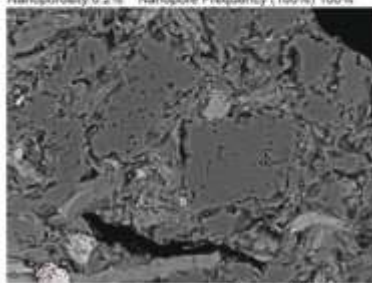
Pore Type: Framboid Pores (FHP)
Total Porosity:0.11%
Microporosity:N/A   Micropore Frequency (100%):N/A
Nanoporosity:0.11%   Nanopore Frequency (100%):100%

no longer be utilized to accurately describe gas flow within extremely small nanopore systems. Instead, a wide variety of non-Darcy flow regimes controlled by increases in intermolecular and molecule-wall collisions (such as viscous flow, slip flow, transition flow, and Knudsen flow) are being realized within these systems (Shen et al., 2017; Zhang et al., 2015). A greater understanding of the dimensions and characteristics of pores and the resulting pore networks within shale gas plays is critical for any further development and exploration (Nie et al., 2018), especially with regard to pore types and sizes as these factors strongly affect the reservoir properties (Goral et al., 2015).

2. GEOLOGICAL SETTING

The Late Carboniferous Pastora Formation is developed in the west-ern part of the Ciñera-Matallana Basin (northern Castilla and Leon, NW Spain), which is home to one of Europe's largest opencast coalmines. The coalmine contains medium to high-rank coals ranging from Bituminous C to Anthracite A. Located 42 km north of Leon and 2.5 km east from the mining village of Santa Lucia (Fig. 1A, B), this small pull-apart basin was formed during the Variscan Orogenesis and takes the form of a complex half-graben system. It extends over 12 km east-west and is considered to have formed as a result of multiple transtensional/transpressional movements along the Sabero-Gordon strike-slip fault (Ayllon et al., 2008). The mine displays in total a 1500m succession of Late Carboniferous (Kasimovian-Gzhelian; Fig. 1C) strata (Colmenero et al., 2008), which rest unconformably on the Asturian discordance (Frings et al., 2004).

Siliciclastic in nature, these sediments are interpreted to be largely swamp-, lacustrine-, fluvial and alluvial fan deposits (Heward, 1978). The Pastora Formation itself is an 85–200 m thick formation consisting of lacustrine and swamp deposits and is one of two stratigraphic formations out of the seven that occupy the mine, which demonstrates the greatest potential for natural gas prospecting (Lemos de Sousa and Pinheiro, 1996). The numerous coal seams which are present within the formations, most notably within the Pastora Formation, which consists of up to 30 separate seams ranging from 0.5 to 15 m in thickness,

initiated the research into the natural gas potential. The largest of these seams can be found in the Mid-Upper Pastora Formation where coal seams are most abundant. The regional-scale facies distribution of this largest coal seam horizon, the so-called "Pastora Coal Seam," provides evidence for an NW-SE striking lake, with large coal deposits forming in past swamp environments located at the lake margins (Wagner, 1971). To-ward the top of the formation, sedimentation appears to have formed in a solely lacustrine environment, characterized by interbedded organic matter (OM)-rich, finely laminated shale successions, very fine-grained siltstones, and intercalated up to meter thick coarse-grained sandstones. These lacustrine successions formed the target of the present study.

Fig. 18. Facies OMILS pore size characterization (50 µm Scale).
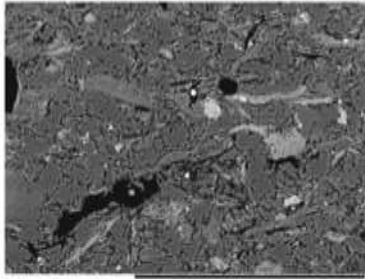
Facies:OM/ILS
Scale:200μm
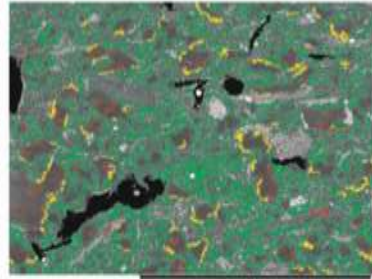
Total Porosity:24.47%
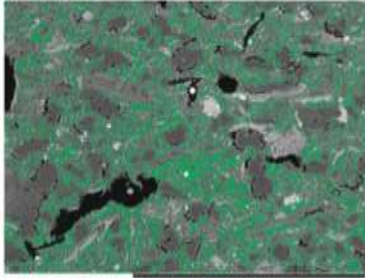
Pore Type:Aluminosilicate Pores (AL)
Total Porosity:21.36%
Porosity (100%):87.29%
Pore Frequency (100%):79.07%
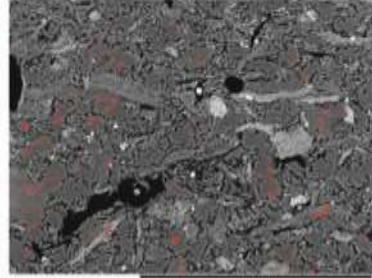
Pore Type:Moldic Pores (MP)
Total Porosity:0.87%
Porosity (100%):3.54%
Pore Frequency (100%):15.09%
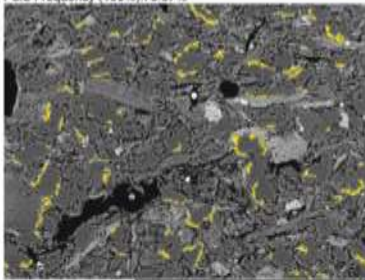
Pore Type:Grain Edge Pores (GEP)
Total Porosity:2.13%
Porosity (100%):8.73%
Pore Frequency (100%):3.63%
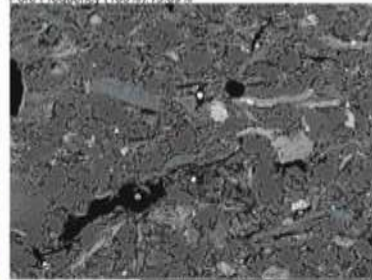
Pore Type:Micaceous Pores (MBP)
Total Porosity:0.06%
Porosity (100%):0.25%
Pore Frequency (100%):1.87%
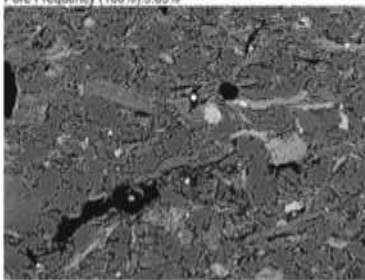
Pore Type:Fracture Pores (FP)
Total Porosity:0.01%
Porosity (100%):0.05%
Pore Frequency (100%):0.17%
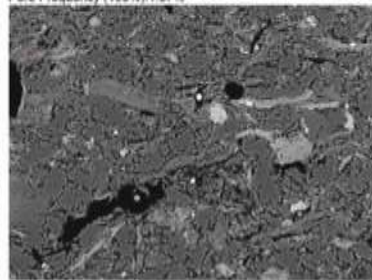
Pore Type:Shrinkage Crack Pores (SCP)
Total Porosity:0.04%
Porosity (100%):0.14%
Pore Frequency (100%):0.17%

3. MATERIAL AND METHODS

3.1. Material

For the present study, a total of 90 samples were extracted in stratigraphic order (bed-by-bed) from the Upper Pastora Formation. Sampling locality was the southern part of the Santa Lucia coal mine (which forms part of the Ciñera-Matallana coal field complex) as it provided the best exposure and accessibility. The samples were taken in conjunction with a high-resolution sedimentary log of a 12 m section of the Upper Pastora Formation (Figs. 2 and 3) which consists of interbedded sandstone/siltstone and shale beds (Fig. 4A–C). A spectral gamma ray log to complement the sedimentary log was generated using a handheld RS-230-BGO gamma ray spectrometer (Radiation Solutions Inc., Canada). Spectral gamma ray data were obtained as a "gliding average" equidistantly every 5 cm with an analytical time of 360s per analytical point. The concentrations of the major element potassium (K) are expressed as weight percentages (wt%), whereas the concentrations of the trace elements thorium (Th) and uranium (U) are given as parts per million (ppm).

3.2. Facies and microfacies analysis

Samples were subject to a detailed facies- and microfacies analysis based on field observations, hand specimens and thin sections in order to identify the hydrocarbon resource potential and to categorize any changes

Fig. 19. Facies OMILS pore type characterization (200 µm Scale).
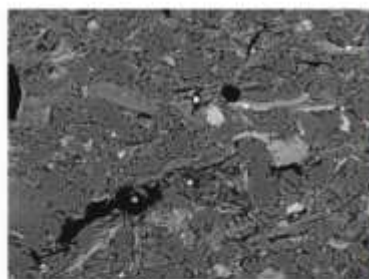
Facies:OM/ILS
Scale:200μm
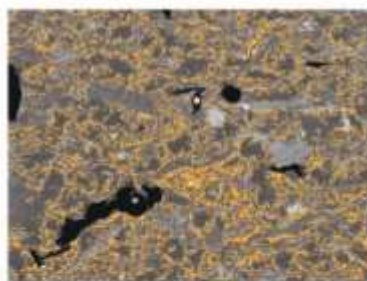
Microporosity:22.95%   200μm
Nanoporosity:1.52%
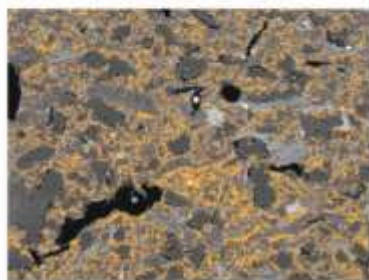
Pore Type:Aluminosilicate Pores (AL) 200μm
Total Porosity:21.38%
Microporosity:20.2%   Micropore Frequency(100%)45.19%
Nanoporosity:1.18% Nanopore Frequency (100%):54.81%

Pore Type:Moldic Pores (MP)   200μm
Total Porosity:0.87%
Microporosity:0.6%   Micropore Frequency(100%):25.55%
Nanoporosity:0.27% Nanopore Frequency (100%):75.45%

Pore Type:Grain Edge Pores (GEP) 200μm
Total Porosity:2.13%
Microporosity:2.11%   Micropore Frequency(100%):76.19%
Nanoporosity:0.02% Nanopore Frequency (100%):23.81%
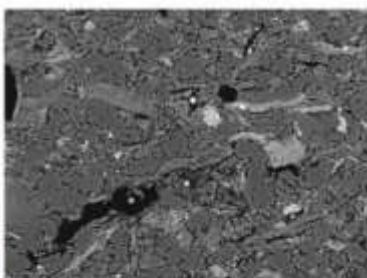
Pore Type:Micaceous Pores (MBP)   200μm
Total Porosity:0.06%
Microporosity:0.02%   Microporosity (100%):9.21%
Nanoporosity:0.04% Nanopore Frequency (100%):90.79%
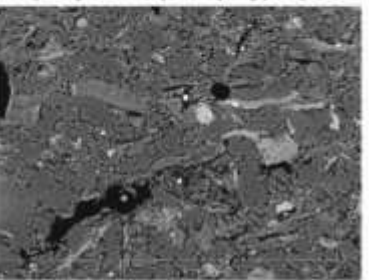
Pore Type:Fracture Pores (FP)   200μm
Total Porosity:0.01%
Microporosity:N/A   Micropore Frequency(100%):N/A
Nanoporosity:0.01% Nanopore Frequency (100%):100%

Pore Type:Shrinkage Crack Pores (SCP) 200μm
Total Porosity:0.04%
Microporosity:0.02%   Micropore Frequency(100%):16.8%
Nanoporosity:0.02% Nanopore Frequency (100%):83.3%

in micro/nanometric porosity and pore-based properties, in association with petrological/mineralogical changes that might impact on hydrocarbon migration and accumulation. Microfacies analysis was conducted using a ZEISS petrological microscope, a HITACHI-TM3000 scanning electron microscope (SEM) equipped with an energy dispersive X-ray analyzer (EDAX) and a NITON-XL3 XRF analyzer. This facies analysis enabled the identification of key mineralogical variations between the shale/ siltstone/sandstone beds and the mineralogical/geochemical subdivision based on geochemical composition, OM observations and sedimentary/ biogenic structures.

3.3. Pore network characterization

To characterize the pore network and identify changes in porosity and pemeability, binarized images were described and pore types quantified, followed by a series of detailed image-based analyses of the pore space. This procedure was executed by generating backscattered electron (BSE) data using a HITACHI-TM3000 SEM. The resulting BSE images were digitally binarized using ImageJ and Corel Draw software packages to generate clear black and white images, with the black parts representing the pores and white parts representing the non-porous background. BSE images were taken systematically at a magnification of 500 times and 1200 times. The 1200 times magnification was identified as the most appropriate scale to analyze nanometric variability whereas the 500 times magnification proved to be effective in analyzing the micrometric variability. The choice of such magnification ranges and scales ran in accordance with the pore size definitions by Loucks et al. (2012; see Fig. 5) and with the limits of SEM resolution. Although the acquisition of representative images of such heterogeneous samples is an inherent problem in pore network modeling (Pak et al., 2016), the scales chosen in this study proved to provide an effective basis for the integration of different scale observations and also allowed for hierarchal data separation and integration.

The acquired BSE images were saved in TIF format; these images were then adjusted appropriately using the software components ImageJ Fiji to acquire a gray range, which contained black, white and intermediate gray levels (Jiang, 2013). The binarized image was then exported

Fig. 20. Facies OMILS pore size characterization (200 µm Scale).
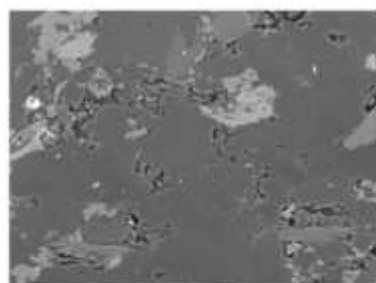
Facies:DOMS
Scale:50μm
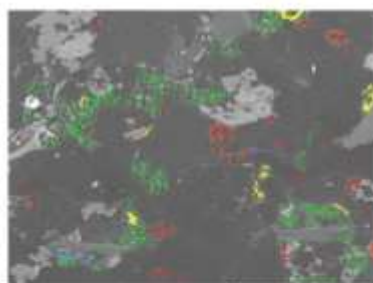
Total Porosity:4.86%
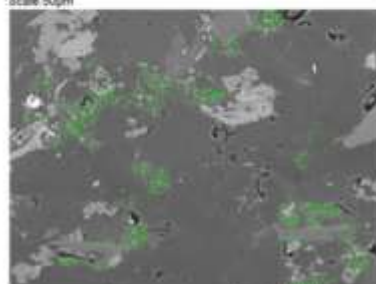
Pore Type:Aluminosilicate Pores (AL)
Total Porosity:3.23%
Porosity (100%):66.49%
Pore Frequency (100%):48.85%
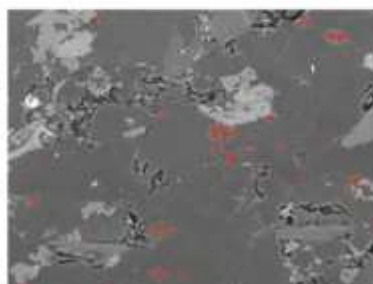
Pore Type:Moldic Pores (MP)
Total Porosity:0.9%
Porosity (100%):18.54%
Pore Frequency (100%):44.78%
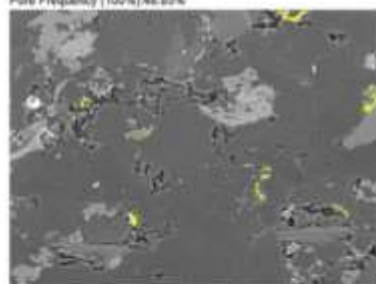
Pore Type:Grain Edge Pores (GEP)
Total Porosity:0.42%
Porosity (100%):8.57%
Pore Frequency (100%):1.53%
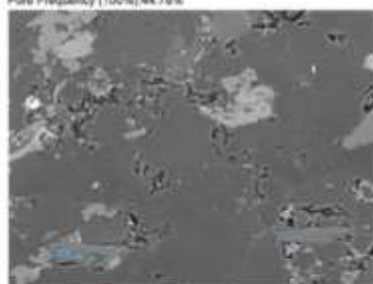
Pore Type:Micaceous Pores (MBP)
Total Porosity:0.11%
Porosity (100%):2.17%
Pore Frequency (100%):1.02%
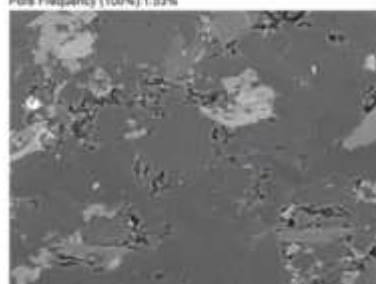
Pore Type:Fracture Pores (FP)
Total Porosity:0.07%
Porosity (100%):1.47%
Pore Frequency (100%):1.27%
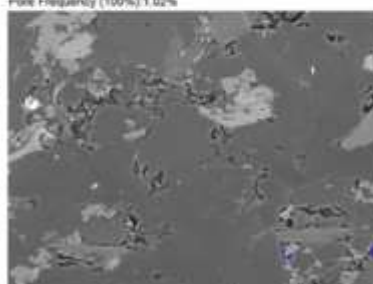
Pore Type: Carbonate Dissolution Pores (CDP)
Total Porosity:0.13%
Porosity (100%):2.76%
Pore Frequency (100%):2.55%

to Corel Draw 2017 and a high-resolution trace of the binarized image was generated. Once generated, the white background was digitally removed and replaced with the original BSE image which allowed for the manual selection of individual and groups of pores in preparation for the pore characterization. Using the BSE image as a base image to guide the pore identification, pore types were identified based on the pore type classification scheme adapted from Loucks et al. (2012) and subsequently color coded, to provide a multicolored binarized BSE image (Figs. 5–7). The pore size- and type classification schemes of Loucks et al. (2012), who analyzed and described a broad and varied spectrum of different pore types within mudrocks, enabled the identification of the most frequent nano- and micropore types found within the various microfacies. Once all pore types were characterized and color coded, specific pore types were digitally extracted from the image and placed on a separate BSE image, thus representing and illustrating a single pore type within a given pore net-work. These images were transformed into a grayscale (8-bit) format and returned to the software package ImageJ and its components for rebinarization and the subsequent analysis and quantification (Fig. 7).

4. RESULTS

4.1. Lithological description

The stratigraphically youngest parts of the Late Carboniferous Pastora Formation are characterized by a continuous succession of interbedded thinly layered fissile shales, very fine-grained siltstones, and sandstones, which generally display weak quasi-planar (QP)/hummocky cross-stratification (HCS) with vitrified bases (Fig. 4A, F). These dominant lithologies also occur with less frequent limestone and calcareous/iron-rich silt-stone intercalations (Fig. 4F). Commonly, this background sedimentation pattern is interrupted by 10–60 cm thick, massive bedded, coarse-grained sandstones (Fig. 4B). These larger sandstone beds typically show the widest variety of textural, bioclastic and sedimentological features, including basal erosional features, (Fig. 4H), bone fragments, palynomorphs, and phytoclastic material (Fig. 4G–I). The largest sandstone

Fig. 21. Facies DOMS pore type characterization (50 μm Scale).

Facies: DOMS
Scale: 50μm

Microporosity: 2.74% :
Nanoporosity: 2.12%

Pore Type: Aluminosilicate Pores (AL)
Total Porosity: 3.23%
Microporosity: 1.98%   Micropore Frequency(100%): 10.42%
Nanoporosity: 1.25%   Nanopore Frequency (100%): 89.58%

Pore Type: Moldic Pores (MP)
Total Porosity: 0.9%
Microporosity: 0.26%   Micropore Frequency(100%): 2.27%
Nanoporosity: 0.64%   Nanopore Frequency (100%): 97.73%

Pore Type: Grain Edge Pores (GEP)
Total Porosity: 0.42%
Microporosity: 0.32%   Micropore Frequency(100%): 50%
Nanoporosity: 0.1%   Nanopore Frequency (100%): 50%

Pore Type: Micaceous Pores (MBP)
Total Porosity: 0.11%
Microporosity: 0.06%   Micropore Frequency (100%): 7.69%
Nanoporosity: 0.05%   Nanopore Frequency (100%): 92.31%

Pore Type: Fracture Pores (FP)
Total Porosity: 0.07%
Microporosity: N/A   Micropore Frequency(100%): N/A
Nanoporosity: 0.07%   Nanopore Frequency (100%): 100%

Pore Type: Dissolution Pores (MP)
Total Porosity: 0.13%
Microporosity: 0.11%   Micropore Frequency(100%): 25%
Nanoporosity: 0.02%   Nanopore Frequency (100%): 75%

bodies (up to 60 cm in thickness) found in this predominantly argillaceous sedimentary succession, are also characterized by a dolomitic diagenetic cement, which greatly reduces porosity, acting as an intermit-tent seal above the more nano- and microporous shale and siltstone facies. Most shales and siltstone facies show evidence of only minor dolomitization (varying between 1% and 5%). However, it can be demonstrated that this varying degrees of dolomitization do have an impact on hydrocarbon migration by reducing the overall porosity and more importantly the pore network connectivity. Generally, all facies types show a strong degree of bioturbation with more diverse ichnofabrics found in the fine-grained sandstones such as the decapod dwelling structure *Thalassinoides* (Fig. 4G) and traces probably produced by annelids within the fine-grained mudstones (Fig. 4C). Organic matter (OM) is ubiquitous and present in all samples as either bed-parallel laminae or pervasive matrix-based OM. Strong enrichments in OM are typically found within the Organic Matter/Illite Rich Siltstone facies (OM/ILS), the Organic Matter Rich/Dolomitized Siltstone facies (DOMS), the Organic Matter Rich Shale facies (OMRS), and the Varved Sandstone facies (VSND, see Fig. 8A, B, F, G). Randomly distributed OM shows a variety of structured morphologies that have been interpreted as woody tissue and other phytoclast fragments. Structures interpreted here as varves are typically formed by bundles of OM rich- and siltstone laminae. These varves most commonly occur in the DSND and VSND facies with up to 60 varves in just 5 cm. As such, this section of the Upper Pastora Formation can be described and interpreted as a multi-layered sealing sequence (sensu Bertoni et al., 2018), in which the paleoenvironment is interpreted to be a hydrologically open lake, located close to a river mouth distributing coarser grained sediment.

4.2. Mineralogy

Mineralogically, all mudstones and siltstones show similar compositions but in varying quantities. The intergranular space is dominated by a mixed clay content, which is predominantly Illite (20–33%) with localized dolomitization (< 6%). The most common grains are detrital quartz grains (40–60%), which show varying textures and structures. Albite (8–14%), biotite (2–8%), muscovite (2–13%) which are prominent

Fig. 22. Facies DOMS pore size characterization (50 µm Scale).
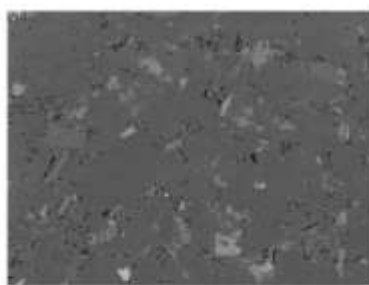
Facies:DOMS
Scale:200μm
200μm
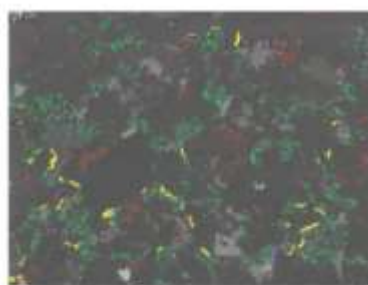
Total Porosity:5.26%
200μm
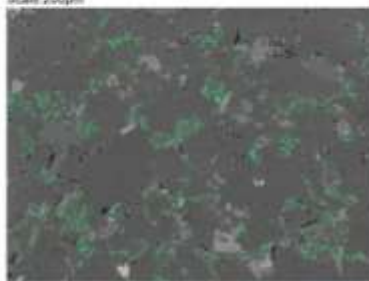
Pore Type:Aluminosilicate Pores (AL)
Total Porosity:3.44%
Porosity (100%):65.6%
Pore Frequency (100%):66.21%
200μm
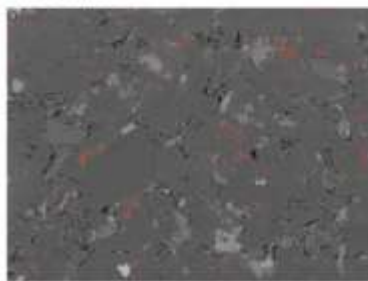
Pore Type:Moldic Pores (MP)
Total Porosity:1%
Porosity (100%):19.06%
Pore Frequency (100%):30.34%
200μm
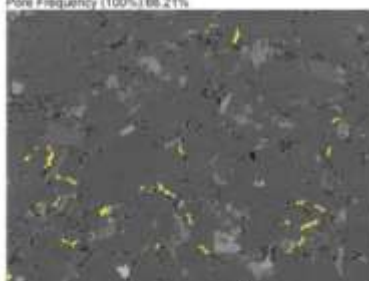
Pore Type:Grain Edge Pores (GEP)
Total Porosity:0.86%
Porosity (100%):12.52%
Pore Frequency (100%):2.05%
200μm
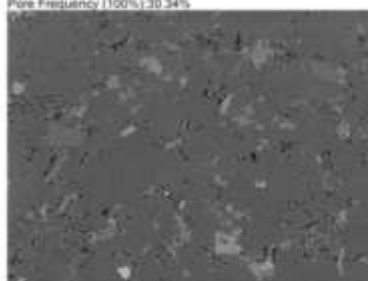
Pore Type:Micaceous Pores (MBP)
Total Porosity:0.04%
Porosity (100%):0.67%
Pore Frequency (100%):0.18%
200μm
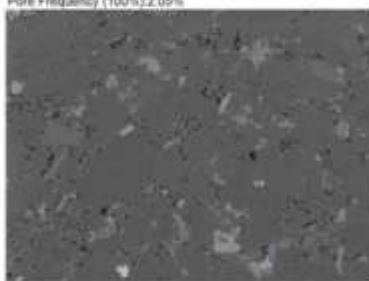
Pore Type:FracturePores (FP)
Total Porosity:0.09%
Porosity (100%):1.67%
Pore Frequency (100%):0.36%
200μm
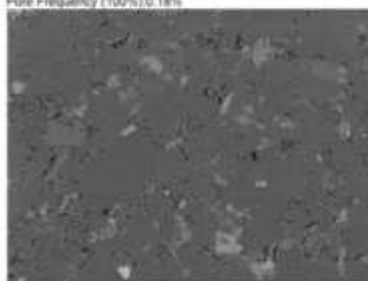
Pore Type:Carbonate Dissolution Pores (CDP)
Total Porosity:0.03%
Porosity (100%):0.48%
Pore Frequency (100%):0.86%
200μm

45

within the shale facies and lithic fragments (1–11%) which are most prominent in sandstones. Accessory minerals include pyrite (2–3%), rutile (< 3%) and zircon (< 1%) (Figs. 8–10).

4.3. Facies types

The overall petrological characteristics of the 90 samples were described and quantified using SEM-EDS, XRF and conventional light microscopy and allowed for the differentiation and establishment of 7 different facies types:

1.   Organic Matter Rich Shale (OMRS)

2.   Organic Matter/Illite Rich Siltstone (OM/ILS)

3.   Organic Matter Rich/Dolomitised Siltstone (DOMS)

4.   Illite Rich Siltstone (ILRS)

5.   Mica Rich Siltstone (MRSL)

6.   Dolomitised Sandstone (DSND)

7.   Varved Sandstone (VSND)

These facies types occur in a repetitive sealing succession, whereby smaller interchanging shale and sandstone/siltstones units are repeatedly capped by much more prominent sandstone bodies. This rhythmic sedimentation pattern has created a dual self-sealing system whereby shales, which already act as a self-sealing and self-sourcing hydrocarbon reservoirs, are locked within a larger sealing system capped by very low porosity sandstones (VSND), confining any escaped gas to these layers (Fig. 2).

4.4. Organic matter content

4.4.1. Pervasive organic matter

Pervasive organic matter (OM) found within the matrix and inter-varve regions have a variety of distinct structured morphologies indicating a diverse range of OM sources. Macerals were identified by variations in morphology which correspond to observations made by the International Committee for Coal and Organic Petrology (ICCP) and other published studies on maceral identification (Cardott and Curtis, 2018; Mastalerz et al., 2010; Pickel et al., 2017). Major maceral groups identified were vitrinite and liptinite, derived from woody tissue, leaf cuticles and cell

Fig. 23. Facies DOMS pore type characterization (200 µm Scale).
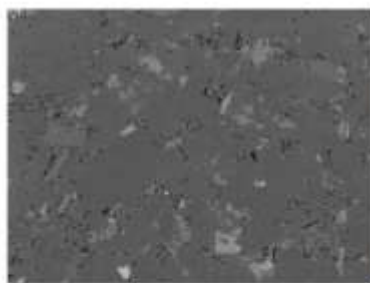
Facies:DOMS
Scale:200µm

Microporosity:4.26%
Nanoporosity:1%
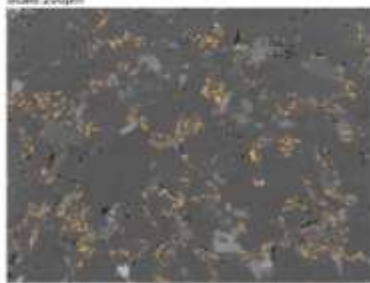
Pore Type:Aluminosilicate Pores (AL)
Total Porosity:3.44%
Microporosity:2.86%   Micropore Frequency(100%):34.54%
Nanoporosity:0.58%   Nanopore Frequency (100%):65.45%
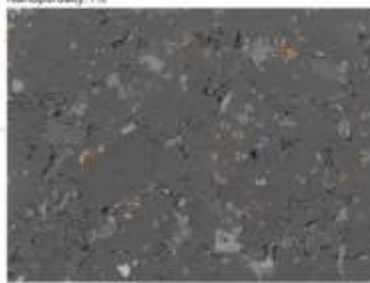
Pore Type:Moldic Pores (MP)
Total Porosity:1%
Microporosity:0.7%   Micropore Frequency(100%):10.6%
Nanoporosity:0.3%   Nanopore Frequency (100%):89.4%
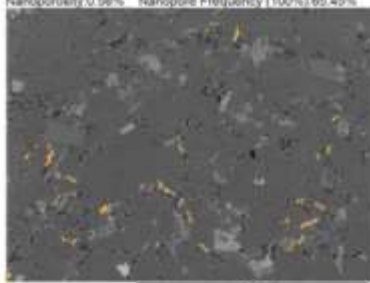
Pore Type:Grain Edge Pores (GEP)
Total Porosity:0.66%
Microporosity:0.65%   Micropore Frequency(100%):93.3%
Nanoporosity:0.01%   Nanopore Frequency (100%):6.7%
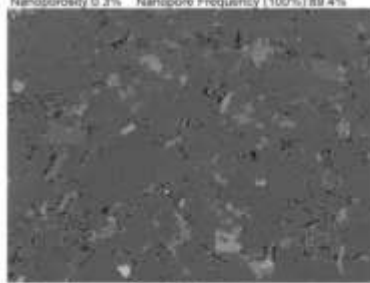
Pore Type:Micaceous Pores (MBP)
Total Porosity:0.04%
Microporosity:0.02%   Microporosity (100%):50%
Nanoporosity:0.02%   Nanopore Frequency (100%):50%
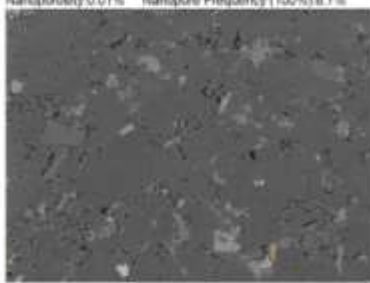
Pore Type:Fracture Pores (FP)
Total Porosity:0.09%
Microporosity:0.01%   Micropore Frequency(100%):N/A
Nanoporosity:0.08%   Nanopore Frequency (100%):100%
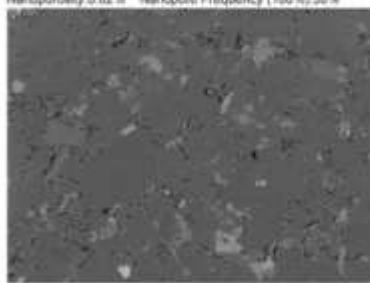
Pore Type:Carbonate Dissolution Pores (CDP)
Total Porosity:0.03%
Microporosity:0.02%   Micropore Frequency(100%):20%
Nanoporosity:0.01%   Nanopore Frequency (100%):80%

walls of plant tissues. Some of the maceral subgroups identified include secretinite with cell lumens filled with clay minerals, cutinite with serrated edges on one side and smooth on the other, and finally various vitrinite subgroups related to woody tissue, characterized by thin elongate and straight edge structures (Fig. 11A–I). Various palynomorph and botryococcoid green algal cysts have also been identified, providing further evidence for a diverse range in secondary sourced OM but also evidence from primary production of OM within the lake.

4.4.2. Organic matter rich varves

Varves, unlike other dispersed organic matter, consist of lateral concentrations of organic matter in a laminar and occasionally, undulatory fashion. There are two distinctive types of varves present throughout the sequence. The most abundant type shows excellent lateral continuity and connectivity, which can display a sinuous flow pattern and, in some cases, large concentrations of pyrite framboids. These varves contain a high and concentrated OM content which appears at lower magnifications to be amorphous. However, at at higher resolution the OM of these varves does show a bubble-like nanomorphology, indicating that the OM within these varves is algal in nature, as they have a similar morphology to unicellular algal colonies found in the Wufeng-Longmaxi Formation in the Sichuan Basin, SW China (Nie et al., 2018). The bundle like nature of these varves could well be a photosynthetic response to solar variations, providing an insight into seasonal variability in lacustrine primary paleoproductivity. More importantly, they provide evidence for a continued and prolonged source of type I kerogen with high H/C values. The second varve type pre-sent is more common in the upper reaches of coarser-grained sandstone bodies and consists of quasi-laminar concentrations of structured organic matter, with a variety of morphologies similar to the pervasive OM structures found in the matrix. These varves lack continuity, displaying poor connectivity, and represent the settling of phytoclastic material located in the catchment basin of the paleolake,

with the rivers transporting this material together with coarser sediments.

Fig. 24. Facies DOMS pore size characterization (200 µm Scale).
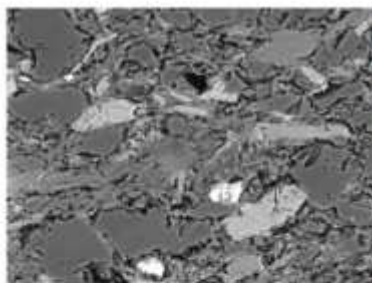
Facies:OMRS
Scale:50μm
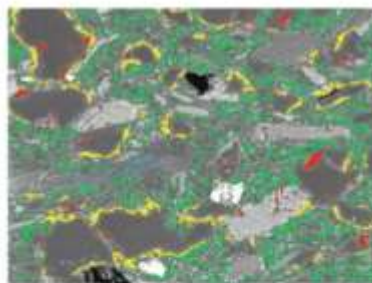
Total Porosity:17.08%
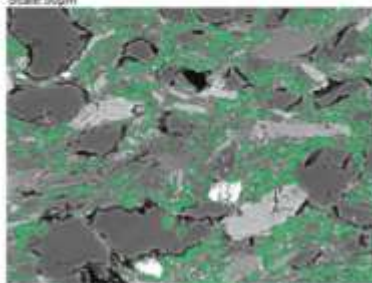
Pore Type:Aluminosilicate Pores (AL)
Total Porosity:12.04%
Porosity (100%):70.5%
Pore Frequency (100%):72.37%
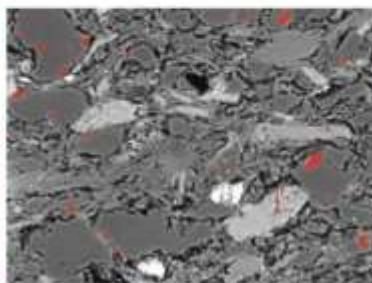
Pore Type:Moldic Pores (MP)
Total Porosity:0.78%
Porosity (100%):4.57%
Pore Frequency (100%):9.5%
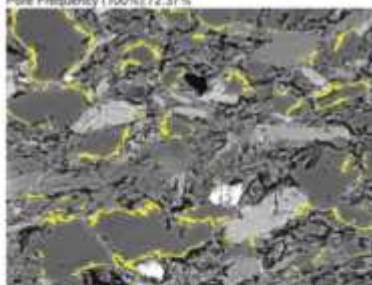
Pore Type:Grain Edge Pores (GEP)
Total Porosity:3.69%
Porosity (100%):21.59%
Pore Frequency (100%):8.78%
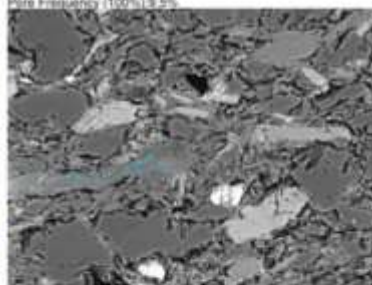
Pore Type:Micaceous Pores (MBP)
Total Porosity:0.28%
Porosity (100%):1.63%
Pore Frequency (100%):4.4%
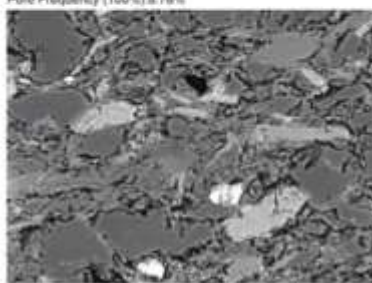
Pore Type:Fracture Pores (FP)
Total Porosity:0.29%
Porosity (100%):1.71%
Pore Frequency (100%):4.95%

4.4.3. Thermal maturation

The most fundamental parameters in controlling the thermal maturation of kerogen and expulsion of hydrocarbons during pyrolysis are temperature, time and pressure. Pressure plays only a subordinate role in the thermal maturation of kerogen, though it can alter chemical reactions involved in the process of thermal maturation. Temperature is more important, and the amount of time kerogen is exposed to higher temperatures. The reconstruction of the paleo-geothermal gradient in the Ciñera-Matallana Basin provides evidence for conditions conducive to the formation of thermo-genic gas. The rapid subsidence of the Pastora Formation during the Late Carboniferous and Permian— estimated to be 0.23 m/1000 years by Frings et al. (2004) and 0.21–0.36 m/1000 years by Heward (1978), has provided a window of around 58 Myrs for the generation of thermogenic gas. Erosion rates increased during the Triassic, which continued to drive the Pastora Formation into the upper reaches of the oil window during a long period of non-deposition, until subsidence resumed associated with the diachronous sedimentation of transgressive sandstones and conglomerates during the Albian-Santonian time interval.

4.5. Gamma ray log

4.5.1. Overview

A 3.4 meter section from the base of the investigated section was analyzed using gamma ray spectrometry to identify important paleoenvironmental parameters that control and influence hydrocarbon formation, storage, and migration (Fig. 12). Chemically reducing and especially anoxic environments are a highly important factor in determining organic matter preservation. Without anoxic water, organic matter is broken down by the activity of aerobic bacteria, resulting in the loss of OM, which would have provided a source for hydrocarbons. Quantifying the changes in reducing and oxidizing conditions within the lake at the time of de-position, will be used to identify organic matter preservation potential through Th/U ratio analysis and whether authigenic U values, which are considered to be associated with total

organic carbon (TOC), re-main constant or fluctuate and to what degree uranium is enriched within the shales. Finally, Th/K ratios were used to aid facies identification

Fig. 25. Facies OMRS pore type characterization (50 μm Scale).
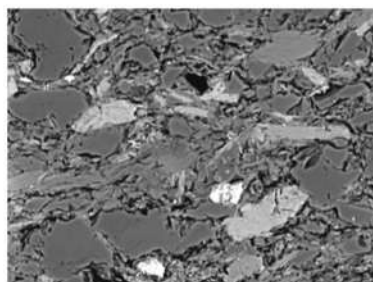
Facies:OMRS
Scale:50μm
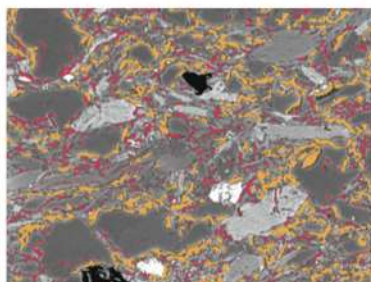
Microporosity:11.89%
Nanoporosity:5.19%
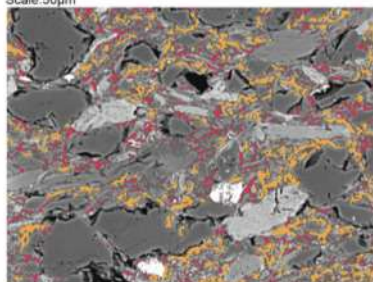
Pore Type:Aluminosilicate Pores (AL)
Total Porosity:12.04%
Microporosity:8.36%   Micropore Frequency(100%):14.1%
Nanoporosity:3.68%   Nanopore Frequency (100%):85.9%
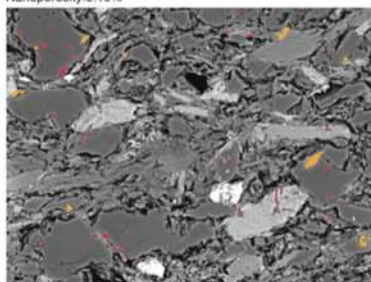
Pore Type:Moldic Pores (MP)
Total Porosity:0.78%
Microporosity:0.43%   Micropore Frequency(100%):7.43%
Nanoporosity:0.35%   Nanopore Frequency (100%):92.57%
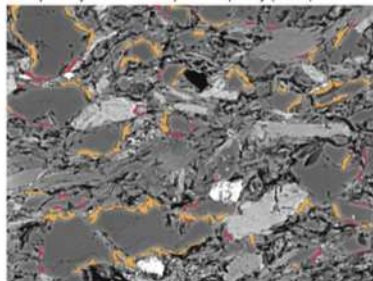
Pore Type:Grain Edge Pores (GEP)
Total Porosity:3.69%
Microporosity:3.04%   Micropore Frequency(100%):39.29%
Nanoporosity:0.65%   Nanopore Frequency (100%):60.71%
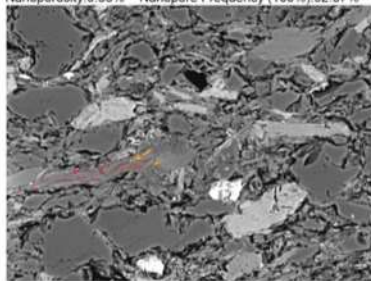
Pore Type:Micaceous Pores (MBP)
Total Porosity:0.28%
Microporosity:0.06%   Microporosity (100%):1.79%
Nanoporosity:0.22%   Nanopore Frequency (100%):98.21%
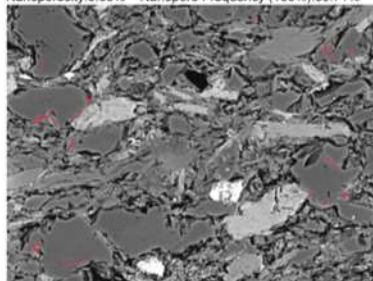
Pore Type:Fracture Pores (FP)
Total Porosity:0.29%
Microporosity:N/A   Micropore Frequency(100%):N/A
Nanoporosity:0.29%   Nanopore Frequency (100%):100%

and grouping as well as an indicator for potential changes in provenance (Rider, 1996).

4.5.2. TOC-U values

The systematic association between TOC and uranium values is well documented and was pioneered by Adams and Weaver (1958) in marine sediments. Because organic matter can extract uranium from solution very efficiently via red/ox-reactions, organic matter rich shales are often enriched in chemically reduced authigenic uranium (U^{IV}). The association between TOC and authigenic uranium within the lacustrine environment is far more complicated and often there is no covariation between TOC and U due to the relative low concentration of uranium within freshwater com-pared to seawater (Lüning and Kolonic, 2003). Uranium values within shales of the Upper Pastora Formation range from 3.2 to 4.3 ppm, which is similar to the "average" uranium value in shale of 3.7 ± 5 ppm reported by Adams and Weaver (1958). When compared with highly productive shale gas plays such as the Late Devonian to Early Carboniferous Wood-ford Shale in Oklahoma (U.S.), which shows a strong correlation between U and TOC and can have U values >100 ppm, the U-TOC systematics of the Pastora mudstones would present little hope for source rock potential. However, the U values presented here are also very similar to those recorded by Felder et al. (2001) in oil shales from the Eocene Prinz von Hessen Lake in Germany, where U values consistently remained between 3 and 4 ppm, which would indicate a poor TOC content. However, a re-visiting of the lake sediments by Hofmann et al. (2005) found that organic matter rich laminae which had shown no correlation between observable high TOC content and uranium values, actually contained a TOC content of between 30% and 45%. It is important to stress that authigenic uranium values alone—even though widely used as red/ox indicators within the published literature—can be misleading and should always be combined with further independent lines of evidence.

4.5.3. Th/U ratios

Th/U ratios throughout the logged section seem to indicate that the Upper Pastora Formation was subject to subtle fluctuations in red/ox conditions. Th/U ratios between 3 and 5.6 and typically higher uranium values associated with a higher TOC content can be correlated with lower Th/U ratios, indicating a more reducing chemical environment. Th/U ratios in average shales vary from 3.26 to 4.73 which, following Adams and Weaver (1958), places these shales between a reducing and oxidizing environment. However, their work was conducted on marine shales and the applicability of such values to the ratios derived from lacustrine successions has remained controversial. According to Jones and Manning (1994), anoxic-oxic conditions in the lacustrine environment are defined as Th/U ratios ranging from anoxic <1.5, dysoxic 1.5–3 to oxic < 3. This would place the OMRS shales in an oxic environment, which shows fluctuations toward a more dysoxic environment. Combined with observations made regarding sedimentary structures which show frequent alter-nations between hummocky cross-stratification and parallel lamination, the environment of deposition likely underwent oxygen fluctuations in response to eolian interactions with the water-sediment interface, indicating that these sediments are shallow, as opposed to deep lacustrine sediments. The interpreted relative proximity to a river, as indicated by the large sandstone bodies, also provides a source for oxygenation. It is observable on the log that the most continuous Th/U ratios can be found within shale bundles which remain uninterrupted from coarser sedimentary influxes.

Fig. 26. Facies OMRS pore size characterization (50 µm Scale).
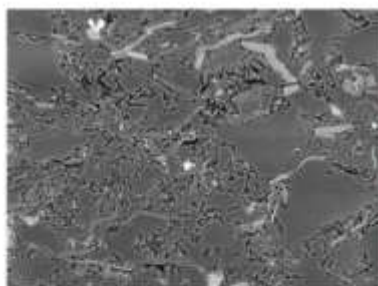
Facies:OMRS
Scale:200μm
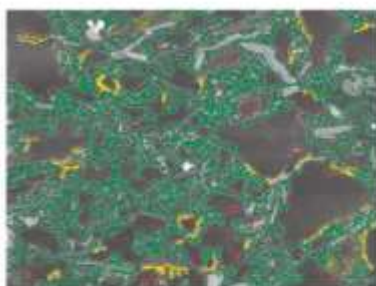
Total Porosity:15.43%
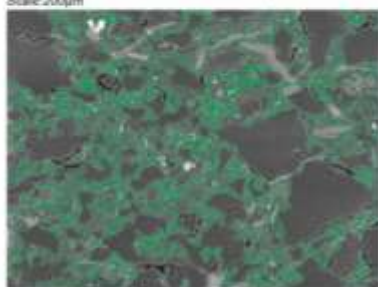
Pore Type:Aluminosilicate Pores (AL)
Total Porosity:12.75%
Porosity (100%):82.66%
Pore Frequency (100%):70.92%

Pore Type:Moldic Pores (MP)
Total Porosity:0.99%
Porosity (100%):6.39%
Pore Frequency (100%):21.36%
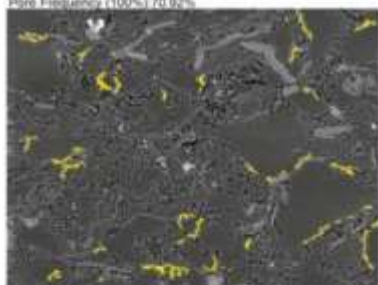
Pore Type:Grain Edge Pores (GEP)
Total Porosity:1.35%
Porosity (100%):8.74%
Pore Frequency (100%):2.12%
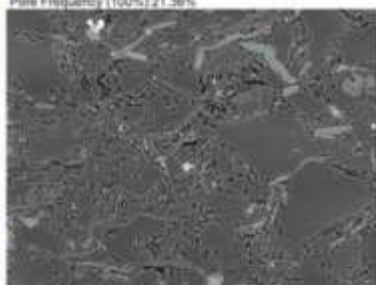
Pore Type:Micaceous Pores (MBP)
Total Porosity:0.05%
Porosity (100%):0.31%
Pore Frequency (100%):1.11%
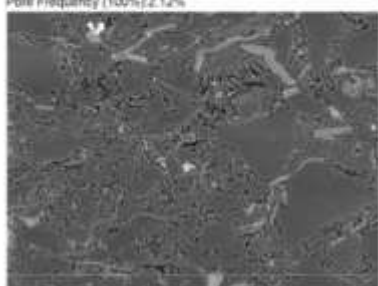
Pore Type: Fracture Pores (FP)
Total Porosity:0.06%
Porosity (100%):0.4%
Pore Frequency (100%):1.04%
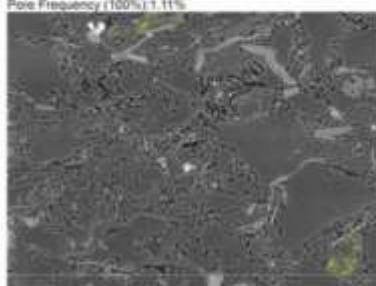
Pore Type:Foldspar Dissolution Pores (FDP)
Total Porosity:0.23%
Porosity (100%):1.5%
Pore Frequency (100%):3.45%

4.6. Pore network characterization (pore type abundance)

4.6.1. Pore network overview

Pore networks within shales are usually heterogeneous and contain a variety of pore types, geometries and sizes spread over several orders of magnitude (Clarkson et al., 2013). To better understand hydrocarbon migration within UHRs the heterogeneous pore network has to be characterized first based on universally accepted pore type classification schemes followed by a quantification of the porosity associated with each pore type. Subsequently, a detailed analysis and quantification of the hydrocarbon storage and migration factors associated with the specific pore types can be carried out. This enables the identification of the potential relationship between changes in the fluid flow activity, the geomechanical behavior during both pre- and post-convective flux and the principal pore type. Finally, systematic changes in the petrological features are linked to the development of distinctive pore type associations and their abundances. This enables the determination of the most relevant pore-scale factors that exert control over both the multiphase fluid flows and the desorption processes. Both of these processes have been documented to be paramount for the assessment and evaluation of well productivity and longevity. Therefore, the pore networks present within the Pastora Formation have been characterized using the pore type and pore size classification schemes established by Loucks et al. (2012). Subsequently, each pore type's total abundance has been quantified together with each pore type's contribution toward the total porosity of the pore network. The same procedure was then applied to the various pre-defined pore sizes, as the size of pores plays a fundamental role in hydrocarbon migration and gives rise to the establishment of non-Darcy flow regimes and multiphase fluid flow (Javadpour, 2009; Shen et al., 2017; Swami et al., 2012; Singh and Myong, 2018; Yang and Bao, 2017; Zhang et al., 2019). The systematic multi-scaled characterization and quantification provides vital information on the multifaceted nature of the different pore networks, on both the microporous and nanoporous scale. In effect this permits the detailed analysis of two seemingly separate systems which, despite being present in one semi-interconnected network, store and mi-grate

hydrocarbons in fundamentally different ways. The wider implications of such an analysis is that more accurate multiphase fluid flow models, even on a reservoir scale, can and have to be generated.

Fig. 27. Facies OMRS pore type characterization (200 µm Scale).
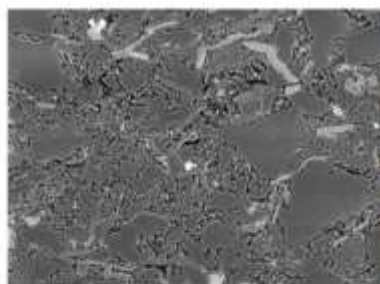
Facies:OMRS
Scale:200μm
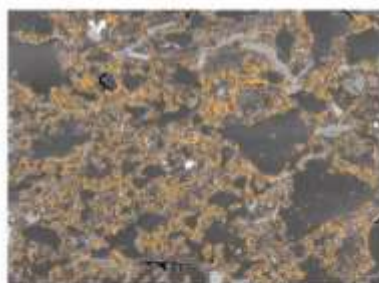
Microporosity:13.76%
Nanoporosity:1.72%
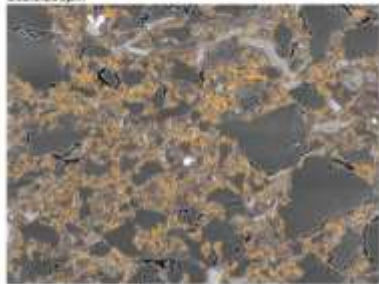
Pore Type:Aluminosilicate Pores (AL)
Total Porosity:12.75%
Microporosity:11.62%   Micropore Frequency(100%):43.48%
Nanoporosity:1.13%   Nanopore Frequency (100%):56.52%

Pore Type:Moldic Pores (MP)
Total Porosity:0.99%
Microporosity:0.58%   Micropore Frequency(100%):21.23%
Nanoporosity:0.41%   Nanopore Frequency (100%):78.77%
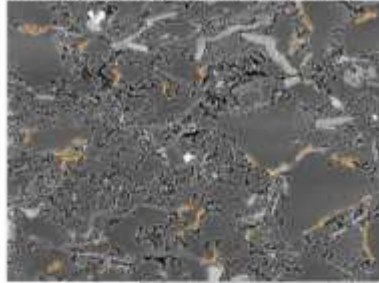
Pore Type:Grain Edge Pores (GEP)
Total Porosity:1.35%
Microporosity:1.3%   Micropore Frequency(100%):95.24%
Nanoporosity:0.05%   Nanopore Frequency (100%):4.76%
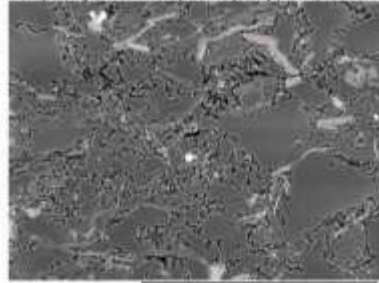
Pore Type:Micaceous Pores (MBP)
Total Porosity:0.05%
Microporosity:0.01%   Micropore Frequency (100%):6.81%
Nanoporosity:0.04%   Nanopore Frequency (100%):93.18%
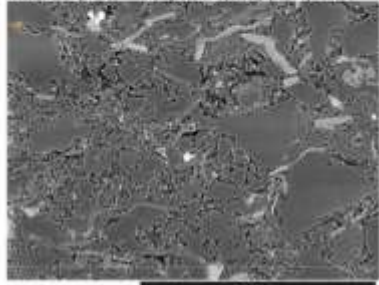
Pore Type:Fracture Pores (FP)
Total Porosity:0.06%
Microporosity:0.03%   Micropore Frequency(100%):19.51%
Nanoporosity:0.03%   Nanopore Frequency (100%):80.49%
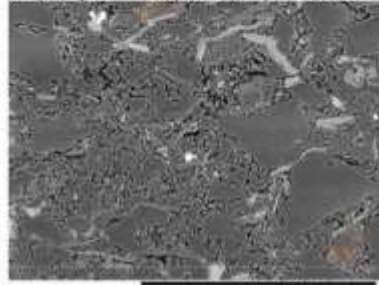
Pore Type:Feldspar Dissolution Pores (FDP)
Total Porosity:0.23%
Microporosity:0.17%   Micropore Frequency(100%):27.21%
Nanoporosity:0.06%   Nanopore Frequency (100%):72.79%

4.6.2. Pore types

The most frequent pore types developed within the nanoporous and microporous systems of the Pastora Formation are aluminosilicate pores (AL), moldic pores (MP) and more variably, pores at the edges of rigid grains (GEP). Among these are the aluminosilicate pores found within the illite matrix by far the most common, followed in abundance by the moldic pores within isolated mineral phases and finally the grain edge pores that are surrounding single grains. These three dominant pore types are referred to as the *primary pore types*, as they make the most significant contributions toward the pore network in both frequency and porosity (Fig. 16). *Secondary pore types* which contribute significantly less

Fig. 28. Facies OMRS pore size characterization (200 µm Scale).
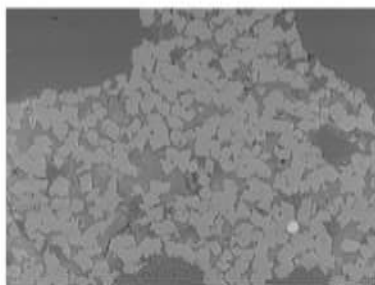
Facies:DSND
Scale:50μm
50μm
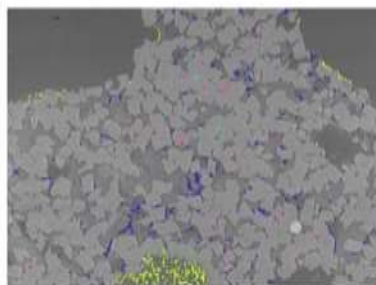
Total Porosity:2.7%
50μm
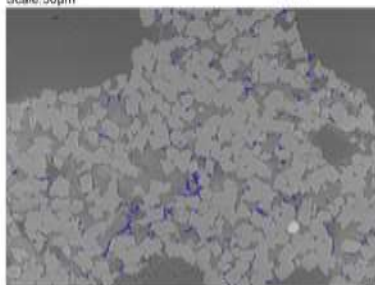
Pore Type:Carbonate Dissolution Pores (CDP)
Total Porosity:1.54%
Porosity (100%):57.4%
Pore Frequency (100%):56.17%
50μm
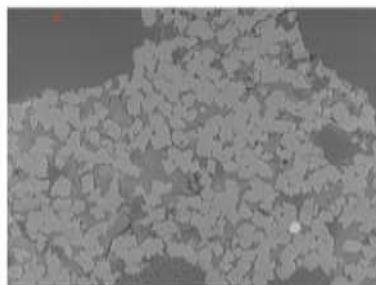
Pore Type:Moldic Pores (MP)
Total Porosity:0.03%
Porosity (100%):1%
Pore Frequency (100%):1.19%
50μm
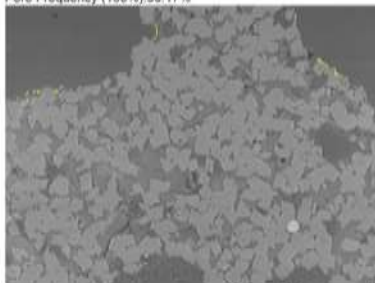
Pore Type:Grain Edge Pores (GEP)
Total Porosity:0.13%
Porosity (100%):4.78%
Pore Frequency (100%):3.86%
50μm
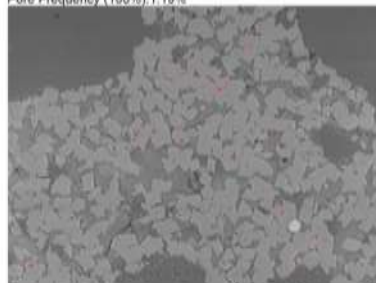
Pore Type:Intracrytalline Pores (ICP1)
Total Porosity:0.35%
Porosity (100%):12.94%
Pore Frequency (100%):27.19%
50μm
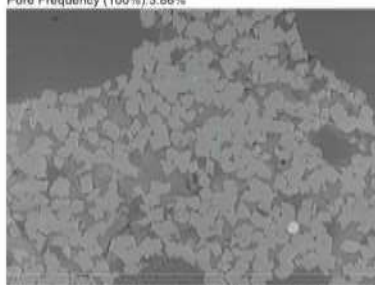
Pore Type:Intracrystalline Pores (ICP2)
Total Porosity:0.08%
Porosity (100%):2.8%
Pore Frequency (100%):1.63%
50μm
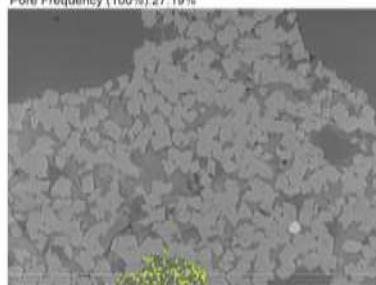
Pore Type:Feldspar Dissolution Pores (FDP)
Total Porosity:0.57%
Porosity (100%):21.08%
Pore Frequency (100%):9.96%
50μm

to the overall porosity and are also significantly less frequent within the pore networks are the fracture pores (FP), the shrinkage crack pores (SCP), the mica bearing pores (MBP), the dissolution pores (DP) and framboidal pores (FHP). In addition to these generally developed pore types, subordinate pore types that only occur within distinct lithological units such as the dolomitized sandstones have been documented. These pores are classed within the present study as *intra*crystalline pores (ICP1) and *inter*crystalline pores (ICP2) and discussed as "additional pore types" in Fig. 6.

4.6.3. Primary pore type abundance

4.6.3.1. Aluminosilicate pores (AL)

Aluminosilicate pores are by far the most abundant pore type found throughout all the different facies- and microfacies types that are associated with an aluminosilicate matrix and are most frequent in the OM/ILS and OMRS. At the two separately analyzed and discussed scales, aluminosilicate pores represent the following percentage of all pore types found throughout the pore network:

- 50 µm Scale: 46.96–73.77%

- 200 µm Scale: 60.46–80.09%

4.6.3.1.1. Nanoporous system (50 µm)

Aluminosilicate nanopores are the most frequent pore type found in the nanopore system, typically developed between detrital grains within the illite matrix. Aluminosilicate nanopores make up 69.08–94.69% of all aluminosilicate pore types pre-sent at this scale, apart from the DSND microfacies, which has undergone diagenetic dolomitization of the intergranular pore space and is characterized by dissolution-based porosity. The microfacies with the largest quantities of aluminosilicate

nanopores are the OMRS and MRSL in which 85.9% and 94.69% of pores are nanoporous. Aluminosilicate nanopores show a great variability in morphology at the 50 µm scale, with larger nanopores becoming increasingly irregular in shape, while the smallest nanopores are diametrically constrained but elongate, showing a fibrous morphology as observed by Desbois et al. (2010).

Fig. 29. Facies DSND pore type characterization (50 µm Scale).
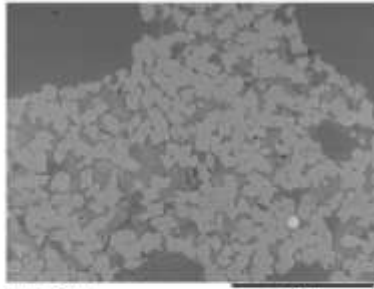
Facies:DSND
Scale:50µm
50µm
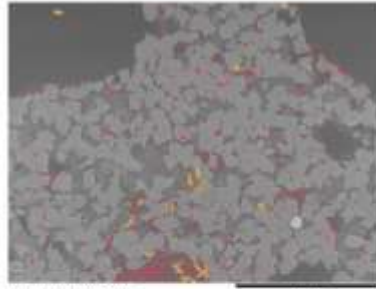
Microporosity:0.55%
Nanoporosity:2.15%
50µm
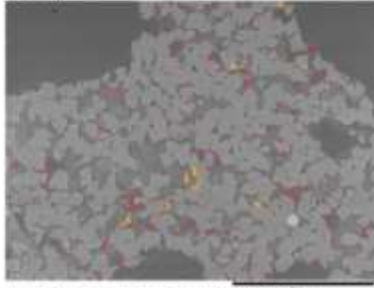
Pore Type:Carbonate Dissolution Pores (CDP) 50µm
Total Porosity:1.55%
Microporosity:0.33%   Micropore Frequency(100%):2.38%
Nanoporosity:1.22%   Nanopore Frequency (100%):97.62%
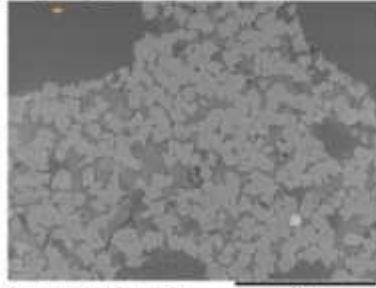
Pore Type:Moldic Pores (MP)
Total Porosity:0.03%
Microporosity:0.01%   Micropore Frequency(100%):12.5%
Nanoporosity:0.02%   Nanopore Frequency (100%):87.5%
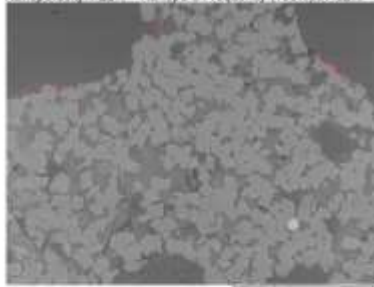
Pore Type:Grain Edge Pores (GEP) 50µm
Total Porosity:0.13%
Microporosity:N/A%   Micropore Frequency(100%):N/A%
Nanoporosity:0.13%   Nanopore Frequency (100%):100%
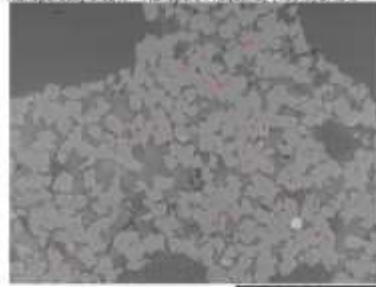
Pore Type:Intracrystalline Pores (ICP1) 50µm
Total Porosity:0.35%
Microporosity:0.02%   Micropore Frequency (100%):1.09%
Nanoporosity:0.33%   Nanopore Frequency (100%):98.91%
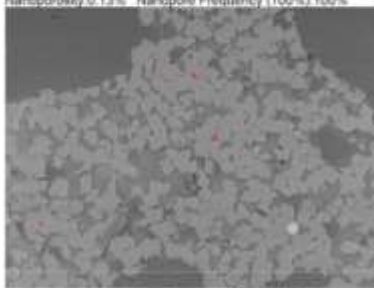
Pore Type:Intercrystalline Pores (ICP2) 50µm
Total Porosity:0.08%
Microporosity:N/A   Micropore Frequency(100%):N/A
Nanoporosity:0.08%   Nanopore Frequency (100%):100%
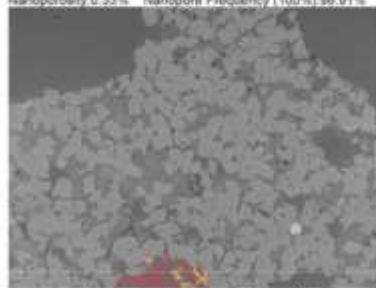
Pore Type:Feldspar Dissolution Pores (FDP) 50µm
Total Porosity:0.57%
Microporosity:0.19%   Micropore Frequency(100%):10.45%
Nanoporosity:0.37%   Nanopore Frequency (100%):89.55%

4.6.3.1.2. Microporous system (200 µm)

Aluminosilicate pores within the microporous system are still the most abundant pore type, however, only 34.54–47.25% of all aluminosilicate pores present are in-deed microporous in size. This indicates that even as the scale increases nanopores are still by far the more frequent pore size. Aluminosilicate micropores are most abundant in the ILRS and VSND microfacies represent-ing 46.21% and 47.25% of the pore network. At this scale, the morphological complexity of aluminosilicate pore types dramatically increases as larger pore structures become apparent. These were potentially formed from pore amalgamations during diagenesis.

4.6.3.2. Moldic pores (MP)

Moldic pores are the second most abundant pore type found throughout all microfacies types, except the DSND. Moldic pore frequency can vary significantly, as does the area occupied by individual pores. Found isolated within mineral phases, predominately quartz grains, their abundance seems to be closely related to quartz grain provenance. At the two separate scales moldic pores represent the following percentage of all pore types found throughout the pore network:

- 50 µm Scale: 1.19–44.78%

- 200 µm Scale: 14.48–36.86%

4.6.3.2.1. Nanoporous system (50 µm)

Because moldic pores are predominately nanoporous in size, they account for 87.5–97.73% of all moldic pores in the nanopore system, a clear evidence that specific pore types are dominated by a certain size. Moldic pores are most abundant in the siltstone and sandstone facies (OM/ILS, DOMS, ILRS, VSND), with a reduced presence in the OMRS and MRSL facies and nearly absent in the DSND facies, accounting there for

only 1.19% of all pore types present. Moldic pores display highly variable morphologies which also accounts for their variable contributions toward the total porosity. This morphometric variability is most prominently documented by variations in area and frequency within the OM/ILS and DOMS microfacies. Despite a similar frequency of nanopores, the area occupied in the OM/ILS microfacies is significantly greater due to the presence of elongated pores (Figs. 14–16). The abundance of these pores shows a strong correlation

Fig. 30. Facies DSND pore size characterization (50 µm Scale).
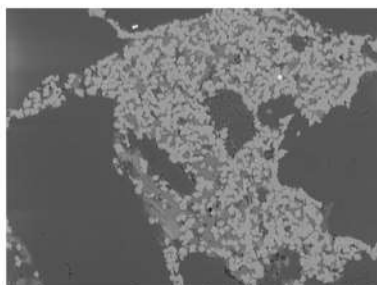
Facies:DSND
Scale:200μm

200μm
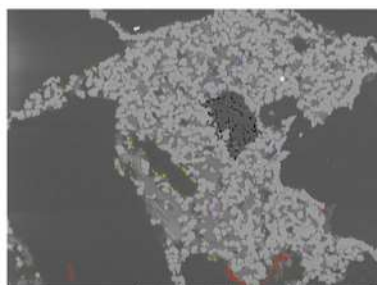
Total porosity:0.91%

200μm
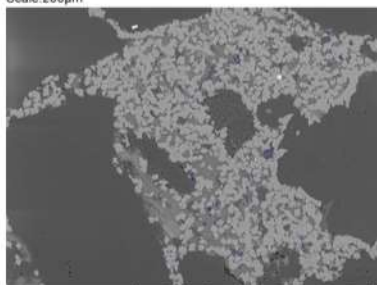
Pore Type:Carbonate Dissolution Pores (CDP)
Total Porosity:0.43%
Porosity (100%):47.5%
Pore Frequency (100%):57.67%
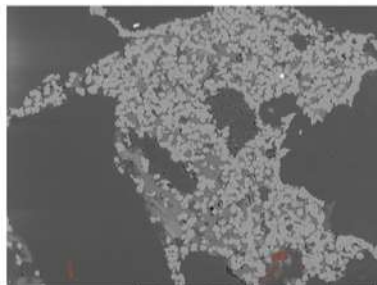
200μm

Pore Type:Moldic Pores (MP)
Total Porosity:0.21%
Porosity (100%):22.54%
Pore Frequency (100%):14.48%
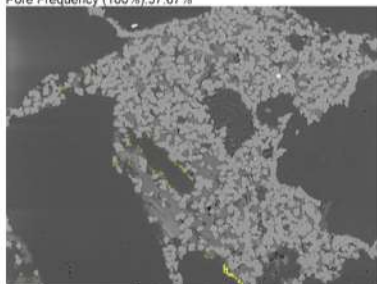
200μm

Pore Type:Grain Edge Pores (GEP)
Total Porosity:0.12%
Porosity (100%):13.13%
Pore Frequency (100%):10.4%
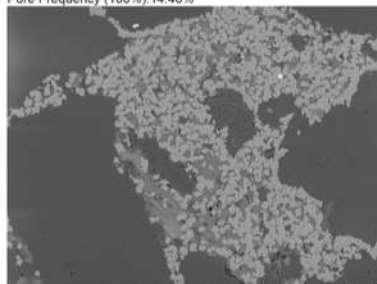
200μm

Pore Type:Fracture Pores (FP)
Total Porosity:0.02%
Porosity (100%):2.12%
Pore Frequency (100%):2.35%
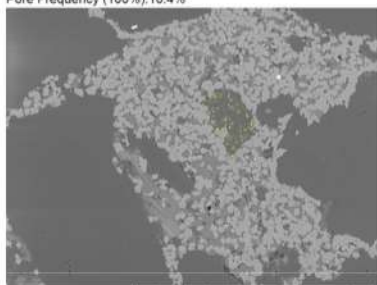
200μm

Pore Type:Feldspar Dissolution Pores (FDP)
Total Porosity:0.13%
Porosity (100%):14.71%
Pore Frequency (100%):15.1%

200μm

with the presence of detrital quartz grains from a presumed secondary source. Larger sandstone bodies with quartz grains exhibiting polycrystallinity and a large lithic fragment content have the lowest quantity of moldic pores, while all other microfacies lacking these quartz grains have much higher moldic porosities (Fig. 13A–G). Observations under SEM provide evidence for quartz grain dissolution. This dissolution process is forming quartz grain remnants with a lower percentage of moldic pores that can be found adjacent to grains with a high abundance of moldic and fracture pores. As to whether the increase in these pore types is a result of selective quartz framework dissolution, a greater degree of weathering of the secondary sourced material prior to sedimentation, or a combination of both is unknown. What is known is that these detrital quartz grains generate another pore type located at the grain's edge, the GEP pores.

4.6.3.2.2. Microporous system (200 μm)

Moldic pores once again are the second most abundant pore type within the microporous system but moldic micropores constitute just 10.6–34.34% of all moldic pores found at the 200 μm scale, with the highest content of micropores found in the ILRS (34.34%), OM/ILS (25.55%) and OMRS (21.23%) microfacies indicating that this primary pore type is dominated by nanopores.

4.6.3.3. Grain edge pores (GEP)

Despite being classified as a primary pore type in the existing literature, GEPs are not always the third most abundant pore type developed. Some-times they form only the fourth or even fifth most frequent pore type within the entire pore network. However, their contributions toward total porosity due to their size is so great, that they are considered a primary pore type nonetheless. Found throughout all the different microfacies types the GEPs are always located at the edges of single grains. Their size varies greatly and can therefore also significantly

increase the overall porosity even if they are only present in low frequencies. Often displaying highly complex but continuous structures, they are predominantly found alongside grains that have undergone selective quartz framework dissolution. At the two separate scales GEPs represent the following percentages of all pore types found throughout the pore network:

**Fig. 31.** Facies DSND pore type characterization (200 μm Scale).

Facies:DSND
Scale:200μm
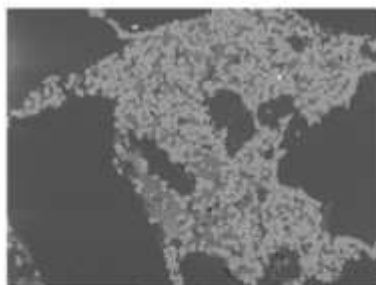
Microporosity:0.51%
Nanoporosity:0.4%

Pore Type:Carbonate Dissolution Pores (CDP)
Total Porosity:0.43%
Microporosity:0.21%   Micropore Frequency(100%):16.52%
Nanoporosity:0.22%   Nanopore Frequency (100%):83.48%

Pore Type:Moldic Pores (MP)
Total Porosity:0.21%
Microporosity:0.14%   Micropore Frequency(100%):18.8%
Nanoporosity:0.07%   Nanopore Frequency (100%):81.2%

Pore Type:Grain Edge Pores (GEP)
Total Porosity:0.12%
Microporosity:0.08%   Micropore Frequency(100%):23.81%
Nanoporosity:0.04%   Nanopore Frequency (100%):76.19%

Pore Type:Fracture Pores (FP)
Total Porosity:0.02%
Microporosity:0.01%   Micropore Frequency (100%):15.79%
Nanoporosity:0.01%   Nanopore Frequency (100%):84.21%

Pore Type:Feldspar Dissolution Pores (FDP)
Total Porosity:0.13%
Microporosity:0.07%   Micropore Frequency(100%):21.31%
Nanoporosity:0.06%   Nanopore Frequency (100%):78.69%

- 50 μm Scale: 1.53–8.78%

- 200 μm Scale: 1.84–3.63% (DSND = 10.4%)

4.6.3.3.1. Nanoporous system (50 μm)

Nanoporous GEPs represent between 29.41% and 100% of all GEPs present within the nanoporous system. Each microfacies type shows a similar quantity of nanoporous GEPs except for those containing more of the aforementioned angular grains, such as the OM/ILS, OMRS and VSND microfacies. The frequency may not vary significantly but the area occupied does. This is due to GEPs being predominantly microporous in size and characterized by a large diameter and an even larger elongate morphology which wraps around detrital grains. The reason for such a high abundance of nanometric GEPs is the discontinuity of larger pores, resulting in the rise of multiple smaller pores wrapping around the same grain. However, although nanoporous GEPs are few in frequency and occupy a smaller area than their microporous counterparts, within the nanoporous system they are still comparatively large in relation to other nanopore types due to their broad and elongate morphology.

4.6.3.3.2. Microporous system (200 μm)

GEPs form a significantly smaller portion of the micropore system, representing only 1.84–3.63% of all pore types present, with the exception of the DSND facies (which displays a total of GEPs of 10.4%, of which 23.8% are microporous). In all other microfacies, micropores are the dominant pore size among GEPs and represent between 59.38% and 95.24% of which most microfacies micropore content is > 60%. GEPs are most abundant in the OM/ILS micro-facies and OMRS, with fewest found in the MRSL microfacies.

4.6.4. Secondary pore type abundance

Pore types that make up significantly less of the pore network yet continue to be present nonetheless, are referred to as secondary pore types and possess unique pore-based properties and features. Secondary pore types consist of fracture, shrinkage, framboidal, micaceous and dissolution pores, and are present in similar abundances throughout all microfacies except the DSND facies. A trend observable across all secondary pore types is an increase in abundance within the nanoporous system. This is a prime example of why downscaling and higher resolution SEM imaging is necessary when analyzing smaller, less frequent pore types. At the two separate scales secondary pores represent the following percentage of all pore types found throughout the pore network:

- 50 µm Scale: 4.82–9.35% (VSND = 0.5%)

- 200 µm Scale: 1.4–5.58% (VSND = 0.4%)

Fig. 32. Facies DSND pore size characterization (200 µm Scale).
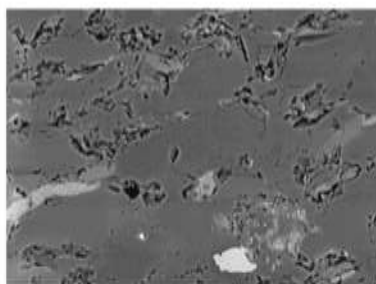
Facies:ILRS
Scale:50µm
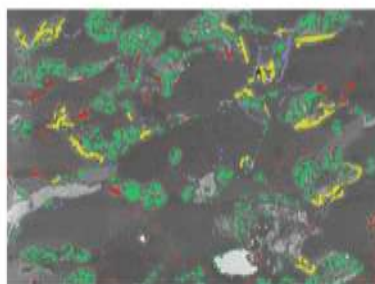
Total Porosity:10.56%
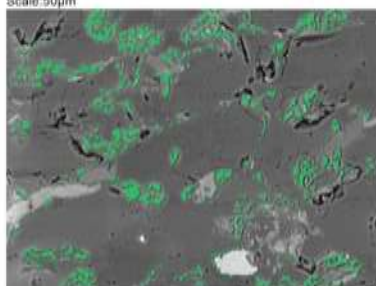
Pore Type:Aluminosilicate Pores (AL)
Total Porosity:7.05%
Porosity (100%):66.76%
Pore Frequency (100%):59.86%
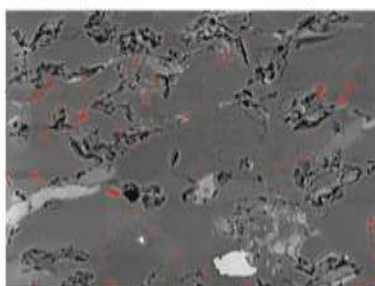
Pore Type:Moldic Pores (MP)
Total Porosity:1.03%
Porosity (100%):9.75%
Pore Frequency (100%):30.08%
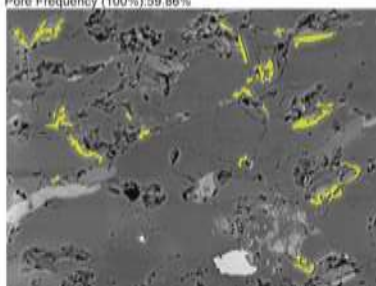
Pore Type:Grain Edge Pores (GEP)
Total Porosity:2.14%
Porosity (100%):20.27%
Pore Frequency (100%):3.56%
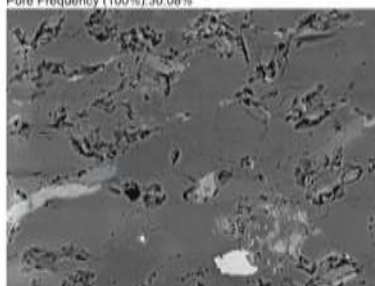
Pore Type: Micaceous Pores (MBP)
Total Porosity:0.02%
Porosity (100%):0.19%
Pore Frequency (100%):0.63%
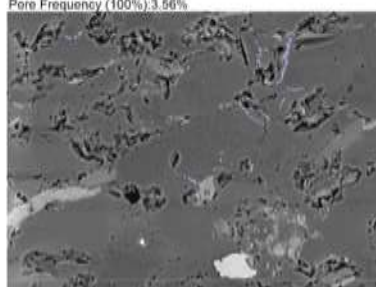
Pore Type:Fracture Pores (FP)
Total Porosity:0.32%
Porosity (100%):3.03%
Pore Frequency (100%):5.87%

4.6.4.1. Fracture pores (FP)

Fracture pores are found throughout all microfacies at both scales in low frequencies, making them one of the most consistently found secondary pore type. At the two separate scales fracture pores represent the following percentage of all pore types found within the entire pore network:

- 50 µm Scale: 1.13–5.87%

- 200 µm Scale: 0.21–2.35%

4.6.4.1.1. Nanoporous system (50 µm)

Nanoporous fracture pores are typically localized phenomena, small in width but pronounced elongate. In the OMRS and MRSL microfacies, where they are most abundant, they display a lack of continuous connectivity across mineral phases. At the 50 µm scale, fracture pores are 100% nanometric in size. Although they only occupy a small area they show the potential to act as conduits for nanometric hydrocarbon migration from adjacent pore types, such as moldic pores, where discontinuous fracture pores cross mineral phases and can transport hydrocarbons isolated within moldic pores. However, fracture pores cannot contribute significant porosity and have a limited potential to serve as an efficient migratory pathway for hydrocarbons due to their low frequency and lack of continuity.

4.6.4.1.2. Microporous system (200 µm)

Fracture pores contribute only a very small proportion to the overall pore network, typically be-tween 0.21% to 2.35%, of which micropores represent <40% of total fracture pores present. However, this data is somewhat unreliable given that so few fracture pores are present within a single area. The largest amount of fracture pores are found within the OMRS microfacies in which facture pores are present, but only at a negligible quantity when considering the proportions of aluminosilicate and moldic pores present within a given network.

Fig. 33. Facies ILRS pore type characterization (50 μm Scale).

Facies: ILRS
Scale:50µm

50µm
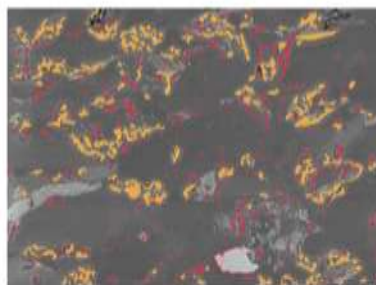
Microporosity:7.41%
Nanoporosity:3.15%

50µm
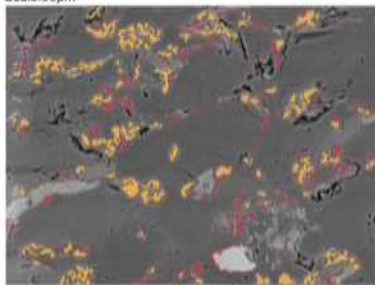
Pore Type:Aluminosilicate Pores (AL)
Total Porosity:7.05%
Microporosity:5.09%   Micropore Frequency(100%):13.84%
Nanoporosity:1.96%   Nanopore Frequency (100%):86.16%

50µm
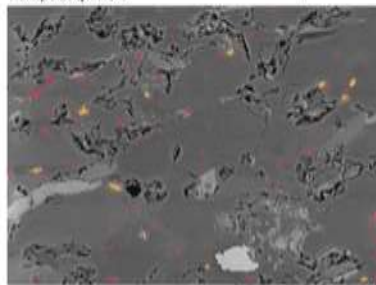
Pore Type:Moldic Pores (MP)
Total Porosity:1.03%
Microporosity:0.26%   Micropore Frequency(100%):3.48%
Nanoporosity:0.77%   Nanopore Frequency (100%):96.52%

50µm
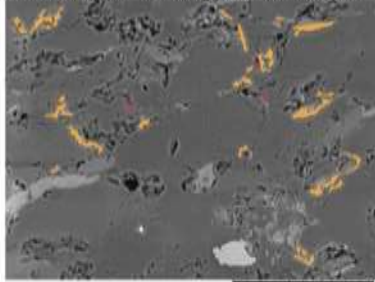
Pore Type:Grain Edge Pores (GEP)
Total Porosity:2.14%
Microporosity:2.06%   Micropore Frequency(100%):70.59%
Nanoporosity:0.08%   Nanopore Frequency (100%):29.41%

50µm
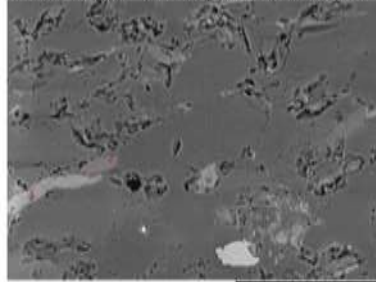
Pore Type:Micaceous Pores (MBP)
Total Porosity:0.02%
Microporosity:N/A   Microporosity (100%):N/A
Nanoporosity:0.02%   Nanopore Frequency (100%):100%

50µm
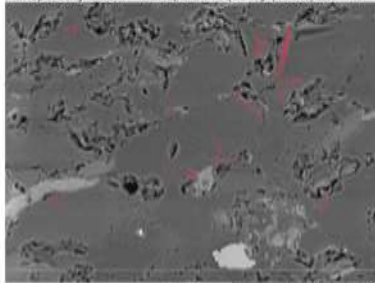
Pore Type:Fracture Pores (FP)
Total Porosity:0.32%
Microporosity:N/A   Micropore Frequency(100%):N/A
Nanoporosity:0.32%   Nanopore Frequency (100%):100%

50µm

4.6.4.2. Shrinkage cracks pores (SCP)

Shrinkage crack pores are microfacies specific and are found isolated within certain areas of the aluminosilicate matrix. At the two separate scales shrinkage crack pores represent the following percentage of all pore types found throughout the pore network:

- 50 µm Scale: 0.4–0.52%

- 200 µm Scale: 0.17–0.19%

4.6.4.2.1. Nanoporous system (50 µm)

Shrinkage crack pores, un-like their fracture pore counterparts, are generally more elongate and larger in diameter, and more continuous. These pore types are not abundant throughout all microfacies and are only developed within the MRSL and VSND microfacies. Representing 0.4-0.52% of the nanoporous net-work of which 80–100% is nanoporous, this pore type is most notable in VSND microfacies where selective diagenetic processes appear to have played a role in their formation. The aluminosilicate matrix, where the shrinkage cracks can be found, is isolated, unlike other cements. This isolation of the cement may be due to the alteration of large feldspar grains, which resulted in the formation of illite, which may serve as an explanation as to why so many shrinkage cracks both large and small are found in confined and isolated spaces. The morphology of the space occupied would also indicate that the illite present is a product of feldspar alteration.

4.6.4.2.2. Microporous system (200 µm)

 Shrinkage pores are equally uncommon, only present in the OM/ILS and VSND, representing 0.17–0.19% of all pore types present, of which only 16.6–20% is micro-porous. With similar properties as fracture pore types, shrinkage cracks are uncommon and where present, predominantly nanoporous, despite decreases in scale.

4.6.4.3. Micaceous pores (MBP)

Mica-based pore types are a small contributor to the nanoporous network, their frequency is marginally variable given that their presence is a function of the quantity of biotite and muscovite present within each microfacies, with most microfacies displaying relatively similar quantities of micas. At the two separate scales mica-based pores represent the following percentages of all pore types found throughout the entire pore network:

•   50 μm Scale: 2.54–7.04%

•   200 μm Scale: 0.18–1.87%

Fig. 34. Facies ILRS pore size characterization (50 μm Scale).
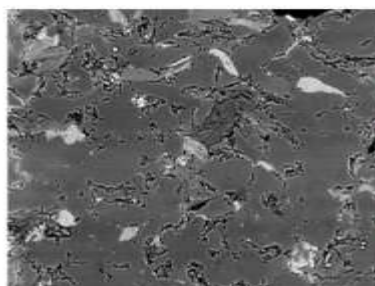
Facies:ILRS
Scale:200μm
200μm
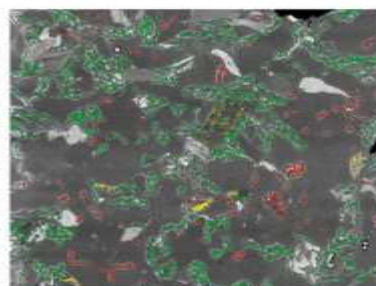
Total Porosity:7.7%
200μm
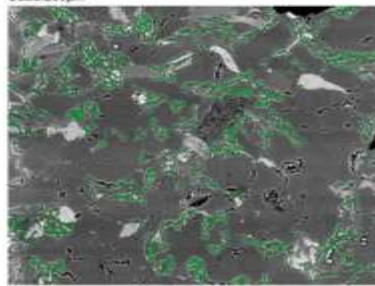
Pore Type:Aluminosilicate Pores (AL)   200μm
Total Porosity:5.96%
Porosity (100%):77.47%
Pore Frequency (100%):73.36%
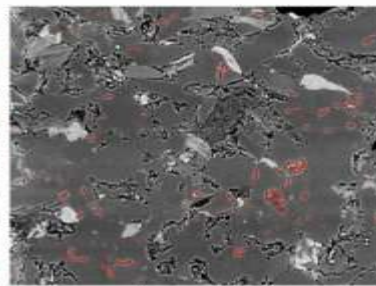
Pore Type:Moldic Pores (MP)   200μm
Total Porosity:0.94%
Porosity (100%):12.16%
Pore Frequency (100%):19.64%
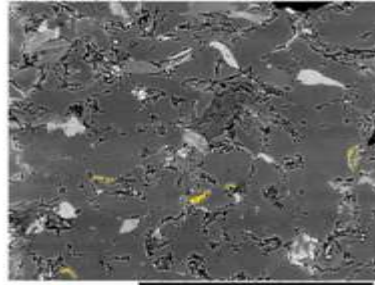
Pore Type:Grain Edge Pores (GEP)   200μm
Total Porosity:0.63%
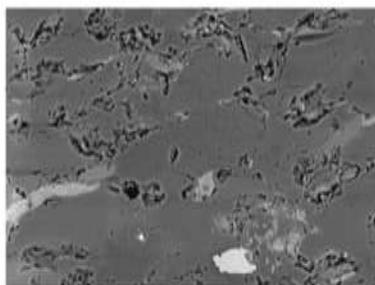Porosity (100%):8.26%
Pore Frequency (100%):2.76%
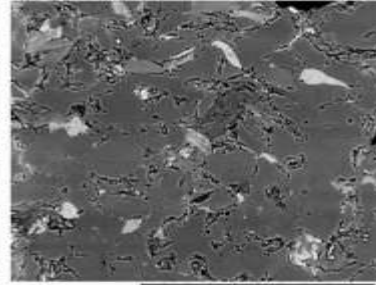
Pore Type:Fracture Pores (FP)   200μm
Total Porosity:0.03%
Porosity (100%):0.4%
Pore Frequency (100%):0.21%

Pore Type:Framboid Pores (FHP)   200μm
Total Porosity:0.02%
Porosity (100%):0.19%
Pore Frequency (100%):0.3%

Pore Type:Feldspar Dissolution Pores (FDP)   200μm
Total Porosity:0.12%
Porosity (100%):1.52%
Pore Frequency (100%):3.73%

4.6.4.3.1. Nanoporous system (50 µm)

Micabased pores represent 0.6–7% of the nanoporous system, of which 92.31–100% of micaceous pores are nanometric. Micaceous nanopores are most abundant in the mica rich MRSL microfacies followed by the OM/ILS and OMRS microfacies. Typically characterized by an elongate, but constrained pore morphology, these pores demonstrate the potential to contribute to nanometric permeability, but their limitations in width will likely result in a complex mode of hydrocarbon migration, due to small pore throat diameters.

4.6.4.3.2. Microporous system (200 µm)

Representing between 0.18% and 1.87% of the microporous system, mica-based pores contribute significantly less to the overall pore network than mica-based pores in the nanoporous system. Microporous mica-based pores represent between 6.81% and 10% (within the DOMS facies up to 50%) of all mica-based pores indicating that this pore type is predominately nanoporous.

4.6.4.4. Framboidal pores (FHP)

Framboidal pore abundance and size is a function of red/ox conditions, with pyrite framboids varying in size from 5 to 11 µm, affecting framboidal pore size. At the two separate scales framboidal pores represent the following percentages of all pore types found throughout the entire pore network:

- 50 µm Scale: 1.65% (OM/ILS)

- 200 µm Scale: 0.06 - 0.3%

4.6.4.4.1. Nanoporous system (50 µm)

Framboidal pores are highly localized and largely confined to varves and large pieces of amorphous OM and are rarely seen residing in the

matrix. Where present, Framboidal pores are 100% nanometric, but that is a function of pyrite framboid size, which across all microfacies ranges from 5 to 11 µm with larger pyrite framboids found in varves, which are consequently more microporous. Representing 1.65% of the pore network in the OM/ILS microfacies, framboidal pores are 100% nanometric.

Fig. 35. Facies ILRS pore type characterization (200 µm Scale).

Facies:ILRS
Scale:200µm

Microporosity:6.86%
Nanoporosity:0.84%

Pore Type:Aluminosilicate Pores (AL)
Total Porosity:5.96%
Microporosity:5.38%   Micropore Frequency(100%):46.21%
Nanoporosity:0.58%   Nanopore Frequency (100%):53.79%

Pore Type:Moldic Pores (MP)
Total Porosity:0.94%
Microporosity:0.74%   Micropore Frequency(100%):34.34%
Nanoporosity:0.2%   Nanopore Frequency (100%):65.66%

Pore Type:Grain Edge Pores (GEP)
Total Porosity:0.63%
Microporosity:0.62%   Micropore Frequency(100%):60%
Nanoporosity:0.01%   Nanopore Frequency (100%):40%

Pore Type:Fracture Pores (FP)
Total Porosity:0.03%
Microporosity:0.03%   Micropore Frequency(100%):40%
Nanoporosity:N/A   Nanopore Frequency (100%):N/A

Pore Type:Framboid Pores (FHP)
Total Porosity:0.02%
Microporosity:0.01%   Microporosity (100%):42.86%
Nanoporosity:0.01%   Nanopore Frequency (100%):57.14%

Pore Type:Dissolution Pores (DP)
Total Porosity:0.12%
Microporosity:0.08%   Micropore Frequency(100%):23.86%
Nanoporosity:0.04%   Nanopore Frequency (100%):76.14%

83

4.6.4.4.2. Microporous system (200 µm)

Framboid pores, as within the nanoporous system, are not only microfacies specific, but the wide and variable distribution within the matrix and preferential concentration in OM varves provide varied results. Most prominent in the ILRS and MRSL microfacies, microporous framboid pores within the microporous system make up a very small portion of the pore network of which 42.86–100% are microporous.

4.6.4.5. Dissolution pores (DP)

Dissolution pores are microfacies specific and are more abundant in microfacies where dolomitization of the intergranular pore space is more pervasive. At the two separate scales dissolution pores represent the following percentages of all pore types found throughout the entire pore network:

- 50 µm Scale: <2.55%

- 200 µm Scale: 0.86–3.73%

**4.6.4.5.1. Nanoporous system (50 µm)** The largest quantity of dolomitic dissolution pores can be found within the DSND facies and occur sporadically throughout most other microfacies, but never in significant quantities. Dolomitic dissolution pores represent <2.55% of the nanopore system of which 75–100% of dolomitic dissolution pores are nanometric. With the exception of the DSND microfacies where dolomitic dissolution pores represent 56.17% of the nanopore system, of which 97.62% is nanometric. Pores associated with dolomitization are dominated by nanopores, not micropores.

4.6.4.5.2. Microporous system (200 µm) Present in only the DOMS and ILRS microfacies at the 200 µm scale, dissolution pores constitute between 0.86% and 3.37% of the pore network of which just 20–23.86%

is microporous, indicating that dolomitic dissolution pores are predominately nanoporous. In the DSND microfacies, where the intergranular space is dominated by dolomite, dissolution pores represent of 62.77%

**Fig. 36.** Facies ILRS pore size characterization (200 μm Scale).
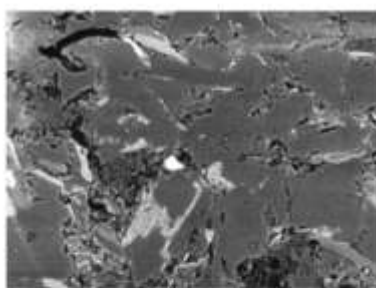
Facies:MRSL
Scale:50μm
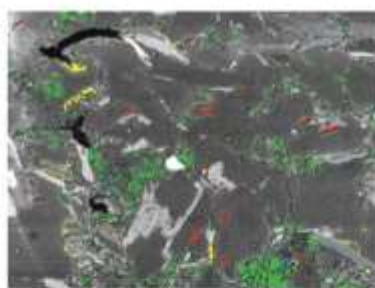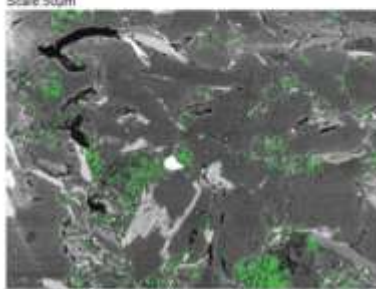
Total porosity:6.84%

Pore Type:Aluminosilicate Pores (AL)
Total Porosity:5.24%
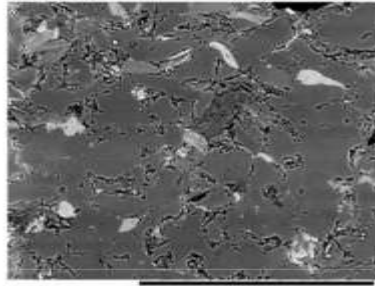Porosity (100%):75.5%
Pore Frequency (100%):73.77%
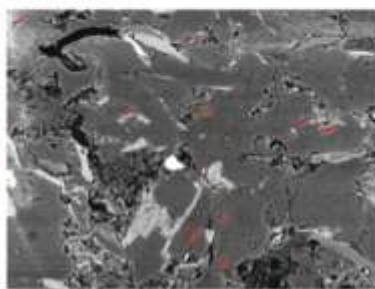
Pore Type:Moldic Pores (MP)
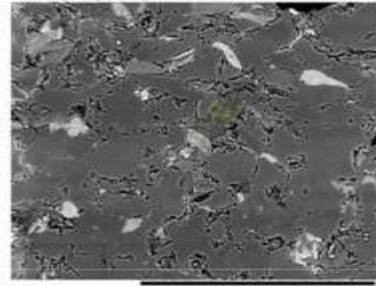Total Porosity:0.53%
Porosity (100%):7.64%
Pore Frequency (100%):13.88%
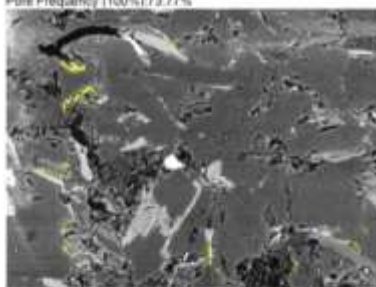
Pore Type:Grain Edge Pores (GEP)
Total Porosity:0.53%
Porosity (100%):7.64%
Pore Frequency (100%):3.72%

Pore Type:Micaceous Pores (MBP)
Total Porosity:0.35%
Porosity (100%):5.04%
Pore Frequency (100%):7.04%

Pore Type:Fracture Pores (FP)
Total Porosity:0.18%
Porosity (100%):2.59%
Pore Frequency (100%):1.41%

Pore Type:Shrinkage Crack Pores (SCP)
Total Porosity:0.11%
Porosity (100%):1.59%
Pore Frequency (100%):0.4%

86

of the pore network, of which 16.52-21.31% are micrometric, depending on the *type* of dissolution.

4.7. Pore network characterization (pore type porosity)

4.7.1. Pore network overview

Porosity is heavily controlled by specific pore types, with the vast majority of porosity found within primary pore types (AL, MP, GEP). However, the latter two contribute significantly less porosity to the overall pore net-work. Combined nano/microporosity across all microfacies ranges from 0.91% to 24.69% (Fig. 16).

Shale microfacies

1. OMRS: Total Porosity (50 µm) = 17.08%. Total Porosity (200 µm) = 15.43%

Siltstone microfacies

1. OM/ILS: Total porosity (50 µm) = 19.35%. Total porosity (200 µm) = 24.47%

2. ILRS: Total porosity (50 µm) = 10.56%. Total porosity (200 µm) = 7.7%

3. MRSL: Total porosity (50 µm) = 6.94%. Total porosity (200 µm) = 6.34%

4. DOMS: Total porosity (50 µm) = 4.86%. Total porosity (200 µm) = 5.26%

Sandstone microfacies

1.   VSND: Total porosity (50 µm) = 8.53%. Total porosity (200 µm) = 6.98%

2.   DSND: Total   porosity   (50 µm) = 2.7%. Total porosity

(200 µm) = 0.91%

4.7.2. Primary pore type porosity

4.7.2.1. Aluminosilicate pores (AL)

Aluminosilicate pores are by far the largest contributor toward total porosity in all microfacies and in both scale systems. The largest aluminosilicate porosity can be found in the OM/ILS and OMRS microfacies with aluminosilicate porosities of 13.36% and 12.04%, respectively, with the lowest aluminosilicate porosity located in the DOMS, MRSL, and VSND microfacies types with porosities of 3.23%, 5.24%, and 5.28%, respectively. The reason for a lack of cement-based porosity in these sand-stone/siltstone microfacies, which characteristically should exhibit high cement-based porosity, is due to more closely spaced grains and diagenetic dolomite destroying the intergranular aluminosilicate porosity. Proportionally, aluminosilicate contributions toward total porosity across all microfacies at the two separate scales are as follows:

•   50 µm Scale: 61.9–75.5%

•   200 µm Scale: 65.6–88.52%

Fig. 37. Facies MRSL pore type characterization (50 µm Scale).
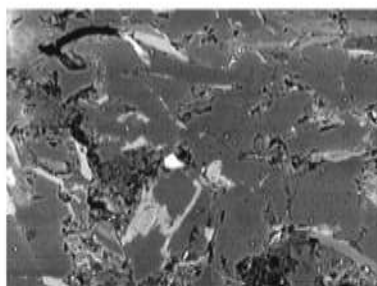
Facies:MRSL
Scale:50μm
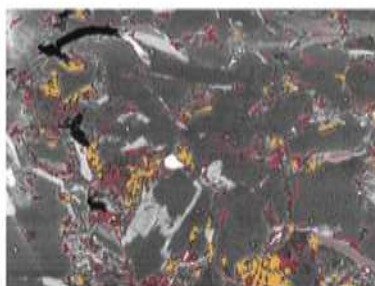
Microporosity:3.36%
Nanoporosity:3.58%
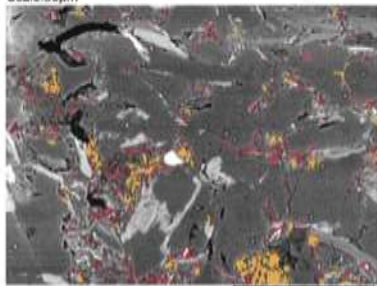
Pore Type:Aluminosilicate Pores (AL)
Total Porosity:5.24%
Microporosity:2.9%   Micropore Frequency(100%):5.31%
Nanoporosity:2.34%   Nanopore Frequency (100%):94.69%
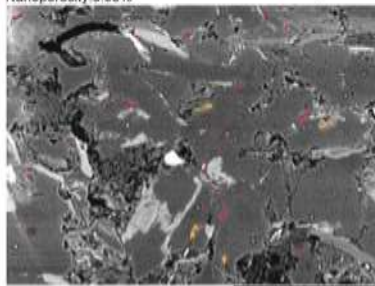
Pore Type:Moldic Pores (MP)
Total Porosity:0.53%
Microporosity:0.17%   Micropore Frequency(100%):2.94%
Nanoporosity:0.36%   Nanopore Frequency (100%):97.06%
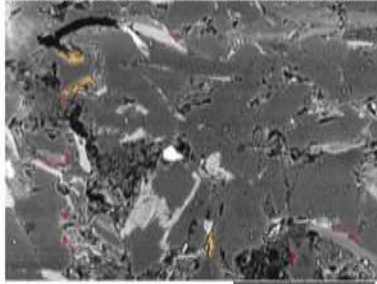
Pore Type:Grain Edge Pores (GEP)
Total Porosity:0.53%
Microporosity:0.29%   Micropore Frequency(100%):16.22%
Nanoporosity:0.24%   Nanopore Frequency (100%):83.78%

Pore Type:Micaceous Pores (MBP)
Total Porosity:0.35%
Microporosity:N/A   Micropore Frequency (100%):N/A
Nanoporosity:0.35%   Nanopore Frequency (100%):100%

Pore Type:Fracture Pores (FP)
Total Porosity:0.18%
Microporosity:N/A   Micropore Frequency(100%):N/A
Nanoporosity:0.18%   Nanopore Frequency (100%):100%

Pore Type:Shrinkage Crack Pores (SCP)
Total Porosity:0.11%
Microporosity:N/A   Micropore Frequency(100%):N/A
Nanoporosity:0.11%   Nanopore Frequency (100%):100%

4.7.2.1.1. Nanopore system (50 µm) Aluminosilicate pores are the largest contributor toward total porosity. They are contributing between 3.23% and 13.36% toward the total porosity, of which nanopores con-tribute 1.25–3.68%, representing 17.31–44.58% of the total aluminosilicate porosity. As Figs. 14 and 15 show, despite being a smaller contributor toward porosity than larger aluminosilicate micropores, nanopore contributions toward porosity cannot be understated or overlooked, with the data highlighting the importance of the matrix being a primary source for hydrocarbon storage in the free gas state. The OMRS microfacies has the greatest amount of nanoporosity held within the cement phase, contributing 3.68% toward total porosity with a limited dolomitic overprint and a smaller grain size which has greatly increased nanoporosity. In total, aluminosilicate nanoporosity equals:

1.   *Siltstone microfacies*: (ILRS, OM/ILS, MRSL, and DOMS) contribute 1.25–2.32% toward total porosity, representing 11.99–33.64% of pore network porosity.

2.   *Sandstone microfacies*: (VSND) contributes 2.34% toward total porosity, representing 27.7% of the pore network.

3.   *Shale microfacies* (OMRS) nanopores contribute 3.68% toward total porosity, representing 21.54% of the pore network.

4.7.2.1.2. Micropore system (200 µm) Aluminosilicate pores are also within the micropore system the largest contributor toward total porosity, contributing between 3.44% and 21.38%,

Fig. 38. Facies MRSL pore size characterization (50 µm Scale).
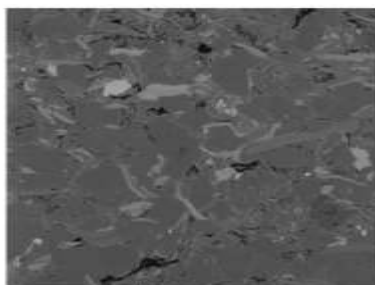
Facies:MRSL
Scale:200μm
200μm
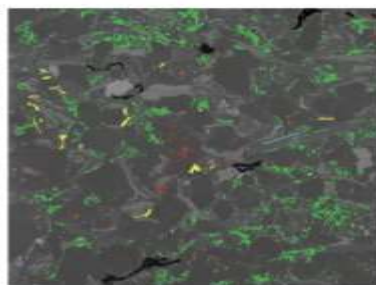
Total Porosity:6.34%
200μm
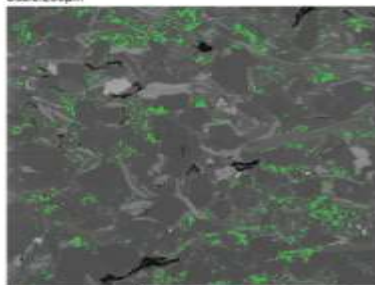
Pore Type:Aluminosilicate Pores (AL):
Total Porosity:5.61%
Porosity (100%):88.52%
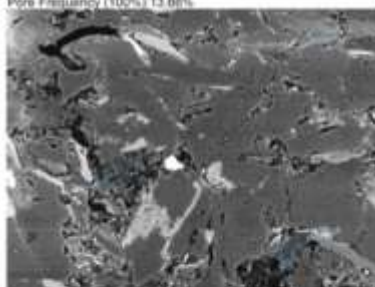Pore Frequency (100%):80.09%
200μm
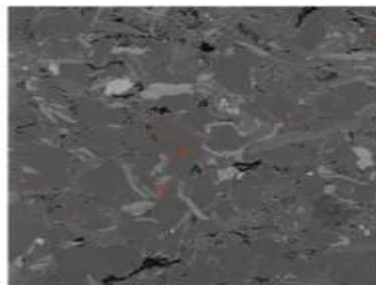
Pore Type:Moldic Pores (MP)
Total Porosity:0.3%
Porosity (100%):4.65%
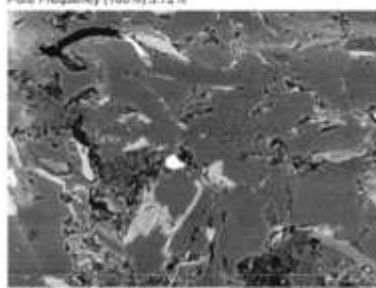Pore Frequency (100%):14.82%
200μm
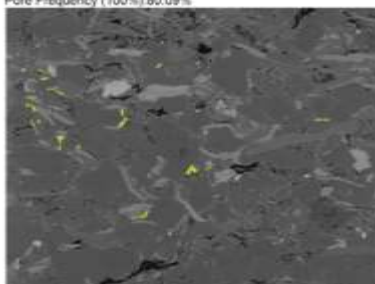
Pore Type:Grain Edge Pores (GEP)
Total Porosity:0.28%
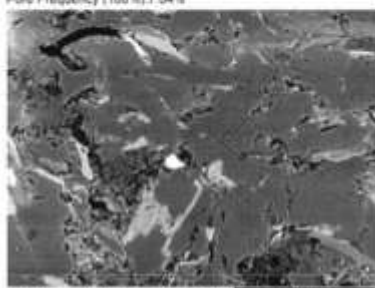Porosity (100%):4.54%
Pore Frequency (100%):1.84%
200μm
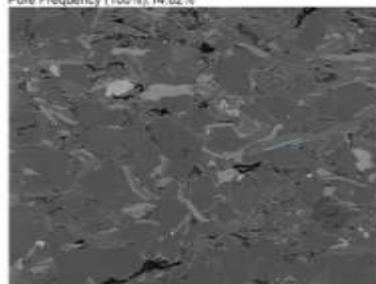
Pore Type: Micaceous Pores (MBP)
Total Porosity:0.07%
Porosity (100%):1.14%
Pore Frequency (100%):1.16%
200μm
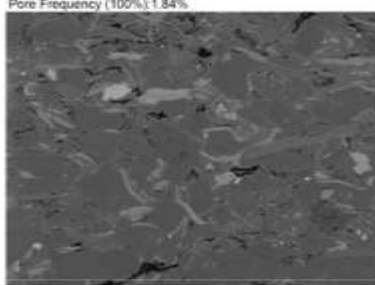
Pore Type:Fracture Pores (FP)
Total Porosity:0.06%
Porosity (100%):0.92%
Pore Frequency (100%):2.07%
200μm
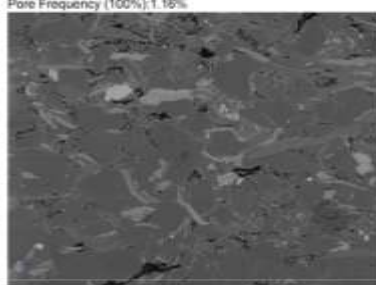
Pore Type:Framboid Pores (FHP)
Total Porosity:0.02%
Porosity (100%):0.2%
Pore Frequency (100%):0.06%
200μm

of which micropores contribute 2.86–20.2% representing 83.05–94.56% of the total aluminosilicate porosity. This close relationship between total aluminosilicate porosity and microporosity demonstrates that at this scale we cannot quantify the role nanopores play, due to their size and the resolution of the BSE image, but at the 50 µm scale we have already identified their increase in frequency and contributions toward porosity. As demonstrated by the nanopore system analysis, the ability of nanopores to contribute significant pore space for free gas, stems from their widespread abundance, thus on the 200 µm scale, where this is not apparent, their total contribution decreases, while micropore contributions increase, as large pore structures become observable. The microfacies with the greatest amount of aluminosilicate porosity, contributing 21.36% toward total porosity of which 94.56% is microporous, is the OM/ILS siltstone microfacies, with no other microfacies being able to contribute similar levels of porosity. The microfacies with the second most abundant aluminosilicate content, and second most porous by far, is the shale OMRS microfacies with aluminosilicate pores contributing 12.75% toward total porosity, of which 91.15% is microporous. The large discrepancy now apparent between the OM/ILS and OMRS microfacies which was not present at the 50 µm scale, is due to the presence of larger micropores in the OM/ILS siltstone microfacies where the OMRS shale microfacies is predominantly more nanoporous. Other microfacies such as DOMS, ILRS, MRSL and VSND have aluminosilicate porosities, which only contribute between 3.44% and 5.96% toward total porosity which is significantly lower than the afore-mentioned microfacies. However, all microfacies continue to show that the aluminosilicate matrix is dominated, almost exclusively, by micropores at this scale with micropores making up 83.05–90.15% of aluminosilicate pore types. Unlike the nanopore system, the role of moldic pores as the second most dominant contributor toward porosity is less apparent, as it often interchanges with pores located at the edge of rigid grains. In total aluminosilicate microporosity equals:

1.   *Siltstone microfacies* (ILRS, OM/ILS, MRSL, and DOMS) contribute 2.86–20.2% toward total porosity and represent 54.5–82.54% of the pore network.

2. *Sandstone microfacies* (VSND) contributing 4.23% toward total porosity, representing 60.64% of the pore network.

**Fig. 39.** Facies MRSL pore type characterization (200 μm Scale).
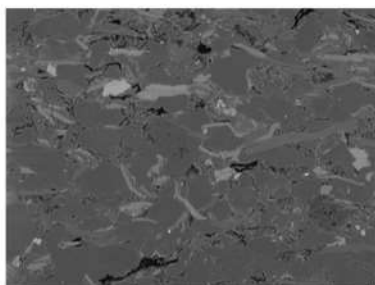
Facies:MRSL
Scale:200μm
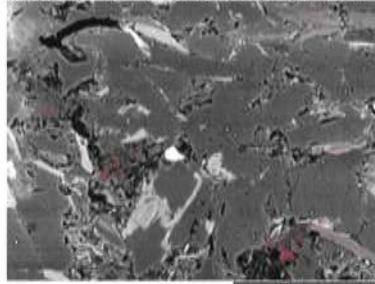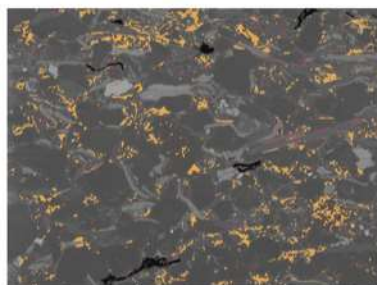

Microporosity: 5.42%
Nanoporosity:0.92%
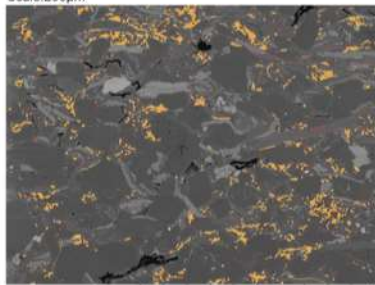
Pore Type: Aluminosilicate Pores (AL)
Total Porosity:5.6%
Microporosity:4.92%   Micropore Frequency(100%):41.08%
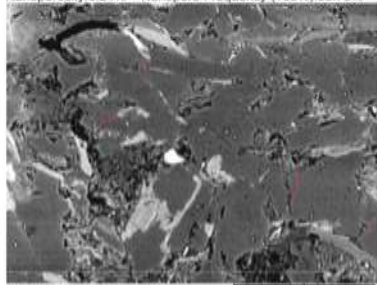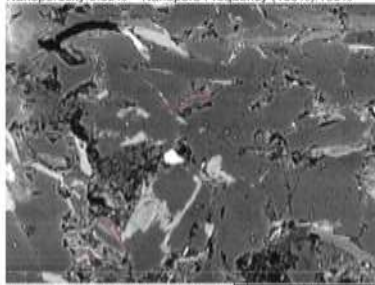Nanoporosity:0.68%   Nanopore Frequency (100%):58.92%
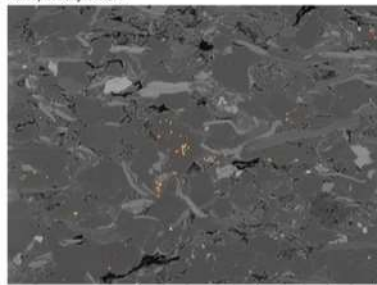
Pore Type: Moldic Pores (MP)
Total Porosity:0.3%
Microporosity:0.17%   Micropore Frequency(100%):20.93%
Nanoporosity:0.13%   Nanopore Frequency (100%):79.07%
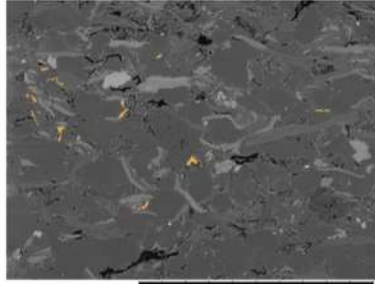
Pore Type: Grain Edge Pores (GEP)
Total Porosity:0.29%
Microporosity:0.28%   Micropore Frequency(100%):59.38%
Nanoporosity:0.01%   Nanopore Frequency (100%):40.62%
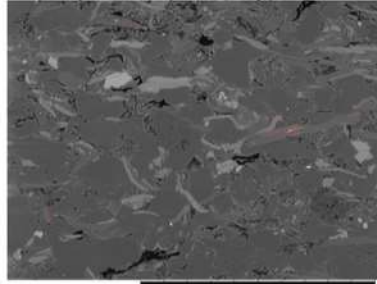
Pore Type: Micaceous Pores (MBP)
Total Porosity:0.07%
Microporosity:0.01%   Microporosity (100%):10%
Nanoporosity:0.06%   Nanopore Frequency (100%):90%
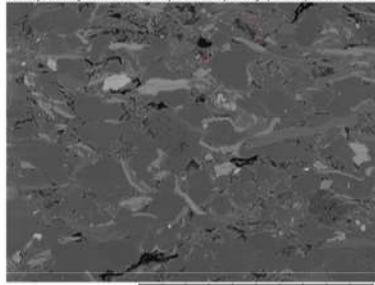
Pore Type: Fracture Pores (FP)
Total Porosity:0.06%
Microporosity:0.02%   Micropore Frequency(100%):11.11%
Nanoporosity:0.04%   Nanopore Frequency (100%):88.89%
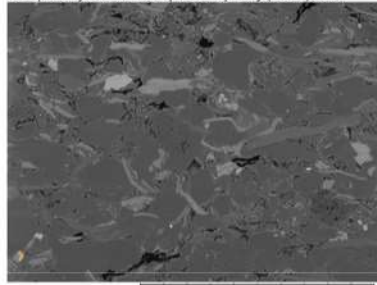
Pore Type: Framboid Pores (FHP)
Total Porosity:0.02%
Microporosity:0.02%   Micropore Frequency(100%):100%
Nanoporosity:N/A   Nanopore Frequency (100%):N/A

3. *Shale microfacies* (OMRS) contribute 11.62% toward total porosity, representing 75.33% of the pore network.

4.7.2.2. Moldic pores (MP)

Despite being the dominant second most abundant pore type present across all microfacies, moldic pores are in some microfacies the third largest contributor toward total porosity or have similar porosity contributions as GEPs due to moldic pores being predominately nanometric. Proportionally, moldic pore contributions toward total porosity across all microfacies at the two separate scales are as follows:

- 50 µm Scale: 4.57–18.54%

- 200 µm Scale: 3.54–22.54%

4.7.2.2.1. Nanopore system (50 µm)

Moldic pores are the second largest contributor toward total porosity, contributing between 0.03% and 2.17%. Unlike the aluminosilicate matrix, moldic pores are dominated by nanopores, while only contributing between 0.02% and 1.34% toward total porosity, nanopores represent 45.04–74.67% of total moldic porosity. The smallest and most frequent moldic nanopores display a pseudospherical morphology, creating a pitted texture, and in other micro-facies display a more elongated pore structure which greatly increases pore size. By far the greatest contributors to overall moldic nanoporosity can be found in the OM/ILS and VSND microfacies, where moldic nanopores contribute 1.34% and 1.08% to total porosity. Other microfacies with high moldic porosity include DOMS, OMRS, and ILRS with the smallest amount located in MRSL and are essentially non-existent in DSND. Quartz grains with a large number of GEP are closely associated with the presence of larger moldic pores which could imply that the elongated moldic pores form in response to selective diagenetic dissolution or that these quartz grains are the product of a highly weathered secondary

sourced material. In addition to the elongated pore structure, there is a second type of moldic pores which is morphometrically dissimilar, forming a diamond shape whereby pore elongation is coupled with an equal increase in diameter. This is creating a much larger and deep-set pore which, although far less abundant, can contribute a large amount toward total porosity. Often these larger moldic pores begin to coalesce and detach segments of the quartz grains to form a separate and more importantly rugged independent grain, which promotes the formation of GEPs

.   Evidence of this selective quartz framework dissolution is very similar to observations made by Leneuf (1973), who observed deeper dissolution features, triangular etch pits, and interconnected networks of grooves

Fig. 40. Facies MRSL pore size characterization (200 μm Scale).

Facies:VSND
Scale 50μm

50μm

Total porosity:8.53%

50μm

Pore Type:Aluminosilicate Pores (AL)
Total Porosity:5.28%
Porosity (100%):61.9%
Pore Frequency (100%):61.34%

50μm

Pore Type:Moldic Pores (MP)
Total Porosity:1.45%
Porosity (100%):17%
Pore Frequency (100%):32.88%

50μm

Pore Type:Grain Edge Pores (GEP)
Total Porosity:1.26%
Porosity (100%):14.77%
Pore Frequency (100%):5.26%

50μm

Pore Type:Shrinkage Crack Pores (SCP)
Total Porosity:0.54%
Porosity (100%):6.33%
Pore Frequency (100%):0.52%

50μm

Fig. 41. Facies VSND pore type characterization (50 μm Scale).

Facies:VSND
Scale:50μm

Microporosity:4.85%
Nanoporosity:3.68%
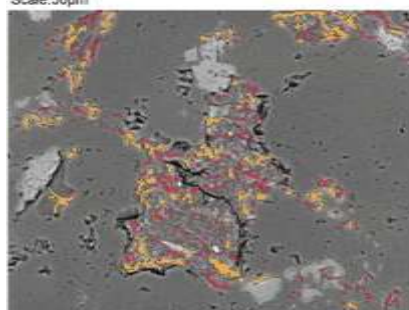
Pore Type:Aluminosilicate Pores (AL)
Total Porosity:5.28%
Microporosity:2.93%   Micropore Frequency(100%):9.92%
Nanoporosity:2.35%   Nanopore Frequency (100%):90.08%
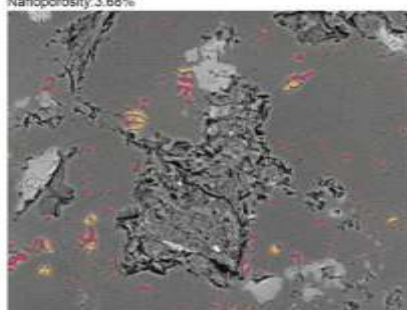
Pore Type:Moldic Pores (MP)
Total Porosity:1.45%
Microporosity:0.37%   Micropore Frequency(100%):4.39%
Nanoporosity:1.08%   Nanopore Frequency (100%):95.61%
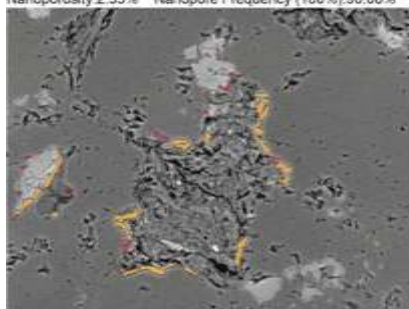
Pore Type:Grain Edge Pores (GEP)
Total Porosity:1.26%
Microporosity:1.07%   Micropore Frequency(100%):33.33%
Nanoporosity:0.19%   Nanopore Frequency (100%):66.67%
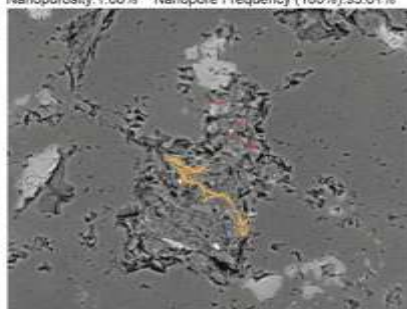
Pore Type:Shrinkage Crack Pores (SCP)
Total Porosity:0.54%
Microporosity:0.48%   Microporosity (100%):20%
Nanoporosity:0.06%   Nanopore Frequency (100%):80%

Fig. 42. Facies VSND pore size characterization (50 μm Scale).

and crevasses in association with increased quartz weathering. In total, moldic nanoporosity equals:

1. *Siltstone microfacies* (ILRS, OM/ILS, MRSL, and DOMS) has contributed 0.36–1.34% toward total porosity, representing 5–13.1% of the pore network.
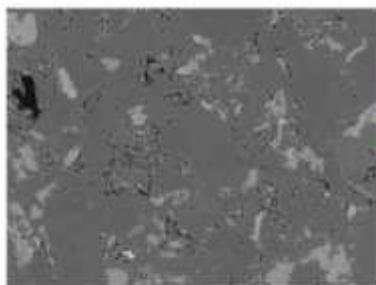
Facies:VSND
Scale:200μm
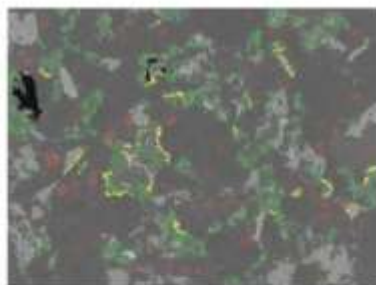
Total porosity:6.98%
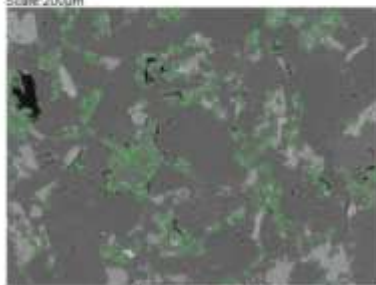
Pore Type:Aluminosilicate Pores (AL)
Total Porosity:4.87%
Porosity (100%):69.84%
Pore Frequency (100%):60.46%
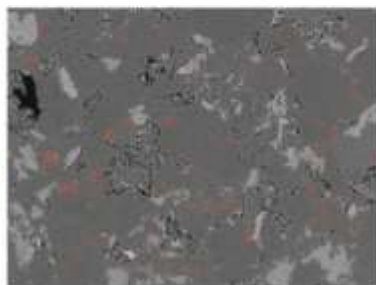
Pore Type:Moldic Pores (MP)
Total Porosity:1.24%
Porosity (100%):17.78%
Pore Frequency (100%):36.86%
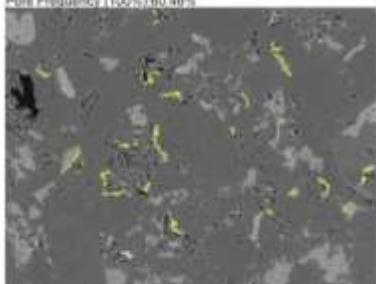
Pore Type:Grain Edge Pores (GEP)
Total Porosity:0.76%
Porosity (100%):10.94%
Pore Frequency (100%):2.26%
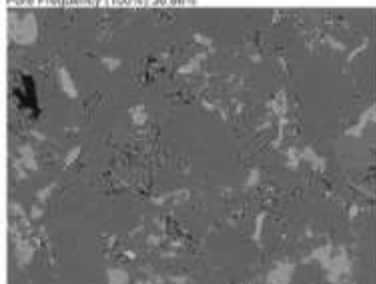
Pore Type:Fracture Pores (FP)
Total Porosity:0.01%
Porosity (100%):0.1%
Pore Frequency (100):0.23%
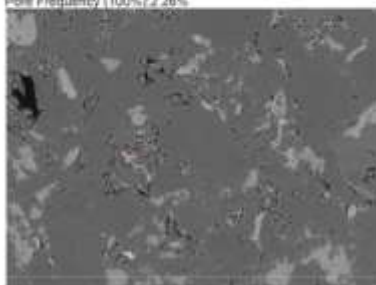
Pore Type:Shrinkage Crack Pores (SCP)
Total Porosity:0.1%
Porosity (100%):1.36%
Pore Frequency (100%):0.19%

2. *Sandstone microfacies* (DSND and VSND) contributes 0.02–1.08% toward total porosity, representing 0.1–12.8% of the pore network.

3. *Shale microfacies* (OMRS) Contributes 0.35% toward total porosity, representing 2.1% of the pore network.

4.7.2.2.2. Micropore system (200 μm)

Moldic pores contribute be-tween 0.21% and 1.24% toward total porosity of which micropores con-tribute 0.14–0.79%, representing 56.58–78.57% of moldic porosity. The five main microfacies which show very similar results are all siltstones and shales, OM/ILS, DOMS, OMRS, ILRS, and VSND and have moldic porosities between 0.87% and 1.24%, while the DSND sandstones exhibit a low porosity of 0.21%. . However, the percentage of micropores present within moldic pore porosity is variable across the two groups ranging from 8.44% to 55.85%. The lower quantity of micropores present with the moldic pore phase indicates that even at a higher resolution moldic porosity still contains significant quantities of nanopores. In total moldic micro-porosity equals:

1. *Siltstone microfacies* (ILRS, OM/ILS, MRSL, and DOMS) contribute 0.17–0.7% toward total porosity and represent 2.46–13.4% of the pore network.

2. *Sandstone microfacies* (VSND and DSND) contributing 0.14–0.79% toward total porosity representing 11.37–16.26% of the pore net-work.

3. *Shale microfacies* (OMRS) contribute 0.58% toward total porosity representing 3.74% of the pore network.

4.7.2.3. Grain edge pores (GEP)

Stressing the disproportionality between pore type abundance and contributions toward total microfacies porosity, predominantly in the OM/ILS and OMRS microfacies, GEPs are the second largest contributor toward total porosity due to their size, not their abundance. Proportionally, GEP contributions toward total porosity across all microfacies are similar and sometimes much greater than moldic pore contributions. At the two separate scales proportional contribution toward total porosity is as follows:
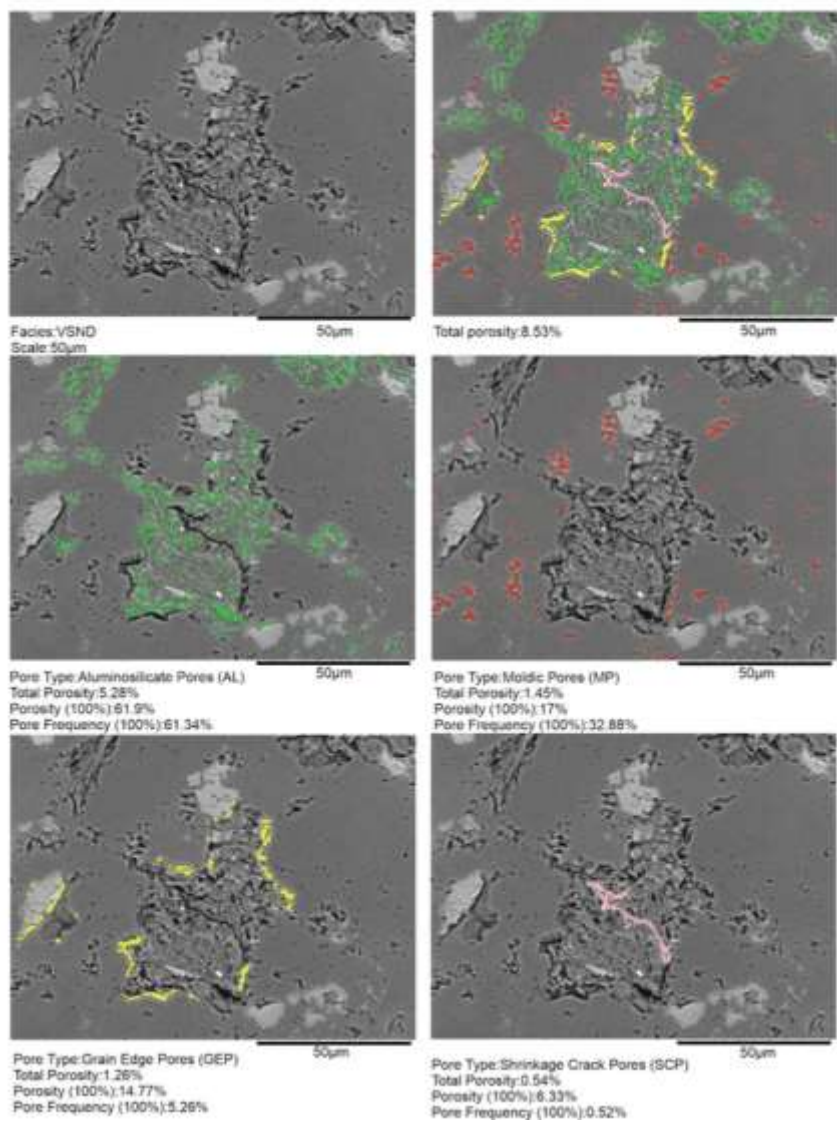
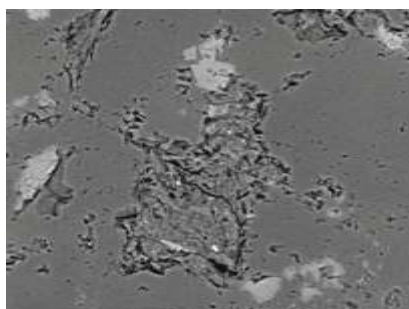- 50 µm Scale: 4.78–21.59%
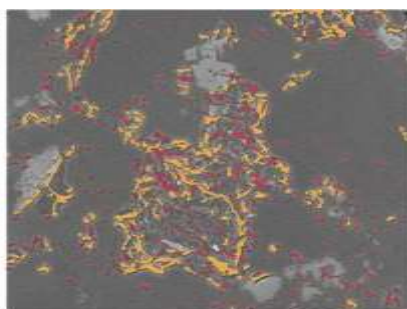
- 200 µm Scale: 4.54–13.13%

Fig. 43. Facies VSND pore type characterization (200 µm Scale).
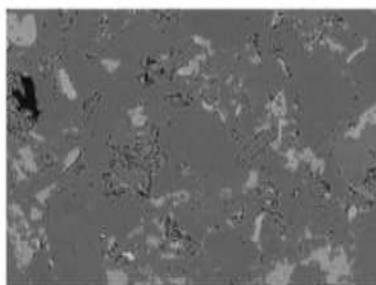
Facies:VSND
Scale:200μm
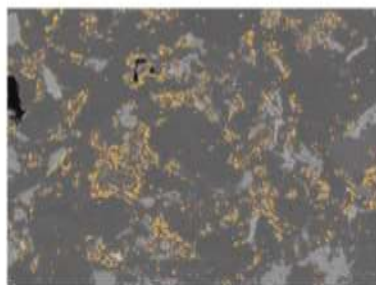
Microporosity:5.86%
Nanoporosity:1.12%
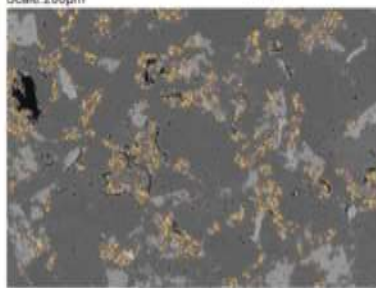
Pore Type:Aluminosilicate Pores (AL)
Total Porosity:4.87%
Microporosity:4.23%   Micropore Frequency(100%):47.25%
Nanoporosity:0.64%   Nanopore Frequency (100%):52.75%
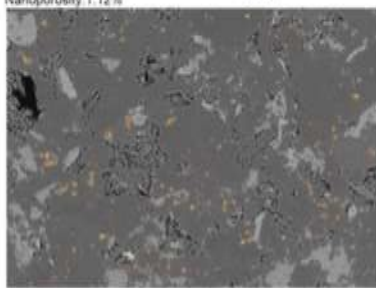
Pore Type:Moldic Pores (MP)
Total Porosity:1.24%
Microporosity:0.79%   Micropore Frequency(100%):26.14%
Nanoporosity:0.45%   Nanopore Frequency (100%):73.86%
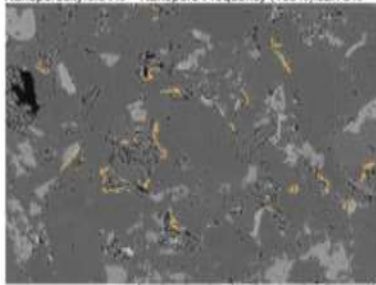
Pore Type:Grain Edge Pores (GEP)
Total Porosity:0.76%
Microporosity:0.75%   Micropore Frequency(100%):79.66%
Nanoporosity:0.01%   Nanopore Frequency (100%):20.34%
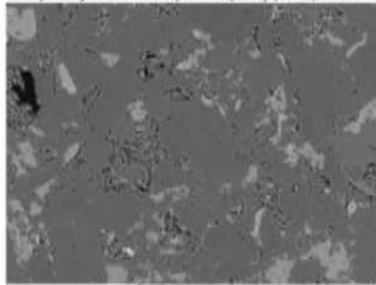
Pore Type:Fracture Pores (FP)
Total Porosity:0.01%
Microporosity:0.006%   Micropore Frequency (100%):33.33%
Nanoporosity:0.004%   Nanopore Frequency (100%):66.67%
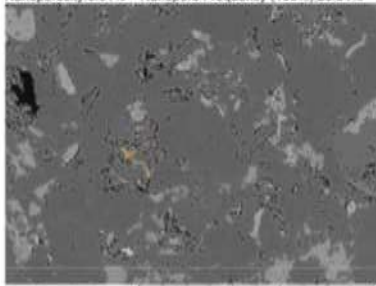
Pore Type:Shrinkage Crack Pores (SCP)
Total Porosity:0.1%
Microporosity:0.09%   Micropore Frequency(100%):20%
Nanoporosity:0.01%   Nanopore Frequency (100%):80%

4.7.2.3.1. Nanopore system (50 µm)

The third-largest contributor to- ward total porosity are GEPs, contributing 0.13–3.69% toward total microfacies porosity. Due to these pores being characteristically microporous in size, GEP nanopores only contribute 0.08–0.65% toward total microfacies porosity representing 3.73–45.28% of the total GEP porosity. This, however, is with the exception of the DSND microfacies in which GEP pores are 100% nanoporous. Characteristically elongate and micro-porous, their nanoporous counterparts contribute very little toward total porosity. Similar to moldic pores these pore types are also grain controlled and are abundant in immature sediments with angular quartz grains. In to- tal grain edge nanoporosity equals:

1. *Siltstone microfacies* (ILRS, OM/ILS, MRSL and DOMS) contributed 0.1–0.43% toward total porosity, representing 0.54–3.46% of the total pore network.

2. *Sandstones microfacies* (DSND and VSND) contribute 0.13–0.19% toward total porosity, representing 2.23–4.81% of the pore network.

3. *Shale microfacies* (OMRS) contribute 0.65% toward total porosity, representing 3.8% of the pore network.

4.7.2.3.2. Micropore system (200 µm)

As previously noted, GEPs are predominantly microporous in nature as they follow the length of rigid grains. GEPs contribute between 0.12% and 2.13% toward the total microfacies porosity, of which micropores contribute 0.28–2.11%. Representing 95.52–99.83% of total GEP porosity. Apart from the DSND microfacies, where microporous GEP pores represent 63.61% of total GEP porosity. The mechanism of their formation has ensured that they remain large and elongate and thus are ideal pore types for facilitating hydrocarbon migration around the matrix and drastically increase gas mobility and freedom to flow. In total grain edge microporosity equals:

1.   *Siltstone microfacies* (ILRS, OM/ILS, MRSL, and DOMS) contribute 0.28–2.13% toward total porosity and represent 4.33–12.5% of the pore network.

2.   *Sandstone microfacies* (VSND and DSND) contributing 0.76% and 0.12% toward total porosity, representing 8.3% and 10.8% of their respective pore networks.

**Fig. 44.** Facies VSND pore size characterization (200 µm Scale).

Pore Size Porosity vs Frequency
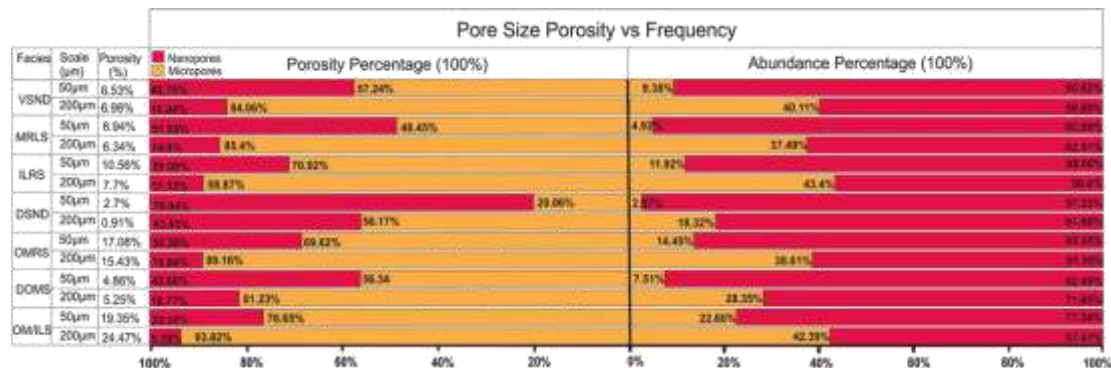
Fig. 45. Pore size abundance and porosity distribution across all facies types within the nanopore system (50 µm) and micropore system (200 µm). The chart shows the abundance of nanopores throughout all facies at all scales is always higher than their microporous counterparts, yet micropores still contribute the majority of porosity except for the DSND (50 µm) and MRSL (50 µm) facies.

3.   *Shale microfacies* (OMRS) contribute 1.35% toward total porosity, representing 8.7% of the pore network.

4.7.3. Secondary pore type porosity

Secondary porosity increases as scale increases, highlighting the importance of factoring in the contributions of secondary pore types in pore net-work modeling. Proportionally, secondary pore type contributions toward total porosity across all microfacies at the two separate scales are as follows:

- 50 µm Scale: 0.7–9.22%

- 200 µm Scale: 0.16–4.13%

4.7.3.1. Nanopore system (50 µm)

Unlike primary pore types, secondary pore types are predominantly nanoporous in size and consist of fractures, shrinkage cracks, framboidal pores, dissolution pores and mica-based pore types. All five types only contributing between 0.06% and 0.64%. Although some of these pore type may be plentiful within the pore network, as confirmed by earlier results in pore abundance, they occupy a very small area (Figs. 14–16), with shrinkage cracks and fractures displaying elongate but dia-metrically constrained morphologies. Nanoporous mica-based pores con-tribute between 0.02% and 0.35% toward total porosity. As these pores are very narrow, 65%–100% of mica pores are nanoporous in all microfacies. Their extremely narrow but elongate morphology prohibits larger contributions toward overall porosity, despite large quantities of micas being present. Fracture nanopores contribute between 0.07% and 0.32% toward total porosity, where present, fractures are predominately nanoporous. Shrinkage crack nanopores are not a

common pore type, in microfacies MRSL and VSND they only contribute 0.11% and 0.06% toward total porosity. Shrinkage cracks in microfacies MRSL are completely nanoporous. However, in the VSND larger microporous shrink-age cracks are present. Framboidal pores are less abundant in the matrix and are primarily concentrated in the varves; where present in the matrix, pores are exclusively nanoporous and contribute only 0.11% toward total porosity. At this scale, combined dissolution-based porosity can only be demonstrated from the DOMS and the DSND microfacies with porosities of 0.13% and 2.12%, of which nanopores contribute 0.05% and 1.59% respectively. Within the DSND microfacies, which is dominated by intergranular dolomitic cement, a significant amount of dissolution-based nanoporosity is present. This nanoporosity contributes 1.22% toward total porosity and represents 45.19% of the total pore network. In total combined secondary pore type nanoporosity equals:

1.   *Siltstone microfacies* (ILRS, OM/ILS, MRSL, and DOMS) contribute 0.14–0.64% toward total porosity, representing 2.23–9.22% of the pore network.

2.   *Sandstone microfacies* (VSND and DSND, excluding the dolomitic dissolution pores in the DSND), contribute 0.06% and 0.78% toward total porosity, representing 0.7% and 21.1% of pore network porosity.

3.   *Shale microfacies* (OMRS) contributes 0.51% toward total porosity, representing 2.99% of total network porosity.

4.7.3.2. Micropore system (200 μm)

The reduction in resolution has reduced the number of observable nanopores and as such the observable porosity that they can contribute. Mica-based porosity is negligible, contributing between 0.04% and 0.07% representing between 0.25% and 1.13% of the total

network. Of this percentage, micropores only constitute 0.01–0.02%. Fracture pores con-tribute even less toward total porosity contributing just 0.01–0.12% of which microporous only contribute between 0.006% and 0.03%. Shrink-age cracks also produce negligible quantities of porosity and microporosity where present. Shrinkage crack porosity ranges from 0.04% to 0.1% of which 0.02–0.09% is microporous. Dissolution-based porosity within argillaceous sediments ranges from 0.12% to 0.57%, of which 0.02% to 0.17% is microporous. The DSND microfacies, which has a dolomite dominated intergranular pore space, has a dissolution-based porosity of 0.43% of which microporosity contributes 0.22%, representing 51.1% of dolomite dissolution based porosity (Figs. 17–44). In total combined secondary pore type microporosity equals:

1. *Siltstone microfacies* (ILRS, OM/ILS, MRSL, and DOMS) contribute 0.04–0.21% toward total porosity, representing 0.07–1.56% of the pore network.

2. *Sandstone microfacies* (VSND and DSND, excluding the dissolution pores in the DSND), contribute 0.1% and 0.08% toward total porosity, representing 1.38% and 8.79% of pore network porosity.

3. *Shale microfacies* (OMRS) contributes 0.21% toward total porosity, representing 1.36% of total network porosity.

5. DISCUSSION

5.1. Resource assessment

5.1.1. Upper Pastora Formation (formation overview)

• The Upper Pastora Formation is characterized by an interbedded succession of organic matter rich shales and siltstones which are intermittently interrupted by massive dolomitized sandstone beds. The negligible porosity of these sandstone units (DSND) and isolation of dissolution based pores within their pore networks, has created a multi-layered sealing sequence. Within this multi-layered sealing sequence, shale gas is confined to shales as a self-sealing, self-sourcing reservoir as well as any escaping gas will be trapped between larger, regularly occurring DSND sandstone units, acting as a seal and trap-ping any gas within the more porous fine-grained siltstones. The presence of interbedded siltstone and sandstones layers within shale gas plays can improve the permeable capacity of shale reservoirs (Zou, 2013), however, the porosities demonstrated here show that most interbedded siltstone are of low porosity.

Pervasive OM content and porosity is highest in the OM/ILS siltstone and OMRS shale facies, with other facies showing more negligible quantities of both.

• Shale microfacies: Demonstrate porosities of 17.08% at the 50 μm scale and 15.43% at the 200 μm scale with an increase in porosity associated with a greater nanopore frequency.

• Siltstone microfacies: Exhibit porosities of 4.86–10.6% at the 50 μm scale and 5.26–7.7% at the 200 μm scale, except for the high degree of porosity found in the OM/ILS siltstone with porosities of 19.35% at the 50 μm scale and 24.47% at the 200 μm scale.

• Sandstone microfacies: DSND microfacies have a porosity of 2.7% at the 50 μm scale and 0.91% at the 200 μm while the VSND microfacies have a porosity of 8.52% at the 50 μm and 6.97% at the 200

μm in the varved sandstone, which is an argillaceous anddolomitic hybrid. This indicates that the microporous system is responsible for the majority of porosity.

- Gamma ray data combined with SEM analysis of organic matter indicate uranium values between 3.2 and 4.3 ppm, and OM identification under the SEM could be an indication of a highly TOC enriched shale which consists of limited type I, and enriched type II and III kerogen.

- Shales were deposited under an environment which underwent oxygenation fluctuations with Th/U ratios between 3.26 and 4.77, which places the Pastora paleolake in an oxicdysoxic environment.

Should exploration occur, these shale/siltstone bundles should be targeted, specifically shale bundles in which OMRS microfacies are located directly above OM/ILS microfacies. Not only the shale self-generating and self-sealing sources but any gas which escapes these shale beds, is likely to accumulate in the more porous OM/ILS siltstone microfacies, which demonstrate the best pore network characteristics for hydrocarbon migration, as mentioned through the nanoporous and more importantly microporous sections. The intermittent occurrence of the DSND micro-facies through the sealing sequence, act as gas seals and keep methane trapped between the coarser sandstone beds, while all other siltstone microfacies (DOMS, ILRS, MRSL) play a significantly less important role in trapping and storing gas, as they have lower porosities, lower effective permeabilities and limited sealing capacity, due to only partial dolimitization. There is currently sufficient evidence for the presence of methane gas migration, as gas between the various lithotypes has already been established by proxy. In 2013, seven miners died in a methane gas blow out in Pozo Emilio de Valle, located in the southeast of the mine. This is an area where a large section of the Upper Pastora Formation crops out and it may very well be that the methane blowout was a result of a penetration into the large

dolomitized sandstones beds (DSND). The initial high porosity prior to diagenetic dolomitization of the intergranular space, may have caused the development of a geopressurized zone. As shale and very fine-grained siltstones, with a high water and gas bearing capacity within the illite matrix, were expelled during lithostatic compaction, they likely migrated into the large porous sandstone beds and were further locked in by later dolomitization. This presents both problems and solutions, in that there is clear evidence of methane generation and migration within the multi-layered sealing sequence and a potential target microfacies has been identified for exploration. We also have a good understanding of the degree of porosity and permeability and which pores can be found. However, it has become clear that rapid sedimentation rates in the Late Carboniferous/Permian, during the primary phase of thermogenic methane generation, may have generated a series of geopressurized sequences marked by gas charged sand bodies. Although it remains a prominent source of blowouts, which complicates extraction, it has been said that geopressurized UHRs contain the greatest quantities of natural gas (Speight, 2019).

5.1.2. Upper Pastora Formation (pore network overview)

As the pore type frequency and porosity data has shown, there is a highly disproportional relationship between these two factors, the most important of which are GEP and moldic pores. Despite moldic pores being the second most abundant pore type, these pore types are predominately nanometric and as BSE imaging shows, isolated from the pore network, indicating that they have an inherent inability to migrate hydrocarbons throughout the pore network. GEP pores however, are lower in frequency but contribute much greater amounts of porosity and are located adjacent to the aluminosilicate matrix, offering great migration potential for gas seeking to escape the matrix. In terms of pore size distribution, we see that as we downscale from the 200 to 50 μm scale there is a 25% average increase in nanopore frequency associated with a 27% increase in nanoporosity throughout the pore network (Fig. 45). This results in an increase in total rock porosity of between 1.12% and 3.47% of which the greatest increase in nanoporosity can be found in the organic matter rich OMILS and OMRS siltstone sand shale facies with an increase of 3% and 3.47%, respectively. This highlights the importance of nanopore contributions toward porosity and the need for multi-scaled imaging, but also the close association between increase in TOC content and nanoporosity.

The two most important microfacies types in the Upper Pastora Formation are the OM/ILS and OMRS. Both show great hydrocarbon potential in response to recovery operations, given the high quantity of porosity found within the aluminosilicate matrix, and the hydrocarbon migration potential offered from the elongate structure of grain edge pores. These two facies offer the greatest potential for shale gas extraction due to the following characteristics:

1. The most abundant pore types are: aluminosilicate pores, moldic pores and grain edge pores. Despite moldic pores being the second most abundant, they are much smaller than GEP pores, contributing less to total porosity and are more isolated from the pore network. The inverse can be said for GEP pores, stressing the disproportionality between moldic and GEP pore type abundance and porosity (Fig. 16).

2. All microfacies demonstrate a low effective porosity, with the greatest potential for effective hydrocarbon migration found in the OM/ILS and OMRS microfacies, due to higher quantities of microporous aluminosilicate and GEP pores. In addition to this, these facies have the highest frequency of aluminosilicate nanopores, which despite contributing proportionally smaller quantities of porosities, can offer further adsorbed gas potential due to a larger specific surface area.

3. Illite-based aluminosilicate porosity, at the 50 µm scale, is the greatest contributor in the two most porous microfacies types OM/ ILS-13.36%, OMRS-12.04%) with nanoporosity more dominant in the shale microfacies (OM/ILS-2.32%, OMRS-3.68%). At the 200 µm scale, Illite-based aluminosilicate porosity is still the biggest contributor toward total microfacies porosity in the OM/ILS (21.36%) and OMRS microfacies (12.75%).

4. In the/OM/ILS and OMRS as we transition from the micrometric system to the nanometric system we see that nanoporosity in primary pore types can increase by up to 2.5%.

As confirmed by the characterized BSE images, specific pore types visually demonstrate varying structures and contributions toward total porosity. Given the level of discontinuity and lack of pore connectivity

within the pore network of shales and siltstone both here, and recorded around the world, we must begin to view the pore network differently. Rather than a collective group of unconnected void spaces, it is vital to identify the importance of their genesis, the morphological variability associated with specific pore types and identify their potential to form effective hydrocarbon migration pathways. This can only be done by first characterizing pore types. Once completed, we can begin to identify pore network properties prior to recovery operations, which indicate conditions most conducive to fluid flow and enhance our ability to predict well longevity and productivity. Furthermore, research and development (R&D) regarding increased hydrocarbon recovery could greatly ben-efit from identifying pore type characteristics which are most conducive to specific types of recovery operations such as acidization. Although in its preliminary stages, combining matrix acidization research in shales, with characterized pore network and geochemical data, could yield interesting results. However, first a deeper understanding of shale mineralogy, permeability, porosity and fluid dynamics is required (Gomez, 2019), something which characterized pore networks from SEM-based binary imagery can provide.

6. CONCLUSION

In this paper with we provide evidence for a multi-layered sealing sequence within the Upper Pastora Formation, consisting of interbedded OM rich shales/siltstones and dolomitic sandstones, which were de-posited in a shallow-intermediate lacustrine setting and contain mostly type II and III kerogen sources, with kerogen type I confined to rhythmic varves. The intermittent presence of larger, low porosity sandstone beds within this sequence has provided a dual sealing sequence which has charged the overlying sandstone bodies with gas. Porosity through-out the sequence is variable, ranging from 2.7% to 19.35% (50 µm) and 0.91% to 24.47% (200 µm), and > 3% within dolomitized sandstones, with the greatest potential for gas in the very fine-grained siltstone microfacies OM/ILS and shale microfacies OMRS. The porosity in these microfacies is dominated by primary pores types, predominantly within the aluminosilicate matrix and then by GEP pores, with moldic pores being isolated from the pore network showing poor migration potential. The structure of these larger microporous GEP pores provides excellent hydrocarbon migration pathways for free gas locked within the aluminosilicate matrix and also adsorbed gas, which shows strong potential due to the large frequency of nanopores within the illite matrix. This characterization of the pore network and quantification of both pore frequency and porosity has highlighted the individual importance of each pore type within the network. Further statistical analysis of the factors associated with pore-scale fluid flow activity such as pore geometry, pore size distribution, spatial distribution and other important morphological parameters, can now be quantified and associated with each individual pore type. With recent work on pore type genesis having greatly improved our understanding of the formation of specific pore types within shales, we can now begin to correlate parameters surrounding pore type gene-sis with changes in the structure of the pore network. This subsequently allows us to identify conditions which are likely to generate pore types which are known to be more conducive to hydrocarbon migration, and contribute the most toward pore network porosity. Although this requires a large amount of data synthesis from a wide range of sources and adoption of a universal characterization scheme, this method can provide valuable data for generating more accurate multiphase fluid flow models and

provide insights into pore-scale geomechanics at both the nanometric and micrometric scale.

REFERENCES

Adams, J., Weaver, C., 1958. Thorium-to-uranium ratios as indicators of sedimentary processes: example of concept of geochemical facies. AAPG Bulletin 42, 387–430.

Álvarez, R., Ordóñez, A., Canteli, P., De Miguel, E., 2018. Unconventional gas resources in the Cantabrian zone (NW Spain): a comprehensive preliminary assessment. Geol. J. 54 (4), 2608–2620.

Ayllon, F., Bakker, R., Warr, L., 2008. Re-equilibration of fluid inclusions in diagenetic anchi zonal rocks of the Ciñera-Matallana coal basin (NW Spain). Geofluids 3 (1), 49–68.

Bazilian, M., Brandt, A., Billman, L., Heath, G., Logan, J., Mann, M., Melaina, M., Statwick, P., Arent, D., Benson, S., 2014. Ensuring benefits from north American shale gas development: towards a research agenda. J. Unconv. Oil and Gas Res. 7, 71–74.

Bertoni, C., Cartwright, J.A., Foschi, M., Martin, J., 2018. Spectrum of gas migration phe-nomena across multi-layered sealing sequences. AAPG Bulletin 102 (6), 1011–1034.

Boyer, C., Clark, B., Jochen, V., Lewis, R., 2013. Shale Gas: A Global Resource. Schlum-berger, 28–39.

Cardott, B., Curtis, M., 2018. Identification and nanoporosity of macerals in coal by scan-ning electron microscopy. Int. J. Coal Geol. 190, 205–217.

Chen, L., Jiang, Z., Liu, Q., Jiang, S., Liu, K., Tan, J., Gao, F., 2019. Mechanism of shale gas occurrence: insights from comparative study on pore structures of marine and la-custrine shales. Mar. Pet. Geol. 104, 200–216.

Chengzao, J., 2017. Breakthrough and significance of unconventional oil and gas to clas-sical petroleum geology theory. Pet. Explor. Dev. 44 (1), 1–10.

Cienfuegos, P., Loredo, J., 2010. Coalbed methane resources assessment in Asturias (Spain). Int. J. Coal Geol. 83 (4), 366–376.

Clarkson, C., Solano, N., Bustin, R., Bustin, A., Chalmers, G., He, L., Melnichenko, Y., Radliński, A., Blach, T., 2013. Pore structure characterization of north American shale gas reservoirs using USANS/SANS, gas adsorption, and mercury intrusion. Fuel 103, 606–616.

Colmenero, J., Suárez-Ruiz, I., Fernández-Suárez, J., Barba, P., Llorens, T., 2008. Genesis and rank distribution of upper carboniferous coal basins in the Cantabrian Mountains, northern Spain. Int. J. Coal Geol. 76 (3), 187–204.

Curtis, M., Sondergeld, C., Ambrose, R., Rai, C., 2012. Microstructural investigation of gas shales in two and three dimensions using nanometer-scale resolution imaging. AAPG Bulletin 96 (4), 665–677.

Desbois, G., Enzmann, F., Urai, J., Baerle, C., Kukla, P., Konstanty, J., 2010. Imaging pore space in tight gas sandstone reservoir: insights from broad ion beam cross-sec-tioning. EPJ Web Conf. 6, 22022.

EIA, 2013. World Shale Resource Assessments. [online] U. S Energy Infomation Admin-istration. Available at:

https://www.eia.gov/analysis/studies/worldshalegas/>, [Ac-cessed 1 Jun 2020].

European Commission, 2016. Overview of the current status and development of shale gas and shale oil in Europe. In: European Unconventional Oil and Gas Assessment (EU-OGA). pp. 90–94.

Felder, M., Harms, H.-J., Liebig, V., Hottenrott, M., Rolf, C., Wonik, T., 2001. Litholo-gische Beschreibungen der Forschungsbohrungen Groß-Zimmern, Prinz von Hessen und Offenthal sowie zweier Lagerstättenbohrungen bei Eppertshausen (Sprendlinger Horst, Eozän, Messel-Formation, Süd Hessen). Geol. Jb. Hess. 128, 29–82.

Frings, K., Lutz, R., de Wall, H., Warr, L., 2004. Coalification history of the Stephanian Ciñera-Matallana pull-apart basin, NW Spain: combining anisotropy of vitrinite 170 reflectance and thermal modelling. Int. J. Earth Sci. 93 (1), 92–106.

Gomez, J., 2019. Design, Set-up, and Testing of Matrix Apparatus. Msc Texas A&M Uni-versity.

González, A., Molinero, R., Crespo, J., Arribas, J., Nita, R., 2017. Proyecto de exploracion de hidrocarburos no convencionales en Espana (HCNC). Ministerio de Economia, In-dustria Y Competitividad.

Goral, J., Miskovic, I., Gelb, J., 2015. Pore network investigation in Marcellus shale rock matrix. In: society of petroleum engineers. In: SPE Asia Pacific Unconventional Re-sources Conference and Exhibitio: Society of Petroleum Engineers. pp. 1–8.

Guo, C., Wei, M., Liu, H., 2018. Study of gas production from shale reservoirs with multi-stage hydraulic fracturing horizontal well considering multiple transport mechanisms. PLoS One 13 (1), e0188480.

Heward, A., 1978. Alluvial fan and lacustrine sediments from the Stephanian a and B (La Magdalena, Ciñera-Matallana and Sabero) coalfields, northern Spain. Sedimentology 25 (4), 451–488.

Hofmann, P., Duckensell, M., Chpitsglous, A., Schwark, L., 2005. Geochemical and organic petrological characterization of the organic matter of lacustrine Eocene oil shales (Prinz von Hessen, Germany):

reconstruction of the depositional environ-ment. J. Paleolimnol. 33 (2), 155–168.

Hu, Q., Ewing, R., Rowe, H., 2015. Low nanopore connectivity limits gas production in Barnett formation. J. Geophys. Res. Solid Earth 120 (12), 8073–8087.

IGME, 1989. MAGNA 50 - Sheet Number 103 (LA POLA DE GORDÓN) Scale 1:50.000. [image] Available at: http://info.igme.es/cartografiadigital/geologica/ Magna50.aspx>, [Accessed 15 October 2019].

Jiang, P., 2013. Pore Morphometrics and Thermal Evolution of Organic-Matter Microp-orosity, Colorado Group, Western Canada Foreland Basin. Msc Western University.

Jones, B., Manning, D., 1994. Comparison of geochemical indices used for the interpreta-tion of palaeoredox conditions in ancient mudstones. Chem. Geol. 111 (14), 111–129.

King, H., Eberle, A., Walters, C., Kliewer, C., Ertas, D., Huynh, C., 2015. Pore architec-ture and connectivity in gas shale. Energy Fuel 29 (3), 1375–1390.

Lemos de Sousa, M., Pinheiro, H., 1996. Prospecting for Coalbed Methane: Preliminary Investigation into the Possibilities in Spain. 90 (1). Real Academia de Ciencias Exac-tas, Físicas y Naturales, 63–74.

Leneuf, N., 1973. Observations stereoscopiques sur les figures de corrosion du quartz dans certaines formations superficielles. Cah. ORSTOM, Serie Pid. 11 (1), 43–51.

Loucks, R., Reed, R., Ruppel, S., Hammes, U., 2012. Spectrum of pore types and networks in mudrocks and a descriptive classification for matrix-related mudrock pores. AAPG Bulletin 96 (6), 1071–1098.

Lüning, S., Kolonic, S., 2003. Uranium spectral gamma-ray response as a proxy for or-ganic richness in black shales: applicability and limitations. J. Pet. Geol. 26 (2), 153–174.

Ma, L., Slater, T., Dowey, P., Yue, S., Rutter, E., Taylor, K., Lee, P., 2018. Hierarchi-cal integration of porosity in shales. Sci. Rep. 8 (1), 11683. https://doi.org/10.1038/ s41598-018-30153-x.

Mackenzie, W., 2018. Cantabrian Basin Shale Gas Unconventional Concept Play. Wood Mackenzie, Edinburgh.

Mastalerz, M., Drobniak, A., Hower, J., O'Keefe, J., 2010. Coal and Peat Fires: A Global Perspective, first ed. Elsevier, 47–62.

McGlade, C., Speirs, J., Sorrell, S., 2013. Methods of estimating shale gas resources – comparison, evaluation and implications. Energy 59, 116–125.

Middleton, R., Carey, J., Currier, R., Hyman, J., Kang, Q., Karra, S., Jiménez-Martínez, J., Porter, M., Viswanathan, H., 2015. Shale gas and non-aqueous fracturing fluids: opportunities and challenges for supercritical CO2. Appl. Energy 147, 500–509.

Middleton, R., Gupta, R., Hyman, J., Viswanathan, H., 2017. The shale gas revolution: barriers, sustainability, and emerging opportunities. Appl. Energy 199, 88–95.

Nie, H., Jin, Z., Zhang, J., 2018. Characteristics of three organic matter pore types in the Wufeng-Longmaxi shale of the Sichuan Basin, Southwest China. Sci. Rep. 8 (1), 7014. https://doi.org/10.1038/s41598-018-25104-5.

Pak, T., Butler, I., Geiger, S., van Dijke, M., Jiang, Z., Surmas, R., 2016. Multiscale pore network representation of heterogeneous carbonate rocks. Water Resour. Res. 52 (7), 5433–5441.

Pickel, W., Kus, J., Flores, D., Kalaitzidis, S., Christanis, K., Cardott, B., Misz-Kennan, M., Rodrigues, S., Hentschel, A., Hamor-Vido, M., Crosdale, P., Wagner, N., 2017. Classification of liptinite - ICCP system 1994. Int. J. Coal Geol. 169, 40–61.

Rider, M., 1996. The Geological Interpretation of Well Logs, second ed. Rider-French consulting LTD, Sutherland, 67–86.

Ross, D., Bustin, R., 2009. The importance of shale composition and pore structure upon gas storage potential of shale gas reservoirs. Mar. Pet. Geol. 26 (6), 916–927.

Scotchman, I., 2016. Shale gas and fracking: exploration for unconventional hydrocar-bons. Proc. Geol. Assoc. 127 (5), 535–551.

Shen, W., Li, X., Xu, Y., Sun, Y., Huang, W., 2017. Gas flow behavior of nanoscale pores in shale gas reservoirs. Energies 10 (6), 751.

Speight, J., 2019. Natural gas, second ed. Gulf Professional Publishing, Oxford, 59–98.

Wagner, R., 1971. The stratigraphy and structure of the Ciñera-Matallana coalfield (Prov Leon N W Spain). In: Wagner, R. (Ed.), Trabajos de Geologia, fourth ed. Universidad de Oviedo, Oviedo, pp. 385–429.

Wang, S., 2018. Shale gas exploitation: status, problems and prospect. Natu. Gas Ind. B 5(1), 60–74.

Zendehboudi, S., Bahadori, A., 2016. Shale Oil and Gas Handbook. Gulf Professional Publishing, Oxford, 1–26.

Zhang, P., Hu, L., Meegoda, J., Gao, S., 2015. Micro/nano-pore network analysis of gas flow in shale matrix. Sci. Rep. 5 (1), 13501. https://doi.org/10.1038/srep13501.

Zou, C., 2013. Unconventional Petroleum Geology, first ed. Elsevier, 149–190.